AN ABSTRACT OF THE THESIS OF

Jeffery W. Samuels for the degree of Doctor of Philosophy in Nuclear Engineering presented on November 1, 1988.

Title: OLAPS: An On-Line Advanced Plant Simulator

Abstract Approved: Redacted for Privacy

A PC based on-line advanced plant simulator (OLAPS) for high quality simulations of Portland General Electric's Trojan Nuclear Facility is presented. OLAPS is designed to simulate the thermal-hydraulics of the primary system including core, steam generators, pumps, piping and pressurizer. The simulations are based on a five equation model that has two mass equations, two energy equations, and one momentum equation with a drift flux model to provide closure. A regionwise point reactor kinetics model is used to model the neutron kinetics in the core. The conservation equations, constitutive models and the numerical methods used to solve them are described. OLAPS results are compared with data from chapter 15 of the Trojan Nuclear Facility's final safety analysis report.

An On-Line Advanced Plant Simulator (OLAPS)

by

Jeffery W. Samuels

A THESIS

Submitted to

Oregon State University

in Partial fulfillment

of the requirements for the

degree of

Doctor of Philosophy

Presented: November 1, 1988

Commencement: June 11, 1989

APPROVED:

Redacted for Privacy

Assistant Professor of Nuclear Engineering,
in charge of major

Redacted for Privacy

Head of Department of Nuclear Engineering

Redacted for Privacy

Dean of

Date thesis presented: November 1, 1988

ACKNOWLEDGEMENTS

This work was performed under the sponsorship of the Portland General Electric Company.

I wish to express my appreciation to my major professor Dr. Jose Reyes and the members of my committee; Dr. Alan Robinson Head of the Department of Nuclear Engineering, Dr. Andrew Klein, Dr. Milton Larson and Dr. Roman Schmitt, for their support and encouragement. I would also like to thank Dr. Samim Anghaie for his help and support during his tenure at Oregon State University.

Most of all I would like to thank my family and friends, both here and abroad for their kind words and support through this sometimes difficult task.

Table of Contents

List of Tables

List of Figures

An On-line Advanced Plant Simulator (OLAPS)

Introduction

The Nuclear Industry has embraced simulators for use in a variety of areas. Three important uses for simulators are ; training of control room personnel, engineering design and safety analysis. Whatever the simulator's use, the common goal is to mimic the behavior of the system without incurring the risks that would be present when using the actual system.

From an engineering point of view a simulator offers the most cost effective way of carrying out these activities. In the training of reactor operators, a full-scope simulator will allow a trainee to manipulate the controls of a realistic control panel without the risk of a costly plant trip that could cause damage to system components. In the design and analysis of a nuclear power plant, engineers often turn to simulators to verify and evaluate system and component designs before construction.

The different activities have different requirements, therefore various kinds of simulators have been developed to perform these diverse tasks. Each of these simulators has their own advantages and disadvantages associated with them. The simulators used in operator training while easy to use, often suffer from poor quality models and the simulators used in engineering calculations have superior simulation models but are generally difficult to use.

The On-Line Advanced Plant Simulator (OLAPS) is designed to bridge the gap between these opposing philosophies.

This work will be concerned with :

- Describing the OLAPS design philosophy,
- Describing the physical and constitutive models,
- Describing the numerical solution methods,
- Presenting OLAPS results
- Comparing the OLAPS results to plant data and results from other computer codes.

1. OLAPS and the State of the Art

1.1. State of the Art

Two major classifications of simulators are the full-scope simulator, primarily used for training purposes; and the engineering simulators used for design and safety analysis. Some of these simulators are reviewed in the following sections.

1.1.1. Full-Scope Simulators

The full-scope simulator[1] provides a full mock-up of the control room control panel giving a realistic environment for operator training. In the full scope simulator, each major system's controls and annunciators are depicted on a control panel. The simulator responds to the manipulation of these controls in a manner that mimics the actual power plant.

These systems have undergone a great deal of development since they first became available in the 1960's. This development paralleled the development of the computers that were driving them. The early versions had hybrid computers based on a combination of analog and digital computers. Today these simulators are primarily based on high speed 32 bit super-minicomputers such as the Gould-SEL CONCEPT/32.

The full scope simulator control panel is often an exact copy of the control panel of the actual plant that it is supposed to simulate. This high level of detail results in a relatively high cost of the system. Also because there is a large amount of computational overhead involved in the monitoring of the various switches and dials, the quality of the physical models of the power plant components is sacrificed in order to maintain real time operation.

The recent advances in computer equipment both in speed and lower costs have begun to alleviate both of these problems.

1.1.2. Engineering Simulators

The engineering simulators are mainly computer programs designed to run on mainframe and super-computers. These programs can generally be divided into two classes; Discrete component codes, and Full system codes. The Discrete component simulators are used to calculate the thermalhydraulic behavior of individual system components (NOTE: while there are a great number of codes available for the simulation of the neutronics and other aspects of a nuclear power plant, the focus here will be on thermalhydraulics). Table 1.1 shows a partial list of some currently available discrete component codes.

Table 1.1
A list of some discrete components type codes used for Nuclear Engineering calculations.

COBRA - IIIc[2]	PNL
COBRA - IV[3]	PNL
TORC[4]	CE
VIPRE[5]	EPRI
MAYOU4[6]	GE
LYNX1[7]	BW
LYNX2[8]	BW

The full system codes, as the name implies are used to simulate the entire plant or at least the entire nuclear steam supply system (NSSS). Not surprisingly, these codes are more complex than the discrete components codes and therefore have a greater requirement for computational resources (time and memory). Table 1.2 list some of the full system codes available.

Table 1.2
Some currently available full system engineering simulation codes.

RETRAN[9]	EPRI
RELAP5/MOD2[10]	INEL
TRAC-PD1[11]	LANL
COBRA/TRAC[12]	PNL
BNL BWR Plant Analyzer[13]	BNL

1.1.3. PC Based Simulators

The recent revolution in the area of personal computer technology has created a great deal of interest in PC based simulators. Currently there are few commercially available PC based simulator systems. These systems are listed in Table 1.3.

Table 1.3
Some current commercially available PC-Based, nuclear system simulators

MC PWR[14]	S. Levy and Associates
PCTRAN[15]	MicroSimulation Technology
CEPAC[16]	CE
COBRA-IV PC[17]	PNL

The chief advantage of the PC based systems is the convenience that they offer. Because they are almost always running on dedicated machines, they can be more interactive than those systems running on a centralized mainframe computer.

Another important advantage that PC based simulators have is the relatively low cost of the computer. The one time investment of $2,000 to $10,000 for a PC provides virtually unlimited access on a one-person-one-machine basis. This is contrasted by the $500,000 - $1,000,000 cost of a multiuser mainframe computer. While the mainframe computer can accommodate many users at once and thereby reduce the dollar-to-user-ratio, the machine performance will decrease with an increase in the number of users.

Because mainframe usage tends to be metered, there is a per run cost associated with mainframe based

simulators that does not exist for the pc based simulator. Therefore for some cases where there is a need for a large number of computer simulation runs to complete a task, as was the case for the pressurized thermal shock overcooling sequences performed for H.B. Robinson Unit 2[18], using a pc based simulator is the only economically feasible alternative.

The primary disadvantage comes from the present limitations of personal computers. The size and speed of today's PC's require that the models used in the PC based simulators must be kept simple. This is particularly important for the real time systems.

1.2. OLAPS

The genesis of OLAPS was to develop a simulator system that could take advantage of future developments and innovations in computational machinery and data processing techniques, to provide high quality simulations in faster than real time. Such a system would have applications in a variety of areas including a control room monitoring system, operational personnel training and safety analysis.

1.2.1. Development Philosophy

Predicting the future always has a measure of risk. However, by looking carefully at the current trends in computer development and past developments, it is possible to reduce these risks. Therefore the development of OLAPS is based on observations made of the current areas of research in the Computer Sciences and projecting how certain break-throughs in these areas may be used.

Another aspect of the design philosophy behind OLAPS was to incorporate many models from other simulators. The idea was to use those models that would give the best results with reasonable speed.

An important OLAPS design decision was to use the FORTRAN programing language. This decision was made based on the wide availability of FORTRAN and its general acceptance in the engineering community.

A major area of current research in the computer sciences is multi- or parallel processing[19]. Multi-processing is the use of multiple processors to perform either similar tasks or different parts of the same task concurrently. This allows the overall speed of the

computation to be increased without increasing the speed of the individual processor.

OLAPS has been designed with the idea that multiprocessing hardware and software will become more readily available. This has been accomplished by using modern software design and data flow techniques[20]. In order to apply the data flow method, the problem is divided into many different sub-problems. This allows the problem to be understood more clearly and will allow easier implementation on a multiprocessor machine in the future.

The data flow method has resulted in a highly modular program, with each module performing different tasks in the overall simulation. This also helps in the readability of the code and in code maintenance.

The great advantages of using a multiprocessor system have been demonstrated by the BNL BWR Plant Analyzer[13]. The BNL BWR Plant Analyzer can run high quality simulations at 10 to 100 times realtime.

1.2.2. Enhancements to the State of the Art

In its current status, OLAPS is a PC based simulator that simulates the thermalhydraulics of a 4-loop Westinghouse PWR. The model of the plant is based on the Portland General Electric (PGE) Trojan Nuclear Facility. The scope of the OLAPS simulation includes the thermalhydraulics of the entire primary system as represented by a 2-loop model, including the core, pressurizer, steam generator, reactor coolant pumps and primary piping.

While many of the models used in OLAPS have been adapted from other simulators, there are some unique features to OLAPS. The most important of which is the Region-wise Point Reactor Kinetics (RWPRK) model[21]. This model allows the axial power shape in the core to change over time without requiring a great increase in computer time. The neutron kinetics model, if available at all in most thermalhydraulics codes, is the point reactor kinetics model. This model does not allow for a variable axial power shape, which can have an impact on the DNBR calculations[25].

Another unique and important feature of OLAPS is the amount of core thermalhydraulic detail that it provides. This feature is unique among the system type simulators which do not provide significant detail about the core condition. The exception to this is the COBRA/TRAC code, which requires the use of a mainframe or supercomputer.

The user interface is interactive for ease of operation. The output is a graphical representation of the plant primary system overlaid with numbers that indicate the values of some of the time dependent parameters at various points in the system. The user has the option of selecting and displaying anyone of several parameters while the simulator is running. In addition to the interactive display OLAPS can save the time dependent values of key parameters to a data file in a format that can be used with a graphics program such as LOTUS 123 or QUATTRO to produces hardcopy graphs. These features are not generally available with many of the current engineering simulators.

The eventual goal of the OLAPS system is to have an on-line connection to the plant computer for continual updates in the plant monitoring mode. This latter feature combined with the faster than real time simulations would provide a look ahead function, that

simulations would provide a look ahead function, that would predict the future condition of the plant based on current conditions and trends. This could be a valuable companion system to the Safety Parameter Display System (SPDS).

In summary OLAPS is a simulator that has been engineered to provide the following features:

- Accurate results(approaching best estimate)
- User friendly (interactive, graphical output)
- State of the art models (RWPRK, core Thermal-hydraulic models detail).

2. Component Models

The conceptual model used in the development of OLAPS is shown schematically in figure 2.1. This model is based on Portland General Electric's (PGE) Trojan Nuclear Facility, a Westinghouse 4-loop PWR. As shown in figure 2.1 the OLAPS model has two loops; one loop representing a single physical loop and the other representing a lumped model of the three remaining loops.

Below, the conceptual models for each of the major components is described.

2.1. Core Model

Conceptually the core is divided into two types of regions, an active region where thermal energy is generated through nuclear fission, and a passive region where no thermal energy is generated. The passive region, which includes; the upper and lower plena; and the downcomer region are lumped together with connecting piping. The pipe model is presented in section 2.7.

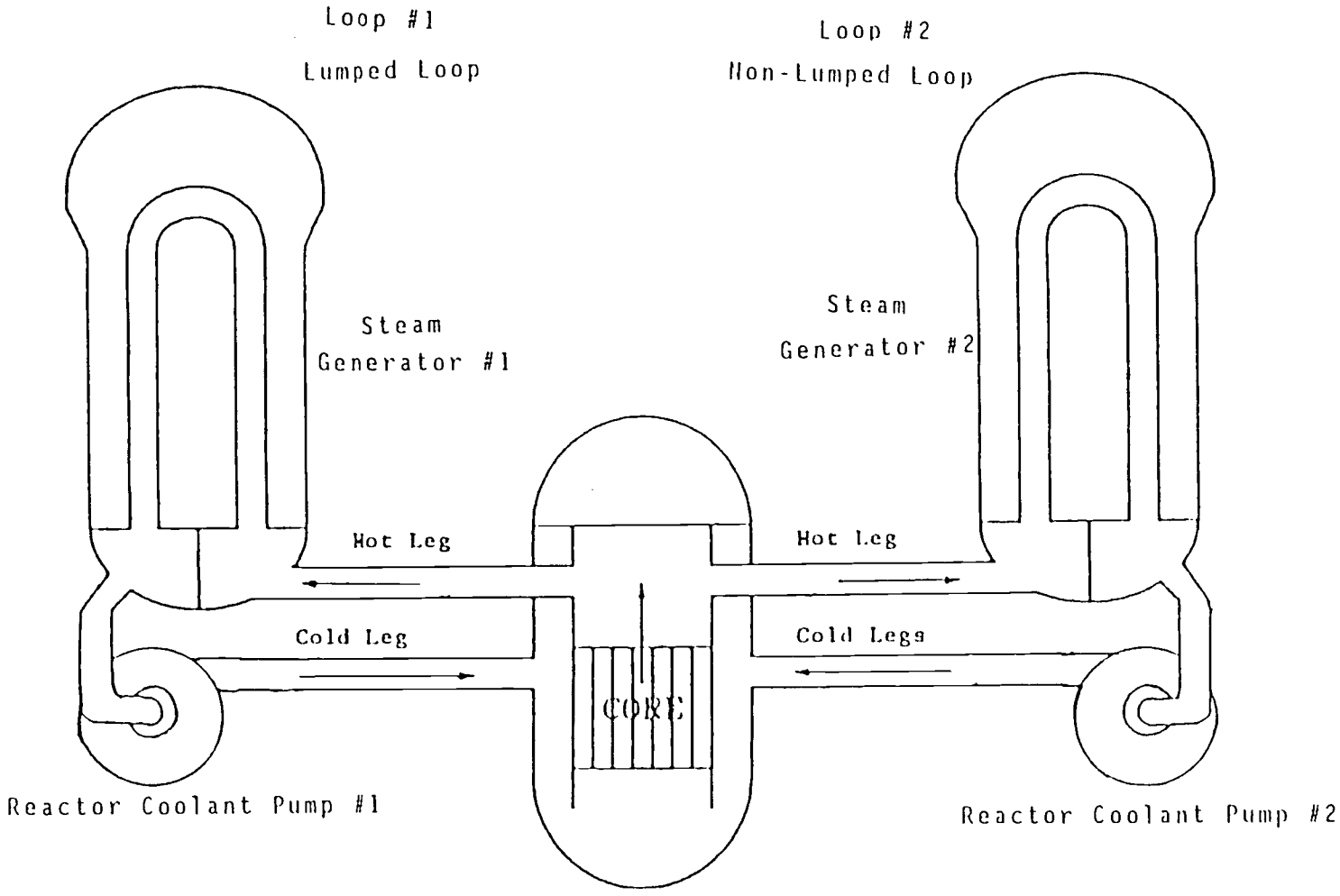

Figure 2.1
Schematic Diagram of OLAPS Model

The active core region is modeled as a single subchannel. This subchannel is taken as the average channel in the core. The subchannel geometry is shown in figure 2.2. This is based on the Trojan Facility's cycle seven fuel geometry [22].

The average channel properties such as average fuel temperature and the coolant temperature are used in the kinetics routines to compute the reactivity feedbacks and power distribution.

Detailed descriptions of the thermalhydraulic, conduction, kinetics, and constitutive models used to calculate the various temperatures, pressure losses and power levels are given in chapters 3, 4, 5 and 6.

2.2. Pressurizer

The OLAPS pressurizer model is based on a model developed and presented by DeGreef at the International Conference on Nuclear Reactor Simulation Technology[23] and the pressurizer of the Trojan Nuclear Facility. The key parameters of the pressurizer are listed in Table 2.1.

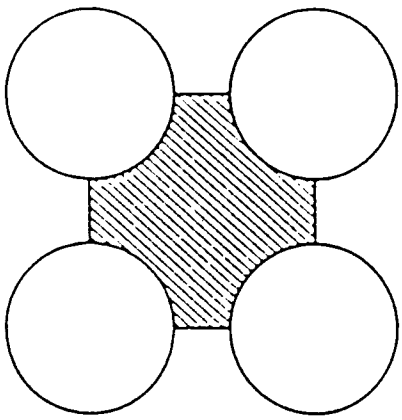

Figure 2.2
Subchannel Geometry

Table 2.1
Trojan Nuclear Facility Pressurizer Data

Volume	1800 cuft
Cross-sectional Area	36.8 sqft
Minimum Spray	1 gpm
Maximum Spray	800 gpm
Maximum Heater	1800 Kw

The basic equations for the pressurizer are derived by using a balance of energy, mass and volume and assuming that both phases are at saturation conditions.

The balance of energy is expressed by:

$$\frac{dE_p}{dt} = P_h - W_{spr}(h_{swp} - h_{spr}) + h_{swp}(W_{sg}) - h_{swp} W_{porv} \quad , \qquad (2\text{-}1)$$

and

$$E_p = h_{sp}M_{sp} + h_{swp}M_{swp} \quad , \qquad (2\text{-}2)$$

where

E_p is the total energy in the pressurizer,

P_h is the heater power,

W_{sg} is the mass flow of the surge line,

h_{spr} is the enthalpy of the sprays

W_{spr} is the spray mass flow rate,

W_r is the mass flow of the water level regulating flow,

h_{sp} is the enthalpy of saturated steam at pressurizer pressure,

M_{sp} is the total mass of saturated steam in the pressurizer,

h_{swp} is the enthalpy of saturated water at the pressurizer pressure,

M_{swp} is the total mass of water in the pressurizer.

The mass balance in the pressurizer is described by:

$$\frac{dM_p}{dt} = W_{sg} - W_{porv} + W_{spr} \quad , \qquad (2\text{-}3)$$

and

$$M_p = M_{sp} + M_{swp} \quad , \qquad (2\text{-}4)$$

where:

M_p is the total mass of water and steam in the pressurizer.

The volume balance simply states that the volume of the pressurizer remains constant, i.e.;

$$\frac{dV_p}{dt} = 0 \quad . \tag{2-5}$$

Where V_p is the pressurizer volume and is given by:

$$V_p = v_{sp} M_{sp} + v_{swp} M_{swp} \quad , \tag{2-6}$$

with v_{sp} being the specific volume of saturated steam, and v_{swp} being the specific volume of saturated water.

The water level in the pressurizer is calculated by :

$$H_p = \frac{M_{swp}}{\rho_l S_p} \quad . \tag{2-7}$$

Where S_p is the cross sectional area of the pressurizer and ρ_l is the density of saturated water.

The pressure in the pressurizer is adjusted as to maintain the pressure at saturation.

The water level and pressure in the pressurizer is maintained by the sprays, heaters and charging flow. The sprays and heaters are controlled in accordance with the controller program shown in figure 2.3 and 2.4.

The spray enthalpy is taken to be that of the cold leg coolant and the surge line enthalpy is taken to be that of saturated water. The surge line flow rate is calculated based on pressurizer pressure, hot leg pressure and the surge line piping characteristics.

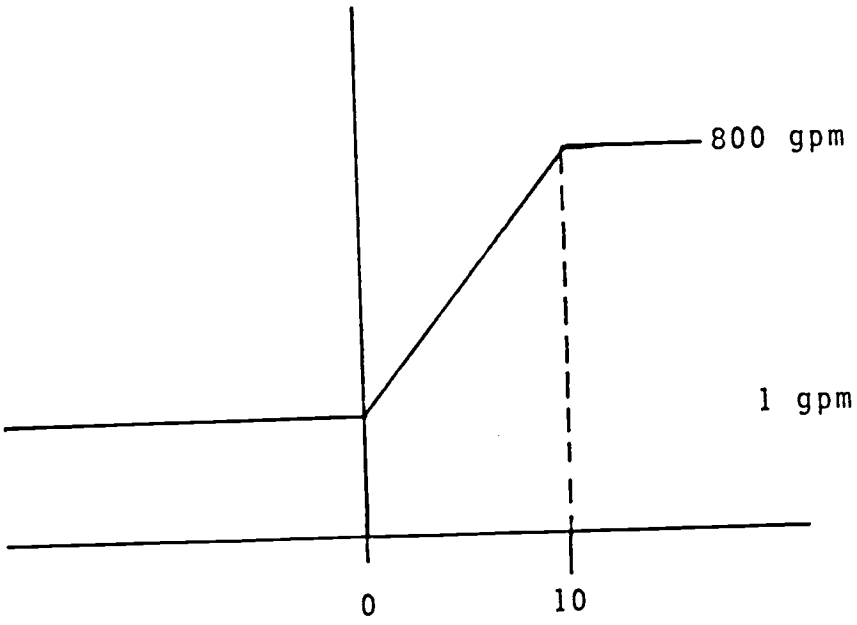

Figure 2.3
Pressurizer Spray Program

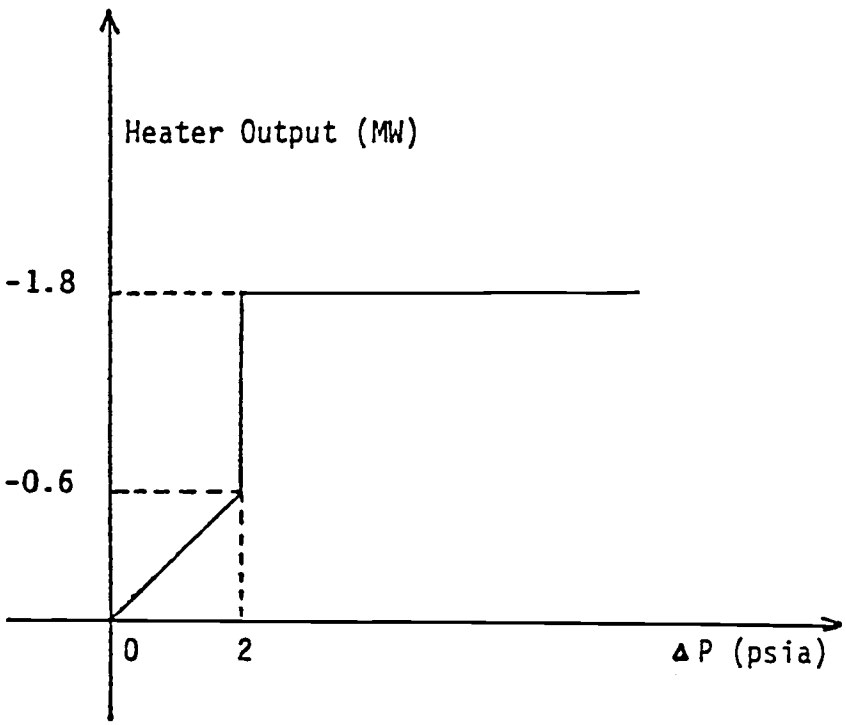

Figure 2.4
Pressurizer Heater Program

2.3. Steam Generator

The OLAPS steam generator is modeled as a simple heat sink. The magnitude of the sink is governed by the expression:

$$q''_{ps} = h_{ps}(T_p - T_s) \qquad (2\text{-}8)$$

where: q" is the average heat flux from the primary to the secondary of the steam generator,

h_{ps} is an overall heat transfer coefficient

T_p is the steam generator average primary coolant temperature,

T_s is the steam generator average secondary coolant temperature.

The value of h_{ps} is assumed to be constant and is calculated by:

$$hps = 1/4 \; \frac{\text{Thermal output @ full power}}{\text{Surface area per steam generator}} \; \frac{1}{(Tp - Ts)}$$

Here T_p and T_s are the primary and secondary temperatures at steady state full power and are derived using the data in the Trojan FSAR (Tp=316 C and Ts=260 C).

2.4. Pumps

The OLAPS reactor coolant pumps are modeled after the Trojan Nuclear Facility's pumps. The flow verses head curve for the pumps is fit to a polynomial which is evaluated to determine the flow rate for a particular pressure rise across the pump.

The pressure rise across the RCP's is matched to the pressure drop around the coolant loop.

The flow verses head curve for the Trojan pumps are shown in figure 2.5. The polynomial fitting coefficients are given in Table 2.2.

Table 2.2
Polynomial Coefficients for RCP pump curve
for W in Kg/s and ΔP in N/m2

$$\Delta P=(A +BW^2+CW^3+DW^4)$$

A = 1.628784×10^6
B = -150180.3
C = 34060.89
D = 264.83866

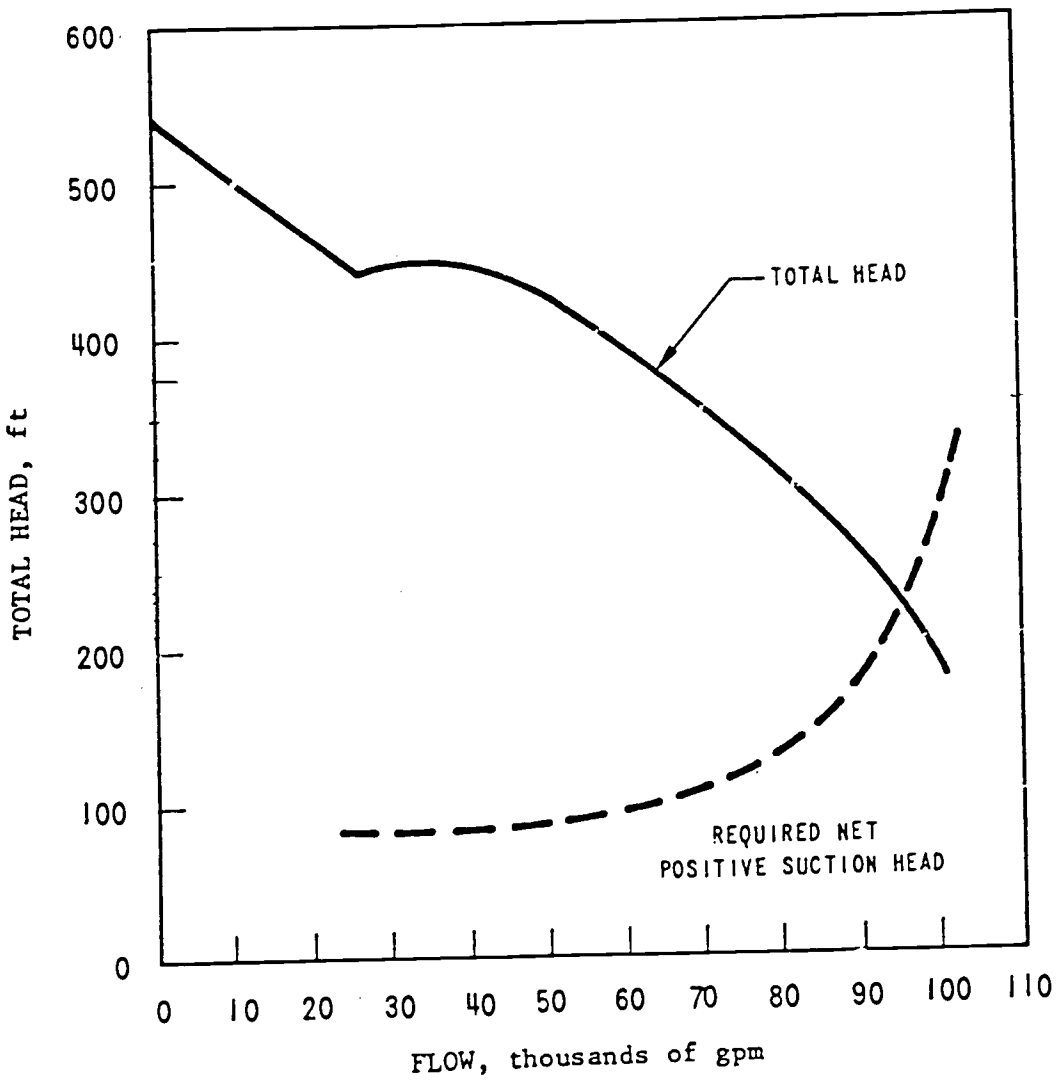

Figure 2.5
RCP Pump Curve

2.5. Valves

The mass flow rates through the power operated relief valves (PORV's) and the safety relief valves on the pressurizer, are calculated using a model developed by Shapiro (39). This model assumes:

- Single phase vapor flow
- Steam behaves as an ideal gas
- discharge coefficients do not depend on flow rates
- flow is quasi steady.

The mass flow through the valve is calculated by multiplying the ideal flow through an orifice by a discharge coefficient C_v which accounts for the friction and flow area contraction in the valve. This ideal flow depends on the ratio of the upstream and downstream pressures given as follows:

$$\chi_v = P_d/P_u \qquad (2\text{-}10)$$

The value of χ_v is limited to be between 0.0 and 1.0, with χ_v=1.0 at equilibrium. The flow is non-choked for values of χ_v in the range: $1.0 > \chi_v > \chi_{v,crit}$. Where $\chi_{v,crit}$ is given by:

$$\chi_{v,crit} = [2/(\kappa+1)]^{\left(\frac{\kappa}{\kappa+1}\right)} \qquad (2\text{-}11)$$

where:

$$\kappa = \rho_0\{p_0[\frac{\partial\rho}{\partial h} + \frac{\partial\rho}{\partial p}]_0\}^{-1}$$

The subscript 0 indicates that these parameters are evaluated at time zero.

The flow rate for non-choked flow is calculated using:

$$W_v = C_v A_v(\frac{2\kappa}{k-1}<p>_0\rho_{g0})^{.5}\ (\frac{p_u}{p_{d0}})^{\frac{\kappa+1}{2\kappa}}\ [\chi^{2/\kappa}(1-\chi)^{\frac{\kappa-1}{\kappa}}]^{.5}$$

When the flow becomes choked ($\chi_v < \chi_{v,crit}$) the flow rates are calculated using:

$$W_v = C_v A_v(\frac{2\kappa}{\kappa-1}<p>_0\rho_{g0})^{.5}\ (\frac{p_u}{p_{d0}})^{\frac{\kappa+1}{2\kappa}}\ (\frac{2}{k+1})^{\frac{\kappa+1}{2(\kappa-1)}}$$

where Av is flow area of the valve,

ρ_{g0} is the initial vapor density,

and $\langle p \rangle_0$ is the initial system pressure.

The values of A_v's and C_v's for the Trojan Facility are given in Table 2.3.

This model is also used to calculate the mass discharge rate through the break during the LOCA transient.

Table 2.3

Discharge coefficients C_v and flow areas A_v for OLAPS Valves. SRVs and break.

Valve	Cv	Av
PORV	.8	.44 sqft.
SRV	.8	.66 sqft.
Break	.8	5.22 sqft.

2.6. Pipes

Pipes are treated as one dimensional adiabatic flow connectors in OLAPS. In the control volume method that is used, each pipe segment is put into a separate

control volume and the conservation of mass, momentum and energy is applied (see Chapter 3.).

Some of the pipe segments may have several components to them such as bends, expansions and contractions. Some include components such as the core and steam generator inlet and exit plena and the core downcomer region. These components are converted to an equivalent length and lumped together with the adjoining pipe segments. The equivalent length of the various hydraulic components are obtained by an iterative process where the equivalent lengths were repeatedly adjusted so that the calculated pressure losses matched those given in the Trojan FSAR. The equivalent lengths obtained are given in Table 2.4.

The pipe segments are assumed to have only one entrance and one exit, and are insulated against heat loss. The exceptions to this are those pipe segments that are connected to the pressurizer surge line and the charging and letdown lines. The flows into and out of these lines appear as source terms in the mass, energy and momentum equations for these pipe segments (see chapter 3.). Other exceptions to the one-inlet-one-outlet rule are the lower-plenum and downcomer and the upper plenum control volumes. The lower-plenum and

downcomer control volume has two inlets and one outlet, while the upper-plenum control volume has one inlet and two outlets.

The pressure loss for two phase flow through pipes is calculated using the correlations for two phase friction factors given in section 6.3.

Table 2.4

Piping and component data for OLAPS

Component	L_e(m)	D_e(m)	Volume (m^3)
Hot Leg	10.45	0.737	7.70
Cold Leg	7.84	0.786	2.94
Core	24.1	0.0111	17.35
Upper Plenum	893.3	3.27	17.35
Lower Plenum and Down comer	897.5	3.36	49.80
Steam Generator	5.48	0.0197	2.085
Suction pipe and Pump	65.10	0.786	10.22

3. Loop Thermalhydraulics

The OLAPS thermalhydraulics model is a one-dimensional, 5 equation, two phase, non equilibrium flow model. In this model, the mass and energy conservation equations are written for each phase and a conservation of momentum equation is written for the mixture. A drift flux model (see section 6.4) is used with this model to provide the phase velocities.

Each of the conservation equations is applied to a two loop representation (see figure 3.1) of a four loop plant and is solved to find the thermodynamic and flow conditions at various points around the loops. OLAPS has one loop which represents a single physical loop and another loop which represents the remaining three physical loops.

Various assumptions were made, in arriving at the equations described below. The most important of which is the assumption of one-dimensional flow. This assumption greatly reduces the complexity of the

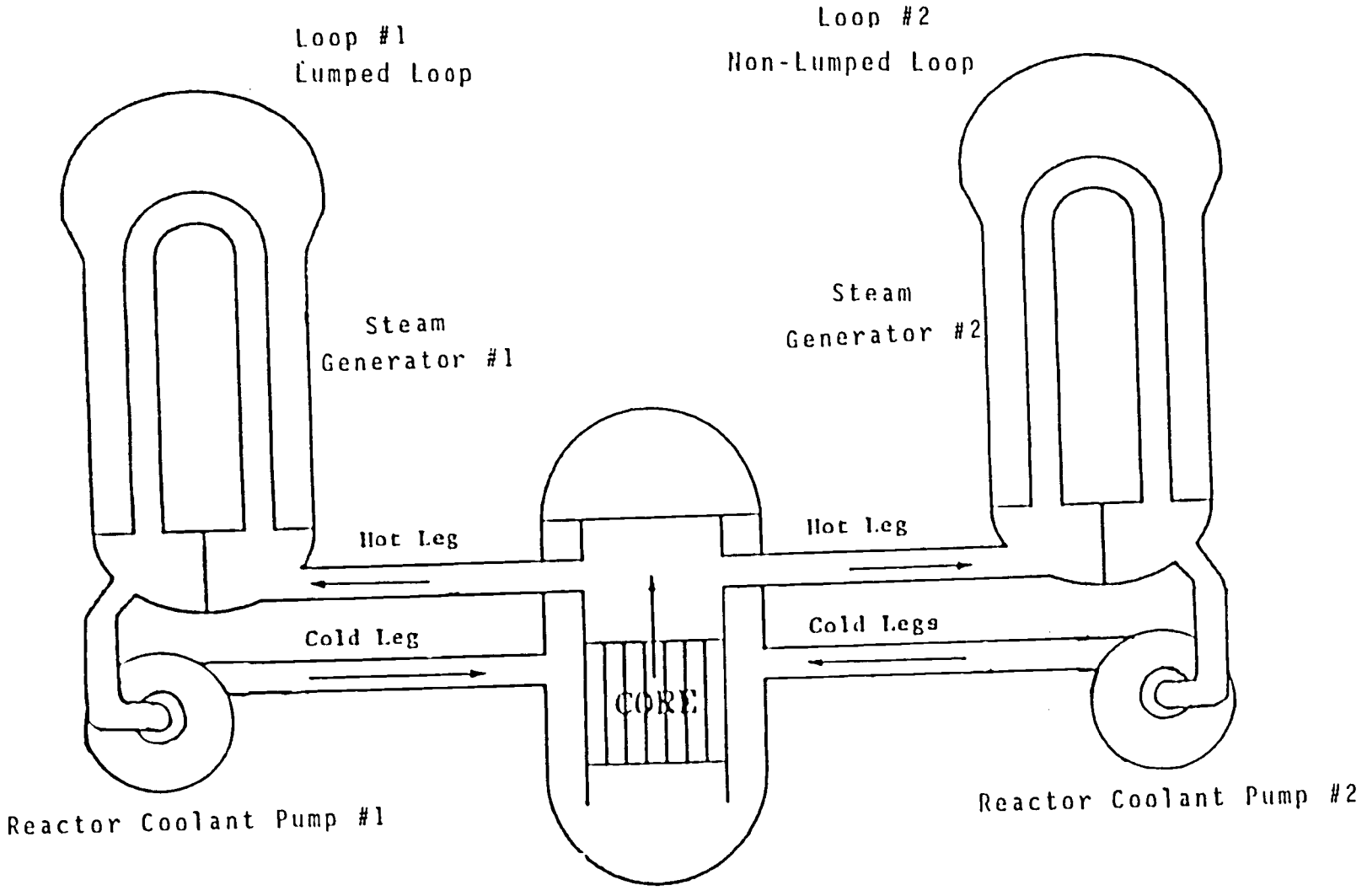

Figure 3.1
2-Loop Model

place limitations on the model. For example there is no cross flow in the calculation and the description of the coolant is limited to the bulk or average conditions. However, since OLAPS is mostly concerned with core average results, this assumption should not be too limiting.

The one-dimensional assumption also implies that the properties across the flow channel are uniform or at least can be described by an average value. This is not of concern because interest lies only in the bulk properties.

Other assumptions include standard assumptions made in most LWR integral system analyses. These include:

- no axial conduction in the coolant, (convection is the dominant heat transfer process)

- Heat transfer and phase change processes dominate over mechanical processes (viscous dissipation, turbulent dissipation, pressure work,etc)

3.1. Mass Equations

The three-dimensional two-fluid equation developed by Ishii[24a] gives a separate mass conservation equation for each phase. The mass conservation equation for the vapor phase is:

$$\frac{\partial \alpha \rho_g}{\partial t} + \nabla \cdot (\alpha \rho_g u_g) = \Gamma_{lg} \tag{3-1}$$

and for the liquid phase:

$$\frac{\partial (1-\alpha) \rho_g}{\partial t} + \nabla \cdot [(1-\alpha) \rho_l u_l] = -\Gamma_{lg} \tag{3-2}$$

where α is the volumetric void fraction,

Γ_{lg} is the volumetric vapor generation rate,

ρ_l and ρ_g are the liquid and vapor phase densities,

u_g and u_l are the liquid and vapor phase velocities.

The averaging operator:

$$\langle \phi \rangle = \frac{\int_{vol} \phi \, dV}{\int_{vol} dV} \tag{3-3}$$

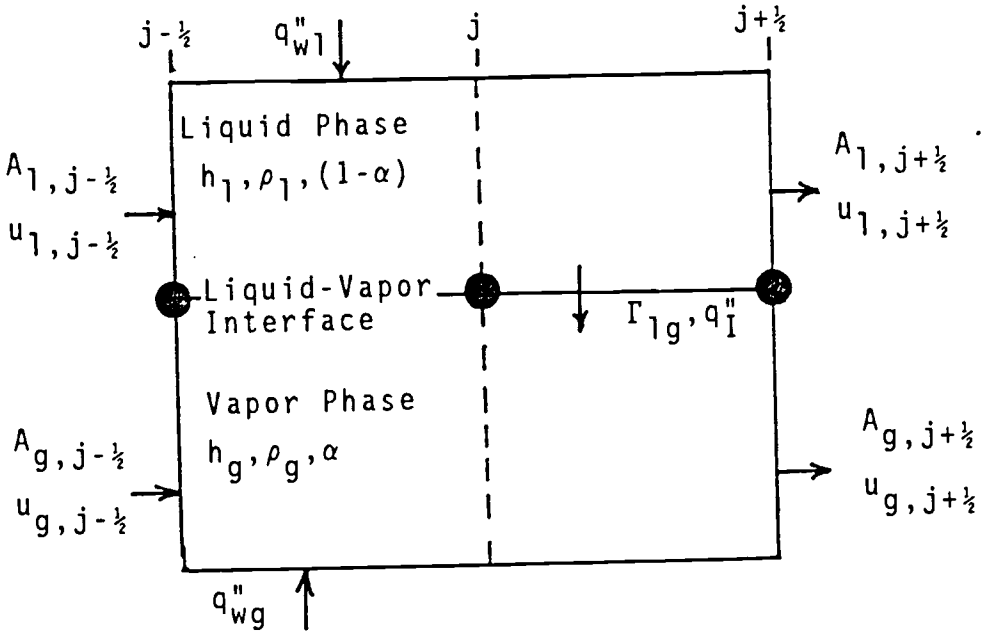

Figure 3.2
Control Volume for Conservation of Mass and Energy

can be applied to these equation to average them over the control volume shown in figure 3.2.

Looking first at the vapor phase equation, the first term becomes:

$$\frac{1}{A\Delta z} \int_A \int_{\Delta z} \frac{\partial \alpha \rho_g}{\partial t} \, dA \, dz \qquad (3\text{-}4)$$

Changing the order of differentiation and integration and using the assumption that the density and void fraction are uniform across the flow area A, This term becomes:

$$\frac{1}{A\Delta z} \frac{\partial}{\partial t} \int_{\Delta z} A \alpha \rho_g \, dz \qquad (3\text{-}5)$$

However $\alpha = A_g/A$, therefore this can be reduced to:

$$\frac{1}{A\Delta z} \frac{\partial \langle \alpha \rho_g \rangle}{\partial t} \qquad (3\text{-}6)$$

where $\langle \alpha \rho_g \rangle$ is the total mass of vapor in the control volume and is calculated by:

$$\langle \alpha \rho_g \rangle = \frac{\int_{\Delta z} A_g \rho_g dz}{A\Delta z} \qquad (3\text{-}7)$$

Averaging the second term over the control volume yields:

$$\frac{1}{A\Delta z} \int_A \int_{\Delta z} \nabla\cdot(\alpha\rho_g u_g)\, dA\, dz \qquad (3\text{-}8)$$

Using Gauss's Divergence Theorem and the assumption of 1-D flow in the z-direction, this term becomes:

$$\frac{1}{A\Delta z} \left\{ \int_{A_{out}} \alpha\rho_g u_g dA \; - \int_{A_{in}} \alpha\rho_g u_g dA \right\} \qquad (3\text{-}9)$$

Again the assumption that the properties of the vapor are uniform over the flow area reduces the term to:

$$\frac{1}{A\Delta z} \Delta(A\alpha\rho_g u_g) \qquad (3\text{-}10)$$

where

$$\Delta(A\alpha\rho_g u_g) = (A\alpha\rho_g u_g)|_{A_{out}} - (A\alpha\rho_g u_g)|_{A_{in}} \qquad (3\text{-}11)$$

With the control volume averaged vapor generation rate the vapor mass equation becomes:

$$\frac{\partial\langle\alpha\rho_g\rangle}{\partial t} + \frac{1}{A\Delta z} \left\{ \Delta(A\alpha\rho_g u_g) \right\} = \langle\Gamma_{lg}\rangle \qquad (3\text{-}12)$$

By analogy the liquid phase control volume average mass conservation equation becomes:

$$\frac{\partial<1-\alpha\rho_l>}{\partial t} + \frac{1}{A\Delta z}\left\{ \Delta(A(1-\alpha)\rho_l u_l) \right\} = -<\Gamma_{lg}> \qquad (3\text{-}13)$$

If equations (3-12) and (3-13) are solved for $<\alpha\rho_g>$ and $<(1-\alpha)\rho_l>$, the mass of the vapor and liquid in the control volume can be calculated by:

$$M_{g,j}=<(\alpha\rho_g)>_j \; Vol_j \qquad (3\text{-}14)$$

and

$$M_{l,j}=<((1-\alpha)\rho_l)>_j Vol_j \qquad (3\text{-}15)$$

Then the void fraction can be calculated:

$$<\alpha_j> = \frac{\frac{M_{g,j}}{\rho_{g,j}}}{\frac{M_{g,j}}{\rho_{g,j}} + \frac{M_{l,j}}{\rho_{l,j}}} \qquad (3\text{-}16)$$

From this the phasic densities can be calculated by:

$$\rho_g = \frac{<(\alpha\rho_g)>_j}{<\alpha_j>} \qquad (3\text{-}17)$$

and

$$\rho_l = \frac{<((1-\alpha)\rho_l)>_j}{<(1-\alpha)_j>} \qquad (3\text{-}18)$$

3.2. Energy Equations

Ishii also gives a three-dimensional two-fluid energy conservation equation for each phase. For the vapor phase this equation is:

$$\alpha\rho_g \frac{Dh_g}{Dt} = - \nabla\cdot q_g'' + \alpha \frac{Dp_g}{Dt} + \Phi_g^t + \Phi_g^\mu + \Gamma_{lg}\Delta h_{Ig} + \frac{q''_I}{L_s} + $$
$$+(p_g - p_I) \frac{D\alpha}{Dt} + M_g^d (u_{gI} - u_g) \qquad (3\text{-}19)$$

and for the liquid phase is:

$$(1-\alpha)\rho_g \frac{Dh_l}{Dt} = - \nabla\cdot q_l'' + (1-\alpha) \frac{Dp_l}{Dt} + \Phi_l^t + \Phi_l^\mu - \Gamma_{lg}\Delta h_{Il} - \frac{q''_I}{L_s} +$$
$$+(p_g - p_I) \frac{D(1-\alpha)}{Dt} + M_g^d (u_I - u_l) \qquad (3\text{-}20)$$

where h_g and h_l are the enthalpies of the vapor and liquid phases,

Δh_{Ig} and Δh_{Is} are the differences between the phase enthalpy and the saturation enthalpy for that phase,

p_g, p_l and p_I are the vapor, liquid and interface pressures,

u_I is the interface velocity,

q''_g is the total heat flux in the vapor,

q''_l is the total heat flux in the liquid,

q''_I is the vapor liquid interface heat flux,

Φ^t and Φ^μ are turbulent and viscous dissipation terms,

M^d_g and M^d_l are the drag forces on the vapor and liquid,

$1/L_s$ is the interfacial area concentration (vapor-liquid surface area per unit volume).

If heat transfer and phase change are the dominant processes, then mechanical effects, such as viscous dissipation, pressure work, etc. can be ignored and the energy equations reduce to :

$$\alpha\rho_g \frac{Dh_g}{Dt} = -\nabla\cdot q''_g + \Gamma_{lg}\Delta h_{Ig} + \frac{q''_I}{L_s} \qquad (3\text{-}21)$$

By expanding the substantial derivative this can be rewritten as:

$$\frac{\partial \alpha\rho_g h_g}{\partial t} + \nabla\cdot(\alpha\rho_g h_g u_g) = -\nabla\cdot q''_g + \Gamma_{lg} h_{g,I} + \frac{q''_I}{L_s} \qquad (3\text{-}22)$$

Averaging the vapor equation over the control volume using a process similar to the one used to arrive at the mass conservation equations (see above) and the assumptions of no axial conduction and 1-D flow the result is:

$$\frac{\partial \langle \alpha \rho_g h_g \rangle}{\partial t} + \frac{1}{A\Delta z} \Delta(A \alpha \rho_g h_g u_g) = \frac{A_{surf}}{A\Delta z} q''_{wg} + \langle \Gamma_{lg} \rangle h_{fg} + \langle q''_I / L_s \rangle \qquad (3\text{-}23)$$

where A_{surf} is the wall surface area in the CV.

q''_{wg} is the wall heat flux to the vapor.

By analogy the liquid energy equation is:

$$\frac{\partial \langle (1-\alpha) \rho_l h_l \rangle}{\partial t} + \frac{1}{A\Delta z} \Delta(A(1-\alpha) \rho_l h_l u_l) = \frac{A_{surf}}{A\Delta z} q''_{wl} - \langle \Gamma_{lg} \rangle h_{fg} - \langle q''_I / L_s \rangle \qquad (3\text{-}24)$$

3.3. Mixture Momentum Equation

In addition to the equations for mass and energy for each phase Ishii also provides a mixture momentum equation:

$$\frac{\partial<\rho_m u_m>}{\partial t} + \nabla\cdot(\rho_m u_m u_m) = -\nabla p + \nabla\cdot\tau + \gamma\rho_m + m_m \qquad (3\text{-}25)$$

where V_m is the mixture velocity,

τ is the total stresses on the mixture including viscous,diffusion and turbulent stresses,

m_m is the mixture momentum source

g is the acceleration of gravity.

Averaging this equation over the control volume shown in figure 3.3, using the same assumptions of 1-d flow and also assuming that m_m =0, yields:

$$\frac{\partial<\rho_m u_m>}{\partial t} + \frac{\Delta(\rho_m u_m u_m)}{A\Delta z} = -\frac{\Delta p}{\Delta z} + \frac{A_{surf}}{A\Delta z}\tau_w + M_m g \qquad (3\text{-}26)$$

where τ_w is the wall stress

M_m is the total mixture mass in the CV.

Evaluating the wall stress term in general is quite complicated. However, using an empirical correlation based on experimental data, the stress term

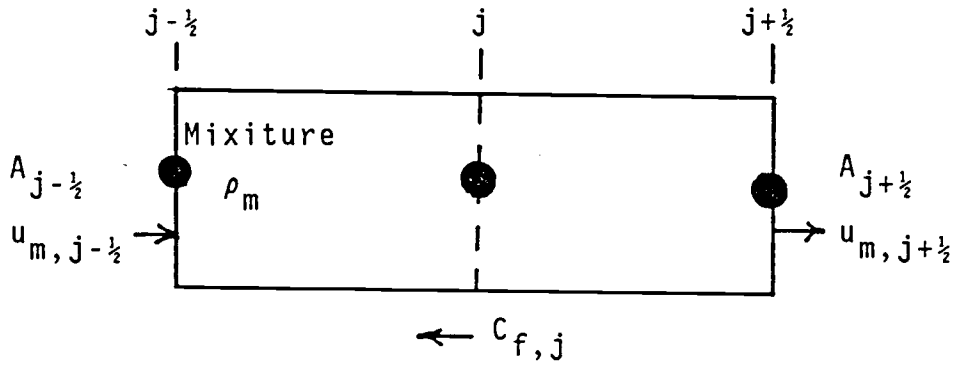

Figure 3.3
Mixture Control Volume

can be written in terms of a friction factor:

$$\frac{A_{surf}}{A\Delta z}\,\tau_w = 2C_f\rho_m\,\frac{u_m^2}{D_e} \qquad (3\text{-}27)$$

where D_e is the hydraulic diameter of the flow channel.

Empirical correlations used to find the friction factor for single and two phase flow are given in section 6.3.

The mixture density used in the above equations is a weighted average of the liquid and vapor densities. The averaging scheme given by Wallis (24) for the drift flux model is :

$$\rho_m = \frac{j_l\rho_l + j_g\rho_g}{j} + (\rho_l - \rho_g)\,\frac{j_{gl}}{j} \qquad (3\text{-}28)$$

where:

j_l is the superficial velocity of the liquid phase,

j_g is the superficial velocity of the vapor phase,

j is the mean volumetric flux,

and j_{lg} is the drift flux.

Details and definitions for the drift flux model are given in section 6.4.

Equation (3-28) can be simplified to :

$$\rho_m = \alpha\rho_g + (1-\alpha)\rho_l \qquad (3\text{-}29)$$

Other correlations for q''_{wg}, q''_{wl}, q''_I, L_s, Γ_{lg} and material properties are also given in chapter 6.

4. Conduction Model

The fuel temperature distribution is calculated using a conduction model based on the model used in the MAYOU4 code. This model applies the one-dimensional heat conduction equation with internal heat generation to the fuel pin geometry shown in figure 4.1. In cylindrical coordinates, the heat conduction equation is given by:

$$\rho C_p \frac{\partial T}{\partial t} = \frac{1}{r} \frac{\partial}{\partial r}(kr \frac{\partial T}{\partial r}) + q''' \qquad (4\text{-}1)$$

where

ρ is the density of the material,

C_p is the specific heat of the material,

T is the temperature,

r is the radial coordinate,

q"' is the volumetric heat generation rate,

k is the thermal conductivity of the material.

The assumptions made in writing the equation are that there is no axial or angular temperature dependence

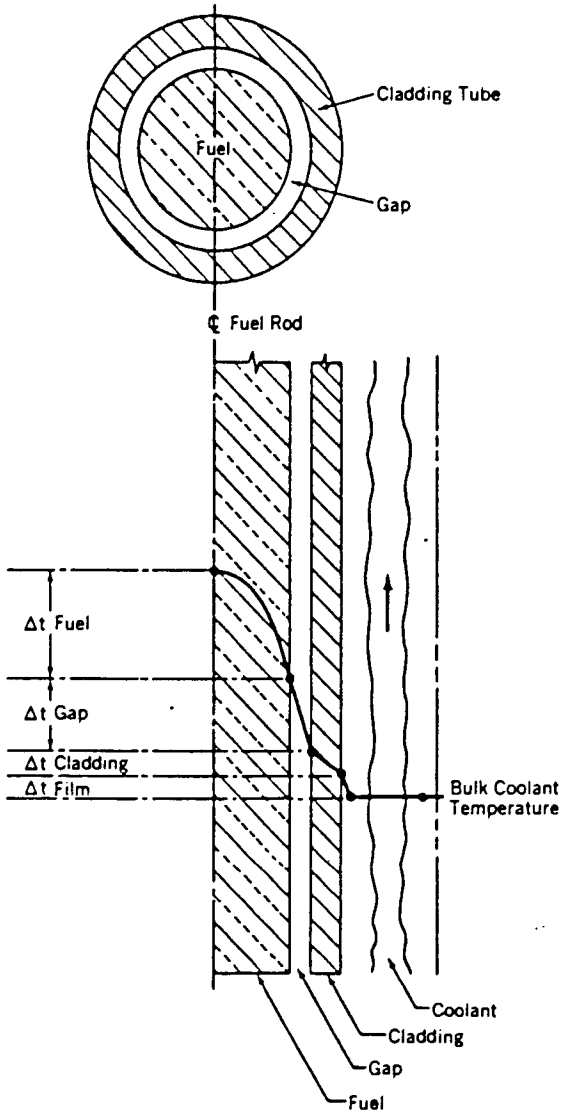

Figure 4.1
Fuel Pin Geometry

(conduction) and the conductivity is a function of temperature and radial position.

This equation is applied to the fuel and cladding regions with the boundary and interface conditions that are given below.

The fuel-clad interface across the gas gap requires two interface conditions. One of these is obtained by setting the heat conducted from the fuel equal to the heat conducted into the clad:

$$k_f r_{fo} \left.\frac{\partial T}{\partial r}\right|_{r=r_{fo}} = k_c r_{ci} \left.\frac{\partial T}{\partial r}\right|_{r=r_{ci}} \qquad (4\text{-}2)$$

where k_f is the fuel conductivity,
k_c is the clad conductivity,
r_{fo} is the fuel pellet radius, and
r_{ci} is the inner cladding radius.

This equation provides a coupling between the temperature gradient at the fuel surface and the temperature gradient at the inner surface of the cladding.

The second interface condition is obtained by setting the heat conducted from the fuel equal to the heat conducted across the gas gap:

$$-k_f \left.\frac{\partial T}{\partial r}\right|_{r=r_{fo}} = H_g(T_{fs} - T_{ci}) \qquad (4\text{-}3)$$

where H_g is a heat conduction coefficient,

T_{fo} is the fuel surface temperature, and

T_{ci} is the inner cladding temperature.

This expression provides a coupling between the fuel surface and cladding inner surface temperatures.

At the cladding surface, the heat flux from the cladding is set equal to the sum of the convective and radiative heat flux to each phase of the coolant:

$$-k_c \left.\frac{\partial T}{\partial r}\right|_{r=r_{co}} = q''_{wl} + q''_{wg} \qquad (4\text{-}4)$$

where r_{co} is the cladding outer radius,

h is the bulk convective heat transfer coefficient,

T_{co} is the cladding surface temperature, and

T_b is the bulk coolant temperature,

q''_{wl} is the total heat flux to the liquid phase,

q''_{wg} is the total heat flux to the vapor phase.

The final boundary condition is provided by the symmetry condition at the fuel centerline:

$$\left.\frac{\partial T}{\partial r}\right|_{r=0} = 0 \qquad (4\text{-}5)$$

The transient heat conduction equations are solved using a Crank-Nicholson numerical method (see section 7.2)

In the fuel region, the volumetric heat generation rate is proportional to the neutron power level. The neutron power level is calculated using a region-wise point reactor kinetics model (see chapter 5). The volumetric heat generation in the cladding is assumed to be zero.

The fuel and cladding conductivity and specific heats, the bulk heat transfer coefficient and the gas gap heat conduction coefficient are all calculated using correlations given in chapter 6.

5. Neutron Kinetics Model

In the selection of a neutron kinetics model there are two important factors that must be taken into consideration, speed and accuracy. The speed of the routine can be measured by the number of mathematical operations it takes to arrive at a solution. The accuracy can be measured by how close the results compare to the actual values. In OLAPS a compromise between speed and accuracy has been made in selecting a kinetics model.

In the development of OLAPS the main interest lies in finding a kinetics model that will adequately predict the changes in the axial power profile (which is proportional to the axial neutron flux shape) with a minimum of computational effort. The axial power profile is important because of its implications to the thermal-hydraulic performance of the reactor; particularly the effects on the minimum departure from nucleate boiling ratio (MDNBR), the maximum linear heat generation rate (LHGR) and the axial power offset [21a][25].

Because only the axial power profile is of interest here, the use of a one-dimensional axially dependent

kinetics model is adequate. The simplification of using a one energy group model is also reasonable provided that the neutron cross sections are properly averaged over the core spectrum.

The kinetics model selected was the region-wise point reactor kinetics (RWPRK) model. This model meets the requirements of having the ability of providing a varying axial power profile and requires little extra effort over the simple point reactor kinetics model. This model is derived and presented below with assumptions and limitations.

5.1. RWPRK

The RWPRK model is essentially a nodal approximation[26][27][28] with the coupling coefficients set to zero. The nodal model and hence the RWPRK model can be derived from the one-dimensional one-energy-group time dependent diffusion equation:

$$\frac{1}{v}\frac{\partial\phi(z,t)}{\partial t} = \frac{\partial}{\partial z} D \frac{\partial\phi(z,t)}{\partial z} + \Sigma_a\phi(z,t) + (1-\beta)\Sigma_f\phi(z,t) + \sum_{i=1}^{6} \lambda_i C_i(z,t) + Q(z,t) \qquad (5\text{-}1a)$$

$$\frac{\partial C_i(z,t)}{\partial t} = -\lambda_i C_i(z,t) + \beta_i \nu \Sigma_f \phi(z,t) \qquad i=1,6 \qquad (5\text{-}1b)$$

Where $\phi(z,t)$ is the neutron flux level,

D is the diffusion coefficient,

β is the delayed neutron fraction,

β_i is the fraction of delayed neutron in the ith group,

ν is the average number of neutron emitted per fission,

$C_i(z,t)$ is the number density for the ith group delayed neutron precursors,

λ_i is the decay constant for the ith group delayed neutron precursor,

Σ_f is the macroscopic fission cross section,

Σ_a is the macroscopic absorption cross section,

v is the average neutron velocity.

For the nodal model the core is divided into regions or nodes. In the case of OLAPS the core is divided into a number of axial regions. The flux in each region R_m, is expressed by:

$$\phi(z) = v_m n_m(t) \psi_m(z) \qquad (5\text{-}2)$$

where $\psi_m(z)$ is a shape function for the region,

$n_m(t)$ is the time dependent neutron density in

the region, and

v_m is the average neutron velocity in the region.

If this expression is substituted into equation (5-1), multiplied by a weighing factor $w_m(z)$ and integrated over the region R_m, The following is obtained:

$$\frac{dn_m}{dt} = L_m - A_m v_m n_m(t) + (1-\beta) F_m v_m n_m(t) + \sum_{i=1}^{6} \lambda_i C_{im}(t) + Q_m(t) \qquad (5\text{-}3a)$$

$$\frac{dC_{im}(t)}{dt} = \beta_i F_m v_m n_m(t) - \lambda_i C_{im}(t) \qquad (5\text{-}3b)$$

where

$$A_m = \frac{1}{\psi_m} \int_{R_m} w_m(z) \Sigma_a \psi_m(z)\, dz \qquad (5\text{-}4)$$

$$F_m = \frac{1}{\psi_m} \int_{R_m} w_m(z) \nu \Sigma_f \psi_m(z)\, dz \qquad (5\text{-}5)$$

$$C_{im}(t) = \frac{1}{\psi_m} \int_{R_m} w_m(z) C_{im}(z,t)\, dz \qquad (5\text{-}6)$$

$$L_m = \frac{1}{\psi_m} \int_{R_m} w_m(z) \left[\frac{d}{dz} D_m \frac{d\psi(z)}{dz}\right] dz \qquad (5\text{-}7)$$

$$Q_m(t) = \frac{1}{\psi_m} \int_{R_m} w_m(z) Q_m(z,t)\, dz \qquad (5\text{-}8)$$

$$\psi_m = \int_{R_m} w_m(z) \psi_m(z) dz \qquad (5\text{-}9)$$

The quantity L_m represents the net streaming of neutrons from the region R_m. A nodal coupling coefficient k_{lm}, can be defined such that L_m can be rewritten as:

$$L_m = v_m n_m(t) \int_R w_m(z) \left[\frac{d}{dz} D_m \frac{d\psi(z)}{dz}\right] dz + \sum_{l \neq m}^{N} k_{lm} n_l(t) \quad (5\text{-}10)$$

The first term of the RHS of equation (5-10) represents the neutrons that stream out of the region and the second term represents the neutrons that stream into the region from the other N-1 regions.

Using equation (5-10) in equation (5-3) yields:

$$\frac{dn_m(t)}{dt} = \sum_{l \neq m}^{N} k_{lm} n_m + \frac{\rho_m - \beta_i}{\Lambda_m} n_m(t) + \sum_{i=1}^{6} \lambda_i C_{im}(t) + Q_m(t) \quad (5\text{-}11a)$$

$$\frac{dC_{im}(t)}{dt} = \frac{\beta_i}{\Lambda_m} n_m(t) - \lambda_i C_{im}(t) \qquad i=1,6 \quad (5\text{-}11b)$$

where

$$\rho_m = \frac{F_m - A'_m}{F_m} \quad (5\text{-}12)$$

$$\Lambda_m = \frac{1}{v_m F_m} \quad (5\text{-}13)$$

$$A'_m = \int_R w_m(z)\left[\frac{d}{dz} D_m \frac{d}{dz} + \Sigma_a\right] \psi_m(z)dz \qquad (5\text{-}14)$$

Equations (5-10)-(5-14) with equations (5-5)-(5-9) constitute the nodal approximation kinetics model.

It is worth noting that equation (5-10) will reduce to the point reactor kinetics model if the entire reactor is represented by a single region (i.e. N=1), or if $k_{lm}=0$.

The latter is exactly what the RWPRK model supposes. To justify the supposition a closer look at the k_{lm}'s is required.

An estimate of the values of the k_{lm}'s can be obtained by using a Green's function method[21][28]. This is done by treating the $\Sigma k_{lm}\ n_l$ term of equation (5-10) as N-1 sources to the region R_m. The strength of these sources is proportional to the neutron populations (or fluxes) in those N-1 regions. In other words this is the contribution to neutron population in the region R_m from all other regions.

The Green's function method gives the flux at some point z as:

$$\phi(z) = \int_{-\infty}^{\infty} G_{p1}(z',z)S(z')dz' \qquad (5\text{-}15)$$

where $G_{p1}(z',z)=L/2D \quad \exp(-|z'-z|/L)$ is the one dimensional diffusion kernel,
and $S(z') = \nu\Sigma_f\phi(z')$ is the fission source.

If the limits of integration are set to cover the region R_1, then equation (5-13) will yield the flux at z due to a fission source in R_1:

$$\phi_1(z)= \int_{R_1} L/2D \exp(-|z'-z|/L) \; \nu\Sigma_f\phi(z')dz' \qquad (5\text{-}16)$$

averaging this expression for the flux over the region R_m gives:

$$\phi_{1m}=\frac{\int_{R_m} L/2D \int_{R_1} \exp(-|z'-z|/L) \; \nu\Sigma_f \phi(z')dz'}{\Delta z_m} \qquad (5\text{-}17)$$

Using the geometry shown in figure 5.1 and carrying out the indicated integration using the region average flux ϕ_1 for $\phi(z')$ in region R_1 will yield:

$$\phi_{1m} = \frac{k_\infty}{2} \phi_1 \left\{ \frac{(e^{[-z_0(|m-1|+1)/L]})(e^{z_0/L}-1)^2}{z_0/L} \right\} \qquad (5\text{-}18)$$

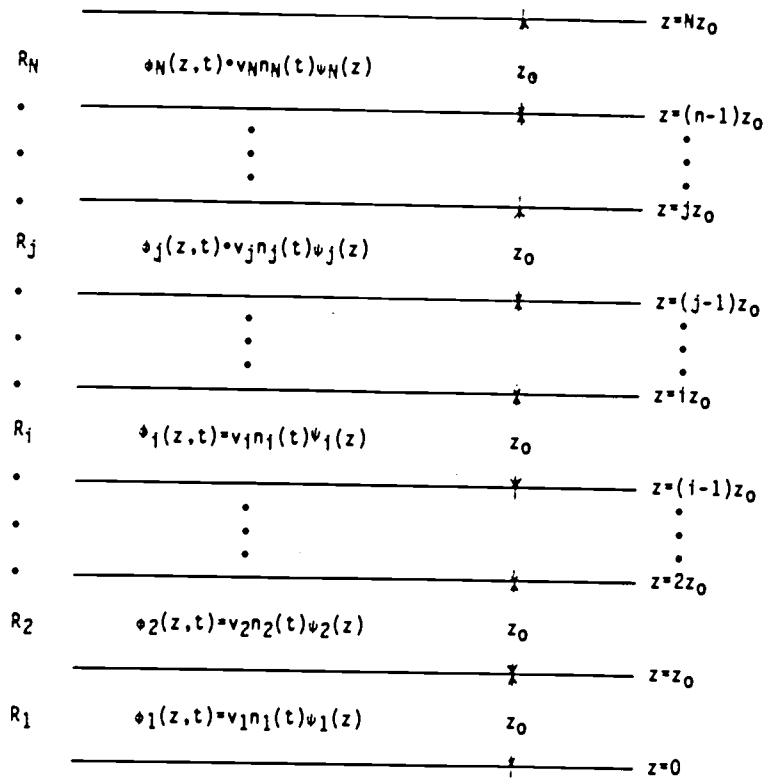

Figure 5.1
Geometry for Calculation of Coupling Coefficients

Comparing equation (5-18) to (5-11a) it can be seen that:

$$k_{1m} = \frac{k_\infty}{2} \left\{ \frac{(e^{[-z_0(|m-1|+1)/L]})(e^{z_0/L}-1)^2}{z_0/L} \right\} \qquad (5\text{-}19)$$

A better approximation would be to use the square root of the migration area M, in place of the diffusion length L in equation (5-19). Table 5.1 list the k_{1m}'s for a typical PWR with N=10.

Table 5.1

Nodal Model Coupling Coefficients

M=56, z0=36.7cm, N=10.

$k_{1,1+1}$	.253
$k_{1,1+2}$	.132
$k_{1,1+3}$	.0683
$k_{1,1+4}$	.0355
$k_{1,1+5}$	.0184
$k_{1,1+6}$	.00596
$k_{1,1+7}$	.00496
$k_{1,1+8}$	.00258
$k_{1,1+9}$	.00134

An order of magnitude estimate of the reactivity worth

of the Σk_{lm} term is obtained by making dn/dt=0 and $dC_{im}/dt=0$. Then equation (5-11) reduces to

$$\frac{\rho}{\Lambda} n_m + \sum_{l \neq m}^{N} k_{lm} n_l = 0 \qquad (5\text{-}19)$$

solving for ρ_{lm} and assuming that $OM(n_l/n_m)=1$ (NOTE: OM() is the order of magnitude function.) then:

$$OM(|\rho|) = \Lambda_m \sum_{l \neq m}^{N} k_{lm} \qquad (5\text{-}20)$$

With $\Lambda=2x10^{-4}$ and $\Sigma k_{lm}=.526$ then $OM(\rho_{lm})=10^{-4}$.

This amount of reactivity is small compared to the reactivity change that can occur as a result of various feedback mechanisms. More importantly this reactivity contribution will remain constant to the extent that the ratio n_l/n_m remains constant. Therefore the reactivity associated with the coupling coefficients is small and unchanging; therefore ignoring them can be justified.

The above argument certainly places some restrictions on the applicability of the RWPRK model, the most important being that the flux tilt must not change too severely during the transient. Experience has shown that for a wide variety of transients this restriction is not limiting(21)(21a)(25).

By setting the coupling coefficients to zero in the RWPRK model, the kinetics problem is reduced from solving a (Nx7)x(Nx7) system to that of solving N systems of 7x7 each. This can represent a significant savings even for moderate values of N.

In OLAPS, the control reactivity, that is, changes in reactivity due to control rod movement etc., are added uniformly throughout the core. The feedback reactivities are computed and added separately for each region.

The feedback reactivity coefficients are calculated using correlations given in chapter 6. Other kinetics parameters used are those of the Trojan Nuclear Facility (22).

6. Constitutive Equations

The models and equations developed in the previous chapters require more information in order to obtain closure. This information is provided in the form of constitutive equations, such as correlations for calculating material properties, heat transfer coefficients, pressure loss coefficients and drift flux relations. The correlations used in OLAPS are described in the flowing sections.

6.1. Material Properties

The material properties used in OLAPS have been borrowed from many sources including; the BNL BWR Plant Analyzer[13], TRAC-PD2[11], and MATPRO[29].

6.1.1. Water Properties

The properties of water are calculated as a function of pressure and enthalpy. The properties that are calculated are:

- Liquid and vapor temperatures,
- Saturation temperature for a given pressure,
- Densities of liquid and vapor,

- Heat of vaporization,
- Constant pressure specific heat for liquid and vapor,
- Thermal conductivity of liquid and vapor,
- Dynamic viscosity of the liquid and vapor,
- Surface tension of liquid.

Unless otherwise noted, all water property correlations are from the BNL BWR Plant Analyzer[13].

The saturation temperature in °C, is calculated for a given pressure in N/m^2, using:

$$T_{sat}(P) = \frac{\sum_{i=0}^{5} a_i P^i}{\sum_{j=0}^{5} b_j P^j} \qquad (6\text{-}1)$$

where: $a_0=-3.84576467\times10^{2}$, $b_0=1.99967470\times10^{1}$,

$a_1=0.570716464$, $b_1=2.09487630\times10^{-2}$,

$a_2=1.04091792\times10^{-4}$, $b_2=1.303093669\times10^{-6}$,

$a_3=1.02949324\times10^{-9}$, $b_3=6.75716812\times10^{-12}$,

$a_4=8.52096126\times10^{-16}$, $b_4=3.17424682\times10^{-18}$,

$a_5=5.56170847\times10^{-23}$, $b_5=1.0\times10^{-25}$.

The density of the saturated liquid in kg/m^3 is calculated using:

$$\rho_l(Tsat) = \frac{\sum_{i=0}^{3} a_i T_{sat}^i}{\sum_{j=0}^{4} b_j T_{sat}^j} \qquad (6\text{-}2)$$

where: $a_0=2.52704355$, $b_0=2.57224487\times10^{-13}$,

$a_1=3.4251011\times10^{-3}$, $b_1=3.36388317\times10^{-6}$,

$a_2=-6.2032234\times10^{-5}$, $b_2=-4.535222\times10^{-8}$,

$a_3=9.27165324\times10^{-8}$, $b_3=3.03855554\times10^{-11}$.

and T_{sat} is in °C.

The density of the saturated vapor in kg/m^3 is calculated from:

$$\rho_g(T_{sat}) = \frac{\sum_{i=0}^{5} a_i T_{sat}^i}{\sum_{j=0}^{3} b_j T_{sat}^j} \qquad (6\text{-}3)$$

where: $a_0=8.86026796\times10^{-4}$, $b_0=1.82518113\times10^{-1}$,

$a_1=5.577964474\times10^{-5}$, $b_1=-7.4969609\times10^{-4}$,

$a_2=1.86320039\times10^{-6}$, $b_2=1.12657020\times10^{-6}$,

$a_3=1.17529683\times10^{-8}$, $b_3=-9.9346951\times10^{-10}$,

$a_4=4.44786646\times10^{-10}$,

$a_5=-1.0776259\times10^{-12}$,

and T_{sat} is in °C.

The density of subcooled and superheated liquid is calculated by:

$$\rho(T_l,P)=\rho_{l_{sat}}(P) + \frac{\partial \rho_l}{\partial T}(T_l-T_{sat}) \qquad (6\text{-}4a)$$

where

$$\frac{\partial \rho_l}{\partial T}_P = \sum_{i=0}^{2} a_i P^i \qquad (6\text{-}4b)$$

where: $a_0=-0.8071$,

$a_1=-0.1774\times10^{-6}$,

$a_2=0.5289\times10^{-14}$.

and P is in N/m^2, T_l is in °C and T_{sat} and ρ_{lsat} are given by (6-1) and (6-2).

The liquid temperature in °C, as a function of enthalpy is given by:

$$T_l(h) \quad \sum_{i=0}^{5} a_i h_l^i \qquad (6\text{-}5)$$

where: $a_0=$ -.241607 ,

$a_2=$ .2440192 ,

$a_2=$ -.1508587x10^{-4},

$a_3 = .1332537 \times 10^{-7}$,

$a_4 = -.1000346 \times 10^{-10}$,

and h is in Ws/kg.

The specific heat at a constant pressure in Ws/(kg°C), of the liquid is calculated by:

$$C_{pl}(P) = \frac{\sum_{i=0}^{4} a_i T_{sat}^{i}}{\sum_{j=0}^{3} b_j T_{sat}^{j}} \qquad (6\text{-}6)$$

where: $a_0 = 9.34851589 \times 10^{3}$, $b_0 = 2.21949939$,

$a_1 = 3.37797785 \times 10^{1}$, $b_1 = 8,92447927 \times 10^{-3}$,

$a_2 = -3.18540182 \times 10^{-1}$, $b_2 = -8.63821184 \times 10^{-5}$,

$a_3 = 4.71558612 \times 10^{-4}$, $b_3 = 1.24688842 \times 10^{-7}$,

$a_4 = -9.93425202 \times 10^{-8}$,

where T_{sat} is calculated from (6-1).

The specific heat at a constant pressure in Ws/(kg°C) of the vapor is given by:

$$c_{pg} = \left(\frac{\partial T_g}{\partial h}\right)_p^{-1} \qquad (6\text{-}7)$$

where

$$T_g(h,P) = \sum_{i=0}^{2} \sum_{j=0}^{2} a_{ij} P^j h^i \qquad (6\text{-}8)$$

where: $a_{00} = 6.565890556 \times 10^{2}$,

$a_{01} = -5.256896914 \times 10^{-4}$,

$a_{02} = 1.622084838 \times 10^{-10}$,

$a_{10} = 9.906585925 \times 10^{-5}$,

$a_{11} = -3.440578369 \times 10^{-11}$,

$a_{12} = 1.867406949 \times 10^{-18}$,

$a_{20} = -2.187860677 \times 10^{-12}$,

$a_{21} = 7.008133640 \times 10^{-19}$,

$a_{22} = -1.456676437 \times 10^{-26}$.

The thermal conductivity in W/(m °C) of the liquid as calculated using:

$$k_l(T_{sat}) = \frac{\sum_{i=0}^{4} a_i T^i}{\sum_{j=0}^{3} b_j T^j}_{sat} \qquad (6\text{-}9)$$

where T_{sat} is given by (6-1) and:

$a_0 = 6.09937000 \times 10^{-1}$, $b_0 = 1.0$,

$a_1 = -2.05611490 \times 10^{-3}$, $b_1 = -5.3887800 \times 10^{-3}$,

$a_2 = -967565800 \times 10^{-6}$, $b_2 = 3.64155290 \times 10^{-6}$,

$a_3 = 3.94689000 \times 10^{-8}$,

$a_4 = -3.1700969910^{-11}$.

The thermal conductivity of the vapor in W/(m °C), is calculated by:

$$k_g(h_g,P) = X_1 + \rho_g(X_2 + C_0\rho_g T_{sat}^{-4.2}) \quad (6\text{-}10a)$$

where:

$$X_1 = \sum_{i=0}^{3} a_i T_{sat}^i \quad (6\text{-}10b)$$

$$X_2 = \sum_{j=0}^{2} b_j T_{sat}^j \quad (6\text{-}10c)$$

where: $a_0 = 1.76\text{x}10^{-2}$, $b_0 = 1.0351\text{x}10^{-4}$,

$a_1 = 5.87\text{x}10^{-5}$, $b_1 = 4.198\text{x}10^{-7}$,

$a_2 = 1.04\text{x}10^{-7}$, $b_2 = -2.771\text{x}10^{-11}$,

$a_3 = -4.51\text{x}10^{-11}$, $C_0 = 2.1482\text{x}10^{5}$,

and T_{sat} is given by (6-1).

The dynamic viscosity of the liquid in kg/(s m), is computed from:

$$\mu_l(T_{sat}) = \frac{\sum_{i=0}^{4} a_i T_{sat}^i}{\sum_{j=0}^{3} b_j T_{sat}^j} \quad (6\text{-}11)$$

where T_{sat} is given by (6-1) and:

$a_0=-7.37828137\times10^{-5}$, $b_0=-4.0980976\times10^{-2}$,

$a_1= 6.51521474\times10^{-7}$, $b_1=-1.03565416\times10^{-3}$,

$a_2=-1.77519264\times10^{-4}$, $b_2=9.45025143\times10^{-7}$,

$a_3= 1.19957482\times10^{-11}$, $b_3=7.94131516\times10^{-8}$,

$a_4=-1.44047622\times10^{-14}$.

The dynamic viscosity of the vapor in kg/(s m) is computed by:

for T $\leq$ 300 °C

$$\mu_g= \mu_0- \rho_g(1.858\times10^{-7}-5.90\times10^{-10}T_{sat}) \qquad (6\text{-}12a)$$

for T > 300 °C

$$\mu_g= \mu_0+ P \left[\sum_{i=0}^{3} f_i T_{sat}^i+\left(\sum_{i=0}^{3} g_i T_{sat}^i \right)\left(\sum_{i=0}^{2} a_i P^i \right)\right] \qquad (6\text{-}12b)$$

where $\mu_0=.407\times10^{-7}T_{sat}+ 8.04\times10^{-6}$ and

where: $a_0=3.53\times10^{-8}$, $g_0=176.0$,

$a_1=6.765\times10^{-11}$, $g_1=-1.60$,

$a_2=1.0211\times10^{-14}$, $g_2=4.8\times10^{-3}$,

$g_3=-4.7407\times10^{-6}$,

$f_0=-2.885\times^{-6}$, $f_1=2.427\times10^{-8}$,

$f_2=-7.7893\times10^{-11}$, $f_3=6.317037\times10^{-15}$.

The surface tension of the liquid in N/m is given by:

for $T_{sat} \leq 374.5$ °C

$$\sigma = .0775(1.0 - T_{sat}/374.5)^{1.2} \qquad (6\text{-}13a)$$

for $T_{sat} > 374.5$ °C

$$\sigma = 0.0 \qquad (6\text{-}13b)$$

The total emissivity, absorptivity and transmissivity for water are required for calculating the radiative heat transfer. These properties are a function of the clad temperature (T_w) in °F, steam temperature (T_g) in °F and the product of pressure and path length (PL) in atm-ft.

The total emissivity of steam is calculated using:

$$\epsilon_{H_2O}(T, PL_g) = 10^{(AT + B)} \qquad (6\text{-}13)$$

where: $A = \sum_{i=0}^{2} a_i P^i$, $B = \sum_{i=0}^{2} b_i P^i$,

$P = \log_{10}(100 PL_g)$,

for T<1000°F

$a_0 = -3.8443 \times 10^{-4}$, $b_0 = -1.50$,

$a_1 = 1.517 \times 10$, $b_1 = .70422$,

$a_2 = -9.5618 \times 10^{-6}$, $b_2 = -9.6888 \times 10^{-2}$,

and for T>1000°F

$a_0 = -3.8472 \times 10^{-4}$, $b_0 = -1.50$,

$a_1 = 1.56767 \times 10^{-4}$, $b_1 = .70989$,

$a_2 = -2.2300 \times 10^{-5}$, $b_2 = -8.81378 \times 10^{-2}$.

This correlation was obtained by fitting the data from Hottel (30).

The total absorptivity of steam according to Edwards[32] is given by:

$$\bar{\alpha}_{H_2O} = (T_g/T_w)^{1/2} \epsilon_{H_2O}(T_w, PL_g) \qquad (6\text{-}14)$$

and the transmissivity of steam is given by:

$$\bar{\tau}_{H_2O} = \frac{\ln(\bar{\alpha}'_{H_2O}/\bar{\alpha}_{H_2O})}{\frac{3}{2}\ln(T_w/T_g)} \qquad (6\text{-}15)$$

where $\bar{\alpha}'_{H_2O} = \bar{\alpha}_{H_2O}(PL'_g)$

and $PL'_g = (T_w/T_g)^{3/2} PL_g$

The emissivity of liquid water in the COBRA/TRAC program is given as:

$$\epsilon_l = 1-\exp(-\alpha_l L_l) \qquad (6\text{-}16)$$

where α_l is the total absorptivity of liquid water and is given by:

For dispersed droplet flow;

$$\alpha_l = .74\ (\pi/4)D_D^2 N_D \qquad (6\text{-}17a)$$

For inverted annular flow;

$$\alpha_l = 1.0 \qquad (6\text{-}17b)$$

where D_D is the mean droplet diameter and is calculated using the Ishii correlation(33):

$$D_D = \frac{4}{9}\ (2\sigma/g\Delta\rho)^{1/2}[\mu_g(\rho_g\sigma\ \sqrt{\sigma/g\Delta\rho}\ )^{-1/2}\ ]^{1/3} \qquad (6\text{-}18)$$

and N_D is given by (see Table 6-1):

$$N_D = \frac{(1-\alpha)}{\frac{\pi}{6}\ D_H^2} \qquad (6\text{-}19)$$

The mean beam lengths for the steam and liquid water are calculated using:

$$L_g = L\,\alpha^{1/2} \qquad (6\text{-}20a)$$

and

$$L_l = L\,(1-\alpha)^{1/2} \qquad (6\text{-}20b)$$

where L=3.5(S-D)
and S is the pitch of the fuel pin array and D is the diameter of the fuel pin.

6.1.2. Fuel (UO_2)

The fuel material (UO_2) properties are calculated as a function of temperature, using the MATPRO correlations. The specific heat of the fuel in Ws/(kg °C) is calculated using:

$$C_{pf} = \frac{k_1 \theta^2 e^{(\theta/T')}}{T'^2 [e^{(\theta/T')} - 1]^2} + k_2 T' + \left(\frac{O/M}{2}\right) \frac{k_3 E_D}{RT'^2} e^{-(E_D/RT')} \qquad (6\text{-}21)$$

where $T' = T + 273.15$

T = Temperature of fuel in °C,

O/M = Oxygen to Metal ratio,

R = 8.314 J/mol °K

θ = 535.285 = Einstein temperature °K

$k_1 = 296.7$

$k_2 = 2.43 \times 10^{-2}$

$k3 = 8.745 \times 10^{7}$

$E_D = 1.577 \times 10^{5}$.

The fuel thermal conductivity in kW/(m °C) is given by:

$$k_f(T) = .001731 \sum_{i=0}^{3} a_i T^i \qquad (6\text{-}22)$$

where: $a_0 = 3.84$,

$a_1 = -1.65485 \times 10^{-3}$,

$a_2 = 2.4374 \times 10^{-7}$,

$a_3 = 6.07334 \times 10^{-12}$,

and T is the fuel temperature in °F.

The fuel density is taken to be a constant and equal to 10960. kg/m^3, and the gas gap conductivity is taken to be a constant at 5680 W/(m °C).

6.1.3. Cladding

The cladding material (Zirc-IV) properties are also calculated as a function of temperature, using MATPRO

correlations. The thermal conductivity in W/(m °C) is given by:

$$k_{clad}(T) = \sum_{i=0}^{5} a_i T^i \qquad (6\text{-}24)$$

where: T is the clad temperature in °K and

$a_0 = 7.51$,

$a_1 = 2.09 \times 10^{-2}$,

$a_2 = 1.45 \times 10^{-4}$,

$a_3 = 7.67 \times 10^{-9}$.

The product of the cladding density and specific heat in Ws/m^3, is given by:

$$\rho C_{clad}(T) = \sum_{i=0}^{4} a_i X^i \qquad (6\text{-}25)$$

where $X = (T - 26.85)/200$, T is the clad temperature in °C and

$a_0 = 1.820453 \times 10^6$,

$a_1 = 3.038627 \times 10^5$,

$a_2 = -1.063741 \times 10^5$,

$a_3 = 2.8102874 \times 10^4$,

$a_4 = -2.72361 \times 10^3$.

The thermal radiation emissivity of the zirc-IV cladding is taken to be a constant :

$$\epsilon_{Zr}=0.8 \qquad (6\text{-}26)$$

6.2. Heat Transfer Package

The primary mode of heat removal from the core is through convective heat transfer from the cladding surface to the coolant flowing around the fuel pin. Under some circumstances radiative heat transfer can become important and must be taken into account.

The heat transfer is dependent on many things including coolant mass flow rate, the temperature of the cladding and the thermodynamic state of the coolant. In OLAPS, the heat transfer to each of the two phases is treated separately.

The OLAPS heat transfer package is essentially the same as that used in the COBRA/TRAC program. The correlations used in OLAPS to determine the heat transfer to each phase and their conditions of applicability, are outlined below.

6.2.1. Single Phase Vapor

Figure 6.1 shows the logic used to select the proper correlation for heat transfer. Following this diagram, when the void fraction is greater than .9999 the flow is considered to be single phase vapor and the heat flux to the vapor is given by:

$$q''_{wg} = h\ (T_w - T_g) \tag{6-27}$$

where

$$h = .023\ \frac{k_g}{D_H}\ \left(\frac{G_g D_H}{\mu_g}\right)^{.8}\ Pr_g^{.4} \tag{6-28}$$

6.2.2. Dispersed Flow Film Boiling

If the cladding surface temperature is greater than the minimum stable film boiling temperature (T_{MIN}) (see below) then the heat flux is given by one of two different correlations depending on the void fraction. For higher void fractions (α<.8) the flow is in the dispersed flow film boiling (DFFB) regime and the heat flux to the vapor phase is given by:

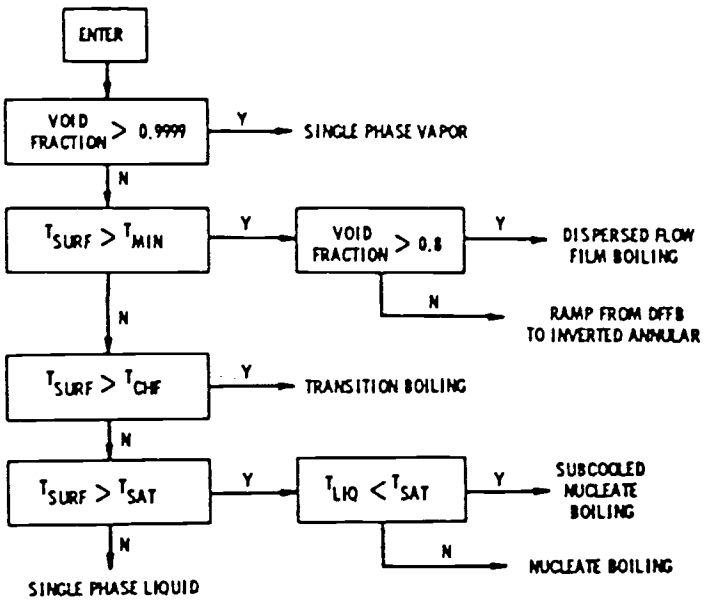

Figure 6.1
Heat Transfer Selection Logic

$$q''_{wg} = q''_{wspv} + q''_{wrg} \qquad (6\text{-}29)$$

where q''_{wspv} is given by (6-18) and q''_{wrg} is heat transfer by thermal radiation. The radiative heat flux as given by Edwards[32] is:

$$q''_{wrg} = \sigma_{SB}\epsilon_{zr} / \left[1-\tau_{bg}(1-\epsilon_{zr})\right] \left[\bar{\alpha}'_{H_2O} T_w^4 - \epsilon_{H_2O} T_g^4\right] \qquad (6\text{-}30)$$

here σ_{SB} is the Stefon-Boltzmann constant,

ϵ_{zr} is the emissivity of Zirc-IV,

τ_{bg} is the transmissivity of water vapor,

$\bar{\alpha}_{H_2O}$ is the total absorptivity of water vapor,

ϵ_{H_2O} is the total emissivity of water vapor.

The heat flux to the liquid phase is divided into components, one due to droplets impinging on the wall and one to radiative heat transfer. The heat transfer due to droplets impinging on the wall is given by the Forslund-Rohsenow correlation[34]:

$$q''_{wl} = .2 \frac{\pi}{4} \left(\frac{6}{\pi}\right)^{2/3} (1-\alpha)^{2/3} \left\{ \frac{g\rho_l \rho_g h_{fg} k_g^3}{(T_w - T_l)\, \mu_g (\pi/6)^{1/3} D_D} \right\}^{1/4} \qquad (6\text{-}31)$$

where D_D is the diameter of the dispersed liquid droplets.

The radiative portion of the wall-liquid heat flux is given by:

$$q''_{wlR} = F_{wl}\sigma_{SB}(T_w^4 - T_l^4) \qquad (6\text{-}32a)$$

$$\text{where } F_{wl} = \left[R_2\left(1 + \frac{R_3}{R_1} + \frac{R_3}{R_2}\right) \right]^{-1} \qquad (6\text{-}32b)$$

$$R_1 = (1-\epsilon_{H_2O})/[\epsilon_{H_2O}(1-\epsilon_{H_2O}\epsilon_l)] \qquad (6\text{-}32c)$$

$$R_2 = (1-\epsilon_l)/\ \epsilon_l(1-\epsilon_{H_2O}\epsilon_l) \qquad (6\text{-}32d)$$

$$R_3 = \frac{1}{(1-\epsilon_{H_2O}\epsilon_l)} + \frac{1-\epsilon_{zr}}{\epsilon_{zr}} \qquad (6\text{-}32e)$$

6.2.3. Inverted Annular Film Boiling

When the cladding surface temperature is above the minimum stable film boiling temperature (T_{MIN}), but the void fraction is less than 0.8 then inverted annular film boiling (IAFB) is assumed. The heat flux to the vapor phase for this situation is the same as for the DFFB. The heat flux to the liquid phase is calculated

from the larger of either DFFB value or the Bromly correlation[35]:

$$q''_{wl} = .107 \left(\frac{D_e}{\lambda}\right) \left\{\frac{g k_g \rho_g (\rho_f - \rho_g)\, h'_{fg}}{D_e \mu_g (T_w - T_l)}\right\}^{1/4} (T_w - T_l) \qquad (6\text{-}33)$$

where $h'_{fg} = h_{fg}(1.0 + .4C_{pg}(T_w - T_l)/h_{fg})$

$$\lambda_c = 2\pi \left[\frac{g\,\sigma}{g(\rho_l - \rho_g)}\right]^{1/2}$$

6.2.4. Transition Boiling

When the wall temperature is greater than T_{CHF}, but less than T_{MIN}, then transition boiling is assumed. The transition boiling heat fluxes are given by:

$$q''_{TB} = \max(.2, 1-a)\ \delta q''_{CHF} + q''_{FB} \qquad (6\text{-}34)$$

where $\delta = [(T_w - T_{MIN})/(T_{CHF} - T_{MIN})]^2$

q''_{FB} is either DFFB or IAFB heat flux, depending on the void fraction.

q''_{CHF} is the critical heat flux for inducing a departure from nucleate boiling (DNB).

The q''_{CHF} is calculated using the Biasi correlation[38]:

$$q''_{CHF} = \max(q''_{B1} , q''_{B2}) \text{ BTU/hr-ft}^2 \qquad (6\text{-}35a)$$

$$q''_{B1} = 5.9695 \times 10^6 \, G^{-1/6} \, (F(p) G^{-1/6} - x) \, D_e^{-n} \qquad (6\text{-}35b)$$

$$q''_{B2} = 11.98 \times 10^6 \, H(p) \, (1-x) \, D_e^{-n} \, G^{-.6} \qquad (6\text{-}35c)$$

$$H(p) = .7249 + .099p \exp(-.032p) \qquad (6\text{-}35d)$$

$$F(p) = -1.159 + .149 \, p \exp(-.019p) + 8.99p \, (10+p^2)^{-1} \qquad (6\text{-}35e)$$

where $n=.6$ if $D_e<1.0$ cm or $n=.4$ if $D_e>1.0$ cm.
with G in g/cm^2-s and P in bars.

6.2.5. Nucleate Boiling

If the wall temperature is greater than the coolant saturation temperature but less than the T_{CHF}, then nucleate boiling is assumed. If the liquid is at saturation then, fully developed nucleate boiling (NB) is assumed. If the liquid is subcooled then it is subcooled nucleate boiling (SCNB).

In the nucleate boiling region, the heat transfer to the liquid is assumed to be forced convection:

$$q''_{wl} = h(T_w - T_l) \tag{6-36a}$$

$$\text{where } h = .023\ F\ (k_l/D_e)\ Re_l^{0.8}\ Pr_l^{0.4} \tag{6-36b}$$

For $x_{tt}^{-1} > 0.1$

$$F = 2.34(x_{tt}^{-1} + .213)^{.736} \tag{6-36c}$$

For $x_{tt}^{-1} < 0.1$

$$F = 1.0$$

and

$$x_{tt}^{-1} = \left(\frac{x}{1-x}\right)^{.9}(\rho_l/\rho_g)^{.5}\ (\mu_g/\mu_l)^{.1} \tag{6-36d}$$

The heat transfer for vapor generation is given by the Foster-Zuber correlation:

$$q''_{wl} = h_{NB}(T_w - T_{sat}) \tag{6-37a}$$

where

$$h_{NB} = 0.00122\ S\ \frac{k_l^{.79}\ c_{pl}^{.45}\ \rho_l^{.49}\ g_c^{.25}}{\sigma^{.5}\ \mu_l^{.29}\ h_{fg}^{.24}\ \rho_g^{.24}}\ (T_w - T_l)^{.24}(P_w - P)^{.75} \tag{6-37b}$$

for $Re'_{TP} < 32.5$

$$S = [1 + .12Re'^{1.14}_{TP}]^{-1}$$

for $32.5 < Re' < 50.9$

$$S = [1 + .42Re'^{.78}_{TP}]^{-1}$$

for $Re'_{TP} > 50.9$

$$S = 0.1$$

$$Re'_{TP} = 1x10^{-4} Re_l F^{1.25}$$

In these correlations all liquid properties are evaluated at their saturation values.

In the subcooled nucleate boiling region, the heat flux is calculated using the same correlations that were used for the nucleate boiling region except that the liquid properties are those of the subcooled liquid and the suppression factor, S, is calculated using the single phase Reynolds number:

$$Re = \frac{G_l D_e}{\mu_l}$$

6.2.6. Single Phase Convection

If the wall temperature is less than the liquid saturation temperature then the single phase convective heat transfer is assumed. The heat flux to the liquid phase is given by:

$$q''_{wl} = h_{spl}(T_w - T_l) \qquad (6\text{-}38)$$

where h_{spl} is calculated using the Dittus-Boetler correlation, equation (6-28), and the liquid properties.

6.2.7. T_{MIN} and T_{CHF}

The minimum stable film boiling temperature, T_{MIN}, and the critical heat flux temperature, T_{CHF}, are needed in a few of the above correlations and are found by using an iterative method. The critical heat flux temperature is found by satisfying the relation:

$$q''_{CHF} = q''_{NB}(T_{CHF})$$

where q''_{CHF} is the critical heat flux given by the Biasi correlation and q''_{NB} is the nucleate boiling heat flux given above.

The minimum stable film boiling temperature is found by satisfying the relation:

$$q''_{MIN} = q''_{FB}(T_{MIN})$$

where q''_{MIN} is the minimum stable film boiling heat flux and q''_{FB} is the film boiling heat flux as given above. q''_{MIN} is calculated from q''_{CHF} using the Zuber(40) correlation:

$$q''_{MIN} = q''_{CHF} \left[(\rho_g + \rho_l)/\rho_g\right]^{-1/2} \qquad (6\text{-}39)$$

6.3. Interfacial Heat Transfer

Because the liquid and the vapor phases are not assumed to be in thermodynamic equilibrium, relations describing the heat transfer rate between the phases is required. In general the interfacial heat transfer rate is given by:

$$\frac{q''_{lg}}{L_s} = \frac{H_{lg} A_I (T_l - T_g)}{L_s} \qquad (6\text{-}40)$$

where H_{lg} is a heat transfer coefficient,

$1/L_s$ is the interfacial surface area concentration,

T_l is the liquid temperature,

T_g is the vapor temperature.

Both H_{lg} and $1/L_s$ are highly dependent on the flow regime. Figure 6.2 shows the logic used to select the proper flow regime. In addition to flow regime, H_{lg} also depends on the thermodynamic state of the liquid and vapor. Separate correlations are used for superheated vapor (SHV), subcooled vapor (SCV), superheated liquid (SHL) and subcooled liquid (SCL).

H_{lg} for the various conditions are given in table 6.1 and correlations for $1/L_s$ are given in table 6.2.

The definitions for the various Reynold's numbers used are given below[12]:

$$Re_g = \frac{D_e \rho_g |u_{lg}|}{\mu_g}$$

$$Re_B = \frac{D_B \rho_g |u_{lg}|}{\mu_{mb}} \quad ; \quad \mu_{mb} = \mu_l (1-\alpha)^{-2.5} \frac{(\mu_g + .4\mu_l)}{(\mu_g + \mu_l)} \quad ;$$

$$D_B = 2 \min(5\sigma/(\rho |u_{lg}|^2), .5D_e, .03606\, \alpha^{1/3})$$

$$Re_D = \frac{D_D \rho_g |u_{lg}|}{\mu_{md}} \quad ; \quad \mu_{md} = \mu_g \alpha^{-2.5} \frac{(\mu_l + .4\mu_g)}{(\mu_g + \mu_l)}$$

Table 6.1
Interfacial Heat Transfer Coefficient
Correlations used in OLAPS

Mode of Heat Transfer	Correlation (BTU/(hr ft^2 °F)	Flow Regime
SHV	1.0×10^4 (a)	Small Bubble
	$\frac{k_g}{D_e}$ $(2.0+.74 Re_g^{.5} Pr_g^{1/3})$	Large Bubble
	$\frac{f_I}{2} \rho_g C_{pg} \lvert u_{lg} \rvert Pr^{-2/3}$ $f_I = .005[1+75(1-\alpha)]$ $\delta = \frac{(1-a)}{4} D_e$	Film
SCV	$1.0 \times 10^4 (a)$	All Regimes

Table 6.1(continued)
Interfacial Heat Transfer Coefficient
Correlations used in OLAPS

Mode of Heat Transfer	Correlation (BTU/(hr ft^2 °F)	Flow Regime
SHL	$\frac{1}{\sqrt{\pi}} \left(\frac{k_l \lvert u_{gl} \rvert}{.5D_B} \rho_l c_{pl}\right)^{1/2}$	Small Bubble
	1.0×10^5 (a)	Large Bubble
	The maximum of: for $Re_l < 1000$ $1.925\ \rho_l c_{pl} \lvert u_l \rvert / (Re_l Pr_l)^{2/3}$ for $Re_l > 1000$ $.2701 \rho_l c_{pl} \lvert u_l \rvert / (Re_l^{.38} Pr_l^{2/3})$ and $2.0\ k_l/\delta$	Film

Table 6.1(continued)
Interfacial Heat Transfer Coefficient
Correlations used in OLAPS

Mode of Heat Transfer	Correlation (BTU/(hr ft^2 °F)	Flow Regime
SCL	$\frac{1}{\sqrt{\pi}} \left(\frac{k_l \lvert u_{gl} \rvert}{.5D_B} \rho_l c_{pl}\right)^{1/2}$	Small and Large Bubble
	For Re_l <1000 $1.925\ \rho_l c_{pl} \lvert u_l \rvert / (Re_l Pr_l)^{2/3}$ For Re_l >1000 $.2701 \rho_l c_{pl} \lvert u_l \rvert / (Re_l^{.38} Pr_l^{2/3})$	Film

(a) Large constant value used to drive phase to equilibrium

Table 6.2
Interfacial Heat Transfer Area Concentration, $1/L_s$
Correlations used in OLAPS

Flow Regime	Correlation (1/meters)
Bubble	$\pi N_B D_B^2$ $N_B = \frac{\alpha}{4\pi/3 \, D_B^3}$
Film	$\frac{4 \alpha^{1/2}}{D_e}$
Chunk, Drop	$N_D \pi D_e^2$ $N_D = \frac{6(1-\alpha)}{\pi D_e^3}$
Inverted Annular	$\frac{4(1-\alpha)^{1/2}}{D_e}$

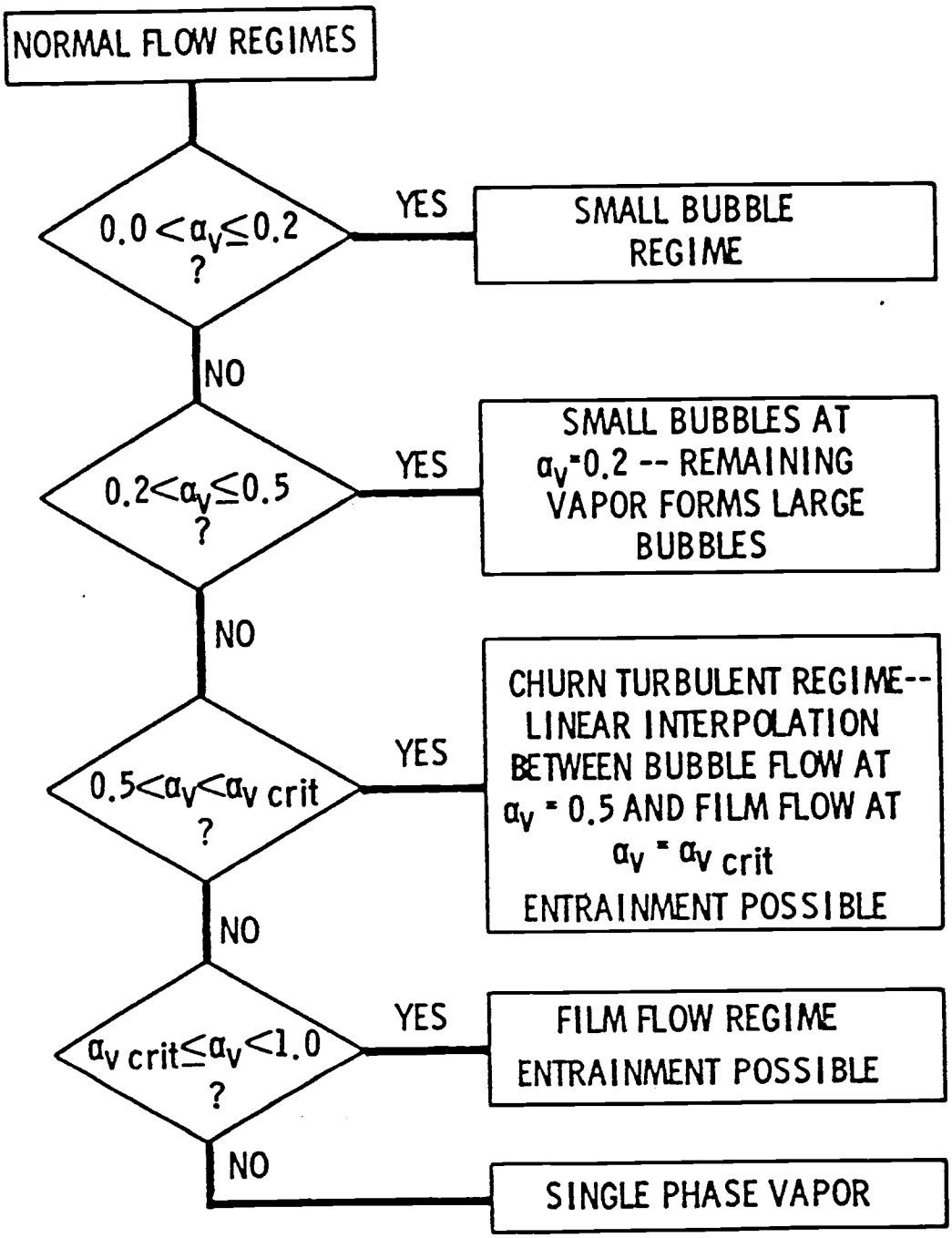

Figure 6.2
Flow Regime Logic

$$Re_l = \frac{D_e \rho_l |u_l|}{\mu_l}$$

6.4. Pressure Loss Coefficients

The frictional pressure loss is required to solve the mixture momentum equation. Obtaining this pressure loss is complicated somewhat by the fact that there are two phases flowing. The usual procedure is to calculate the pressure loss as if the liquid were flowing alone, and then make a correction by using a two phase multiplier. OLAPS uses this method in evaluating the frictional pressure loss.

The pressure loss due to friction for a single phase liquid is given by:

$$\Delta p = -\Delta z \frac{2 C_f \rho_l u_l}{D_e} \qquad (6\text{-}41)$$

where C_f is a friction factor and is calculated using a modified Blasius equation:

$$C_f = .0055 + .55Re_l^{-1/3} \qquad (6\text{-}42)$$

This is corrected for two-phase flow by using a Martinelli-two-phase multiplier:

$$\Delta p_{2p} = \phi_l^2 \, \Delta p_{sp} \qquad (6\text{-}43)$$

This multiplier was developed using the two fluid model and is calculated using :

$$\phi_l^2 = 1 + C/X + 1/X^2 \qquad (6\text{-}44)$$

Where $X = (dp/dz)_l / (dp/dz)_g$

$$(dp/dz)_l = 2 \frac{C_{fl} \, \rho_l \, u_l^2}{D_e}$$

and

$$(dp/dz)_g = 2 \frac{C_{fg} \, \rho_g \, u_g^2}{D_e}$$

Chisholm has correlated the C parameter in the Martinelli equation for a wide variety of flow conditions:

For $G \leq G^*$

$$C = [\lambda + (C_2 - \lambda)(\rho_g/\rho_l)^{1/2}][(\rho_g/\rho_l)^{1/2} \mp (\rho_g/\rho_l)^{1/2}] \quad (6\text{-}45)$$

$$\lambda = .75$$

$$C_2 = G^*/G$$

For $G > G^*$

$$\phi_l^2 = [1 + \bar{C}/X + 1/X^2] \psi$$

$$\psi = [1 + C/T + 1/T^2]/[1 + \bar{C}/T + 1/T^2]$$

$$\bar{C} = [(\rho_l/\rho_g)^{1/2} + (\rho_g/\rho_l)^{1/2}$$

$$T = [x/(1-x)]^{.9} (\mu_l/\mu_g)^{.1} (\rho_g/\rho_l)^{.5}$$

$$G^* = 2000 \text{ kg/m}^2\text{s}$$

The above expressions are for unheated surfaces. For heated surfaces, Tarasova gives a correction as:

$$\phi^2_{l,\text{heated}} = \phi^2_{l,\text{unheated}} [1 + 4.4 \times 10^{-3} (q''_w/G)^2] \quad (6\text{-}46)$$

where q''_w is the total wall heat flux in watts/m^2.

6.5. Drift Flux Model Correlation

The solution of the mixture momentum equation gives the mixture velocity. In order to find the phasic velocities needed for the mass and energy equations, another relation is needed. This is provided through the drift flux model correlation.

In general the drift flux model uses drift flux parameters to relate the mixture velocities to the phasic velocities. These drift flux parameters, C_0 and V_{gj}, are defined by:

$$C_0 = \frac{\langle \alpha\, j \rangle}{\langle \alpha \rangle \langle j \rangle} \qquad (6\text{-}47)$$

$$V_{gj} = \frac{\langle \alpha\, u_{gj} \rangle}{\langle \alpha \rangle}$$

where j is the total volumetric flux, volume flow rate per unit area,
u_{gj} is the drift velocity (the vapor velocity relative to the mixture center of mass).

The velocities of each phase can then be calculated as:

$$u_g = \frac{j_g}{\alpha} \qquad (6\text{-}48a)$$

and

$$u_l = \frac{j_l}{(1-\alpha)} \tag{6-48b}$$

The volumetric flux j, and the superficial velocities j_l, j_g are related through the conservation of mass by:

$$j = j_g + j_l \tag{6-49}$$

Applying the conservation of momentum to the mixture yields:

$$\rho_m u_m = \rho_g j_g + \rho_l j_l \tag{6-50}$$

The definitions given by equation (6-47) can be used to give[24]:

$$-\alpha C_0 j + j_g = \alpha V_{gj} \tag{6-51}$$

This gives three equations for the three unknowns j, j_g and j_l in terms of α, ρ_m, u_m, C_0 and V_{gj}. The mixture velocity u_m is obtained by solution of the mixture momentum equation. The values of α and ρ_m are obtained by solving the vapor and liquid mass conservation equation. Various correlations have been derived to relate the values of C_0 and V_{gj} to the flow conditions.

With the values of α, ρ_m, u_m, C_0 and V_{gj} known, equation (6-49) - (6-51) can be solved to find j, j_g, and j_l. These can then be used in equations (6-48) to calculate the phasic velocities.

To get the values of C_0 and V_{gj}, a drift flux correlation is needed. After considering several different drift flux correlations[36], the Ohkawa-Lahey[37] correlation was chosen for use in OLAPS. The Ohkawa-Lahey model, which was originally devised for use in the analysis of BWR's, was selected based on the wide range of applicability and ease of implementation. This model uses empirically derived coefficients to correlate the drift flux parameters as:

For $\alpha < d$

$$V_{gj} = V_{gj1} \tag{6-52a}$$

$$C_0 = C_{01} \tag{6-52b}$$

For $\alpha \geq d$

$$V_{gj} = \min(V_{gj1}, V_{gj2}) \tag{6-52c}$$

$$C_0 = \min(C_{01}, C_{02}) \tag{6-52d}$$

where

$$V_{gj1} = 2.9[(g g_c \sigma(\rho_l - \rho_g))/\rho_l^2]^{1/4} \tag{6-52e}$$

$$V_{gj2} = Y\, V_{gj1}\{1-[(\alpha-d)/(1-d)]\}^2 \qquad (6\text{-}52f)$$

$$C_{01} = [1.2 - .2(\rho_g/\rho_l)^{1/2}][1-\exp(-18\alpha)] \qquad (6\text{-}52g)$$

$$C_{02} = 1.0 + .2[1-(\rho_g/\rho_l)^{1/2}]\{1-[(\alpha-d)/(1-d)]^2\} \qquad (6\text{-}52h)$$

$$d = .5881164 - 1.81701(\rho_g/\rho_l)^{1/2} + 2.00025(\rho_g/\rho_l) - 3.34398(\rho_g/\rho_l)^{3/2} \qquad (6\text{-}52i)$$

$$Y = \max(3.136, Y_1) \qquad (6\text{-}52j)$$

$$Y_1 = 4.72085 - 17.26736(\rho_g/\rho_l)^{1/2} + 56.14833(\rho_g/\rho_l) + 113.21605(\rho_g/\rho_l)^{3/2} - 1250.603\,(\rho_g/\rho_l)^2 - 3039.7669(\rho_g/\rho_l)^{5/2} - 2431.8228(\rho_g/\rho_l)^3 \qquad (6\text{-}52k)$$

6.6. Reactivity Feedback Coefficients

The feedback reactivities used in the neutron kinetics equations are calculated using various reactivity coefficients. These coefficients represent the change in reactivity with respect to changes in some core

parameter, such as fuel and moderator temperature. That is :

$$\alpha_X(X) = \frac{\partial \rho_X}{\partial X}$$

where X is the changing core parameter.

Assuming that at time equal to zero the core is in steady state, then at some time t, the reactivity change due to changes in X are given by:

$$\rho(t) = \int_{X(0)}^{X(t)} \alpha_X(X)\,dx$$

If the coefficients are fitted to a polynomial of the form:

$$\alpha_X(X) = \sum_{1=0}^{n} a_i X^i$$

Then the reactivity could be calculated by:

$$\rho(t) = \sum_{i=0}^{n} \frac{a_X^i}{i+1} [\, X(0)^{i+1} - X(t)^{i+1}]$$

The various reactivity coefficients for the Trojan reactor were fit using data from the Trojan Cycle-7 Report(xx), the results are given in Table 6.3.

Table 6.3
Reactivity Feedback Coefficient Parameters

$$\alpha_X(X) = \sum_{1=0}^{n} a_i X^i$$

i	Moderator Temperature $\frac{\alpha_{MT}}{(i+1)}$	Fuel Doppler $\frac{\alpha_D}{(i+1)}$	Moderator Void Fraction $\frac{\alpha_{MV}}{(i+1)}$
0	-4.83×10^{-4}	-1.7587×10^{-5}	
1	1.961×10^{-6}	6.7860×10^{-9}	
2	-2.046×10^{-9}	-1.8660×10^{-12}	
3		2.0600×10^{-16}	

6.7. Vapor Generation Rate

The mass and energy conservation equations both require the vapor generation rate Γ_{lg}. There are two components that contribute to the amount of vapor generated. The first component is the generation of vapor at the walls. This occurs during nucleate and subcooled nucleate boiling. There are two components to

the heat transfer to the walls during boiling. One due to convection to the liquid, described by the Dittus-Boetler correlation, and one due to vapor generation described by the Chin correlation. This vapor generation rate is given by:

$$\Gamma_{lg,wall} = \frac{q''_{NB} \; A_{surf}}{h_{fg}} \tag{6-53}$$

The second component of the vapor generation rate is due to vapor generation at the vapor-liquid interface and is related to the interfacial heat transfer rate by:

$$\Gamma_{lg,I} = - \frac{(\xi''_{g,I} + \xi''_{l,I}) \; A_I}{h_{fg}} \tag{6-54}$$

Then the total generation rate is given by:

$$\Gamma_{lg} = \Gamma_{lg,I} + \Gamma_{lg,wall} \tag{6-55}$$

7. Numerical Methods

The complex nature of the conservation and constitutive equations makes an analytical solution impossible. Therefore numerical methods must be employed to obtain a solution. Several different methods were used to solve the loop conservation equations, the conduction equations for the fuel pin and the neutron kinetics equations. Each of these methods is described below.

7.1. Loop Thermalhydraulics

The conservation equations in chapter 3 were derived based upon a control volume approach. In order to apply these equations it is necessary to divide the system up into control volumes or nodes. The nodalization scheme used in OLAPS is shown in figure 7.1

There are 2 loops in the model; loop-1 represents a lumped model of 3 physical loops and loop-2 represents a single physical loop. In each loop there are 16 nodes, with 12 of these being common to both loops (nodes 1-11

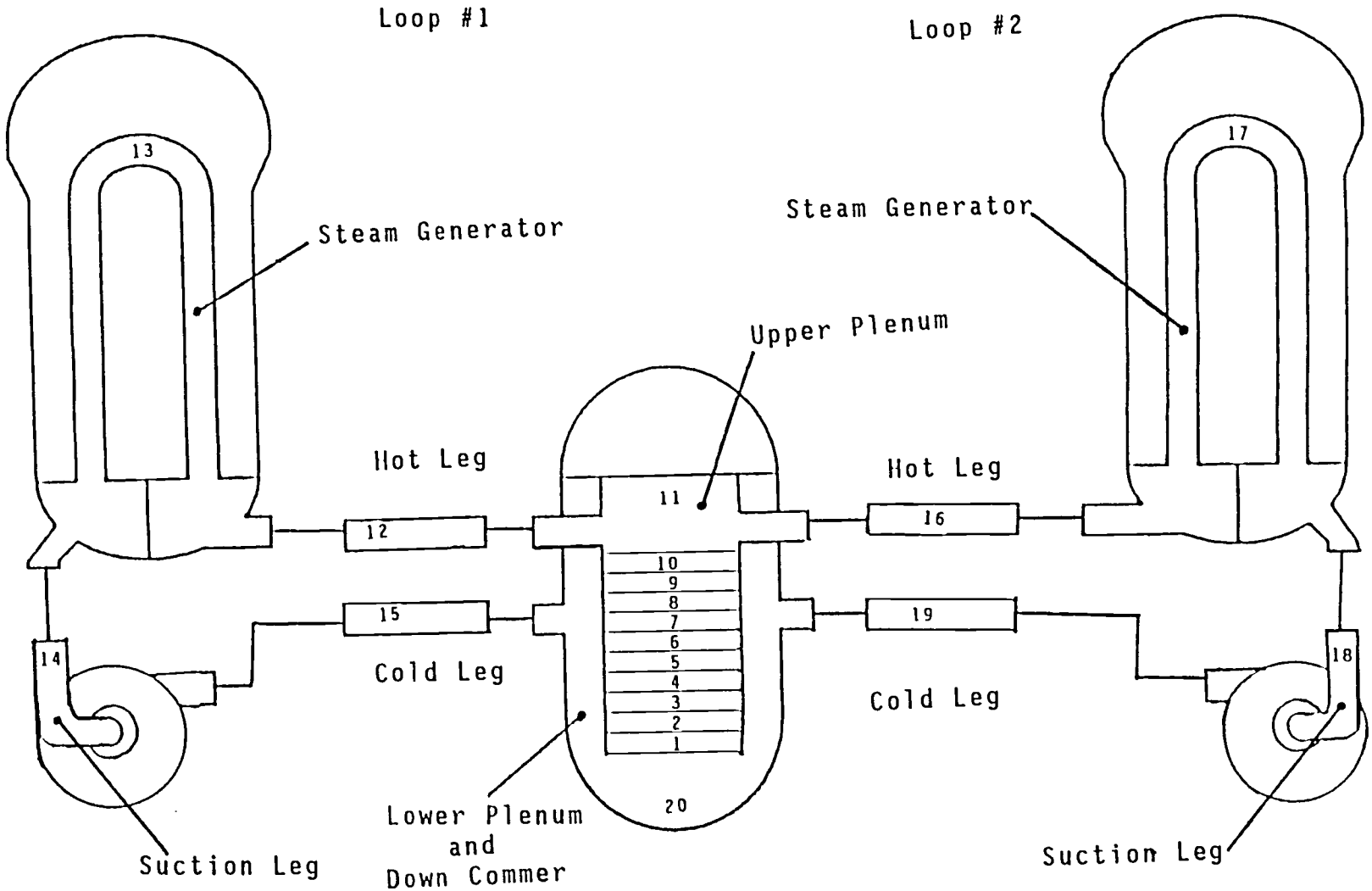

Figure 7.1
Loop Nodalization

and node 20). The common nodes represent the core (nodes 1-10), the upper plenum (node 11) and the lower plenum and downcomer (node 20). The other nodes in each of the loops represent the hot leg pipe (nodes 12 and 16), the primary side of the steam generators (nodes 13 and 17), the coolant pump and suction legs (nodes 14 and 18) and the cold legs (nodes 15 and 19). The 10 nodes (1-10) that represent the core region supply a greater level of detail than is available in most other PC based simulators.

The 20 nodes shown have 21 distinct interfaces through which coolant can pass from node to node. These interfaces are numbered as shown in figure 7.1.

7.1.1. Difference Operator

The numerical method used to solve the loop thermal-hydraulics equations is a finite difference method. This method converts differential equations into difference equations that can be solved algebraicly. This is accomplished by the use of the difference operator:

$$\frac{d\phi(t)}{dt} = \frac{\phi^{i+1} - \phi^{i}}{\Delta t} \qquad (7\text{-}1)$$

where ϕ^i is the value of $\phi(t)$ at the ith or present time step, and ϕ^{i+1} is the value of $\phi(t)$ at the i+1 or future time step and Δt is the time step size.

In addition to the difference operator a finite difference integration operator is needed. In OLAPS a simple box integration technique is used:

$$\int \phi(x)dx = \sum_j \phi(x_j)\, \Delta x_j \qquad (7\text{-}2)$$

7.1.2. Mass Equations

The difference operator is applied to the mass conservation equations (3-12) and (3-13) for the jth node giving:

$$\frac{(\alpha\rho_g)_j^{i+1} - (\alpha\rho_g)_j^i}{\Delta t} + \frac{1}{j}\left\{(A(\alpha\rho)_g^{i+1} u_g)_{j+\frac{1}{2}} - (A(\alpha\rho_g)^{i+1}\, u_g)_{j-\frac{1}{2}}\right\} = \Gamma_{lg,j} \qquad (7\text{-}3)$$

and

$$\frac{((1-\alpha)\rho_l)_j^{i+1}-((1-\alpha)\rho_l)_j^{i}}{\Delta t} \quad +$$

$$\frac{1}{Vol}\left\{(A((1-\alpha)\rho_l)^{i+1}\ u_l)_{j+\frac{1}{2}}-(A((1-\alpha)\rho_l)^{i+1}\ u_l)_{j+\frac{1}{2}}\right\}$$

$$= -\Gamma_{lg,j} \qquad (7\text{-}4)$$

In these equations the subscript j indicates that the variable is evaluated at the center of the control volume and the subscript j+1/2 or j-1/2 indicates that the variable is evaluated at the interface of the node.

Note that the properties are assumed to be constant in a control volume and the property values at the interface are set equal to those of the upstream node. The upstream node for the j-1/2 interface may be the jth node or the j-1th node depending on the direction of flow. If u_g or u_l are positive then the upstream node is the j-1th node; if u_g or u_l are negative then the upstream node is the jth node. Similarly for the j+1/2 interface.

The mass difference equations can be solved for the future time step values of $(\alpha\rho_g)$'s and $((1-\alpha)\rho_l)$'s:

$$\text{Vol}_{j-\frac{1}{2}}\left\{(\alpha\rho_g)_j^{i+1} + (\alpha\rho_g)_{j+\frac{1}{2}}^{i+1}\right\} Dt(Au_g)_{j+\frac{1}{2}} - (\alpha\rho_g)_{j-\frac{1}{2}}^{i+1}\Delta t(Au_g)$$

$$= \Delta t\ \text{Vol}_j \Gamma_{lg,j} + (\alpha\rho_g)_j^i\ \text{Vol}_j \qquad (7\text{-}5)$$

and

$$\text{Vol}_j[(1-\alpha)\rho_l]_j^{i+1} + (1-\alpha)\rho_l]_{j+\frac{1}{2}}^{i+1}\ \Delta t(Au_l)_{j+\frac{1}{2}} \qquad (7\text{-}6)$$

$$-[(1-\alpha)\rho_l]_{j-\frac{1}{2}}^{i+1}\Delta t(Au_l)_{j-\frac{1}{2}} = -\Delta t\ \text{Vol}_j\Gamma_{lg,j} + [(1-\alpha)\rho_l)]_j^i\text{Vol}_j$$

This forms a set of 20 simultaneous equations (j=1-20) that can be solved using a linear equation solver.

7.1.3. Energy Equations

Applying the difference operator to energy equations (3-17) and (3-18) gives:

$$\frac{\alpha_j\rho_{gj}h_{gj}^{i+1} - \alpha_j\rho_{gj}h_{gj}^i}{\Delta t} + \frac{1}{\text{Vol}_j}[(A\alpha\rho_g h_g^{i+1}u_g)_{j+\frac{1}{2}} -$$

$$(A\alpha\rho_g h_g^{i+1} u_g)_{j-\frac{1}{2}}] = \frac{1}{Vol_j} A_{surfj} q''_{wgj} + \Gamma_{lgj} h_{fg} + (q''_i/L_s)_j \quad (7\text{-}7)$$

and

$$\frac{(1-\alpha)_j \rho_{lj} h_{lj}^{i+1} - (1-\alpha)_j \rho_{lj} h_{lj}^{i}}{\Delta t} +$$

$$\frac{1}{Vol_j} [(A(1-\alpha)\rho_l h_l^{i+1} u_l)_{j+\frac{1}{2}} - (A(1-\alpha)\rho_l h_l^{i+1} u_l)_{j-\frac{1}{2}}]$$

$$= \frac{1}{Vol_j} A_{surfj} q''_{wlj} - \Gamma_{lgj} h_{fg} - (q''_i/L_s)_j \quad (7\text{-}8)$$

Like the mass equations the values of α, ρ and h at the interfaces are dependent on the direction of flow and take on the values for the upstream node.

Equations (7-7) and (7-8) can be rearranged so that the terms with future time step values appear on the left hand side and the terms involving the present values are on the right hand side of the equation, ie;

$$h_{gj}^{i+1}[\alpha_j \rho_{gj} Vol_j] - h_{gj-\frac{1}{2}}^{i+1} \Delta t[A\alpha\rho_g u_g]_{j-\frac{1}{2}} + h_{gj+\frac{1}{2}}^{i+1} \Delta t[A\alpha\rho_g u_g]_{j+\frac{1}{2}}$$

$$= \Delta t(A_{surfj} q''_{wgj} + Vol_j \Gamma_{lgj} h_{fg} + Vol_j (q''_I/L_s)_j) + h_{gj}^{i} Vol_j \alpha_j \rho_{gj}$$

and

$$h_{lj}^{i+1}[(1-\alpha)_j \rho_{lj} Vol_j] - h_{lj-\frac{1}{2}}^{i+1} \Delta t[A(1-\alpha)\rho_l u_l]_{j-\frac{1}{2}}$$

$$+h_{lj+\frac{1}{2}}^{i+1} \Delta t[A(1-\alpha)\rho_l u_l]_{j+\frac{1}{2}} = \Delta t(A_{surfj} q''_{wlj} - Vol_j \Gamma_{lgj} h_{fg}$$

$$Vol_j (q''_I / L_s)_j + h_{lj}^{i} Vol_j \alpha_j \rho_{lj} \qquad (7\text{-}10)$$

This forms a set of 20 simultaneous equations similar to the mass equation, and can also be solved using a linear equation solver.

7.1.4. Mixture Momentum Equation

The difference operator is not directly applied to the mixture momentum equation. Instead, the momentum equation is integrated around each loop:

$$\oint \frac{\partial \rho_m u_m}{\partial t} dz + \oint \frac{1}{Vol} (A \rho_m u_m u_m) \quad dz = -\oint \frac{\Delta p}{\Delta z} dz$$

$$+ \oint \frac{2C_f \rho_m u_m^2}{D_e} dz \quad + \oint M_m g dz \qquad (7\text{-}11)$$

This is done in order to eliminate the pressure gradient term, ie:

$$\oint \frac{\Delta p}{\Delta z}\, dz = 0 \qquad (7\text{-}12)$$

Now both the difference operator and the integration operator are applied to the modified mixture momentum equation. Taking (7-11) by terms:

$$\oint \frac{\partial \rho_m u_m}{\partial t}\, dz = \sum_{j=1}^{21} \left(\frac{\rho_{m,j} u_{m,j}^{i+1} - \rho_{m,j} u_{m,j}^{i}}{\Delta t}\right) \Delta z \qquad (7\text{-}13)$$

$$\oint \frac{1}{Vol_j} (A \Delta \rho_m u_m u_m) dz = \sum_{j=1}^{21} \frac{1}{Vol_j} (\rho_{m,j+\frac{1}{2}} u_{m,j+\frac{1}{2}}^{i+1} u_{m,j+\frac{1}{2}}^{i})\, \Delta z_j$$

$$- \sum_{j=1}^{21} \frac{1}{Vol_j} (\rho_{m,j-\frac{1}{2}} u_{m,j-\frac{1}{2}}^{i+1} u_{m,j-\frac{1}{2}}^{i})\, \Delta z_j \qquad (7\text{-}14)$$

$$\oint \frac{2 \rho_m C_f u_m^2}{D_e}\, dz = \sum_{j=1}^{21} 2\, C_{f,j} \rho_{m,j} \left(\frac{u_{m,j}^{i}}{D_{e,j}}\right)^2 \qquad (7\text{-}15)$$

where

$$u^{i}_{m,j} = \frac{u^{i}_{m,j+\frac{1}{2}} + u^{i}_{m,j-\frac{1}{2}}}{2}$$

collecting terms:

$$u^{i+1}_{m,j-\frac{1}{2}}\left[\sum_{k=1}^{20}\left(\frac{\rho_{m,k}}{2\Delta t} - \frac{\rho_{m,k-\frac{1}{2}}u^{i}_{m,k-\frac{1}{2}}}{Vol_k}\right)\right]$$

$$+ u^{i+1}_{m,j+\frac{1}{2}}\left[\sum_{k=1}^{20}\left(\frac{\rho_{m,k}}{2\Delta t} - \frac{\rho_{m,k+\frac{1}{2}}u^{i}_{m,k+\frac{1}{2}}}{Vol_k}\right)\right] =$$

$$\sum_{k=1}^{20}\left[\left(\frac{\rho_{m,k}u^{i}_{m,k}}{\Delta t} + \frac{C_{f,k}\rho_{m,k}L_{e,k}}{2D_{e,k}}\left(u^{i}_{m,k}\right)^2\right]\right. \qquad (7\text{-}16)$$

Writing this equation for each loop gives 2 of the 21 equations needed to be solved for the 21 nodal interface mixture velocities, $u^{m,j+\frac{1}{2}}$'s. The remainder of the 21 equations are obtained by assuming incompressibility and applying the conservation of mixture mass to each node:

$$\nabla\cdot(\rho_m u_m) = 0 \qquad (7\text{-}17)$$

applying the difference operator:

$$\rho_{m,j+\frac{1}{2}} u_{m,j+\frac{1}{2}} - \rho_{m,j-\frac{1}{2}} u_{m,j-\frac{1}{2}} = 0 \qquad (7\text{-}18)$$

7.2. Conduction Equation

The conduction equation (4-1) is solved using the Crank-Nicholson numerical method. To use this method the fuel pin is divided into 12 concentric radial nodes, 10 in the fuel and 2 in the cladding (see figure 7.2). The fuel pin is also divided into 10 axial nodes, one for each of the thermal-hydraulic nodes in the core (see figure 7.1).

The Crank-Nicholson scheme approximates the conduction equation as:

$$(\rho c_p)_j^{j+\frac{1}{2}} \left(\frac{T_j^{i+\frac{1}{2}} - T_j^{i-\frac{1}{2}}}{\Delta t}\right) = \frac{1}{2} \left(L_j^{i+1}\left\{\frac{1}{r}\left[\frac{\partial}{\partial r}\left(rk\frac{\partial T}{\partial r}\right)\right]\right\}\right.$$

$$\left. - \left(L_j^{i}\left\{\frac{1}{r}\left[\frac{\partial}{\partial r}\left(rk\frac{\partial T}{\partial r}\right)\right]\right\}\right) + q_i'''^{i+1} \qquad (7\text{-}19)$$

where L_j^i is a finite difference operator defined as:

$$L_j^i\{\frac{1}{r}[\frac{\partial}{\partial r}(rk\frac{\partial T}{\partial r})]\} = (1+\frac{r_{j-1}}{r_j})(\frac{k_{j-\frac{1}{2}}}{(r_{j+1}-r_{j-1})(r_j-r_{j-1})})T_{j-1}^i$$

$$-(1+\frac{r_{j-1}}{r_j})(\frac{k_{j-\frac{1}{2}}}{(r_{j+1}-r_{j-1})(r_j-r_{j-1})})T_j^i$$

$$+(1+\frac{r_{j+1}}{r_j})(\frac{k_{j+\frac{1}{2}}}{(r_{j+1}-r_{j-1})(r_{j+1}-r_j)})T_j^i$$

$$+(1+\frac{r_{j+1}}{r_j})(\frac{k_{j+\frac{1}{2}}}{(r_{j+1}-r_{j-1})(r_{j+1}-r_j)})T_{j+1}^i \qquad (7\text{-}20)$$

Equation 7-19 is written for each of the fuel interior nodes. In order to satisfy the boundary conditions outline in chapter 5. special difference operators are used for the fuel centerline, fuel surface, cladding inner surface and the cladding outer surface nodes.

For the fuel centerline the finite difference operator L is defined as:

$$L_1^i\{\frac{1}{r}[\frac{\partial}{\partial r}(rk\frac{\partial T}{\partial r})]\} = -\frac{k_1}{r_2^2}T_1^i + \frac{k_1}{r_2^2}T_2^i \qquad (7\text{-}21)$$

The fuel surface node boundary condition is satisfied by using the finite difference operator:

$$L^i\{\frac{1}{r}[\frac{\partial}{\partial r}(rk\frac{\partial T}{\partial r})]\} = (1+\frac{r_{fs-1}}{r_{fs}})(\frac{k_{fs-\frac{1}{2}}}{(r_{fs}-r_{fs-1})^2})T^i_{fs-1}$$

$$-[(1+\frac{r_{fs-1}}{r_{fs}})(\frac{k_{fs-\frac{1}{2}}}{(r_{fs}-r_{fs-1})^2})+(\frac{r_{ci}}{r_{fs}})(\frac{2H_g}{(r_{fs}-r_{fs-1})^2})]T^i_{fs}$$

$$+(\frac{r_{ci}}{r_{fs}})(\frac{2H_g}{(r_{fs}-r_{fs-1})^2})]T^i_{ci} \qquad (7\text{-}22)$$

where Hg is the gas gap conductance and the subscripts fs and ci stand for fuel surface and clad inner radius respectively.

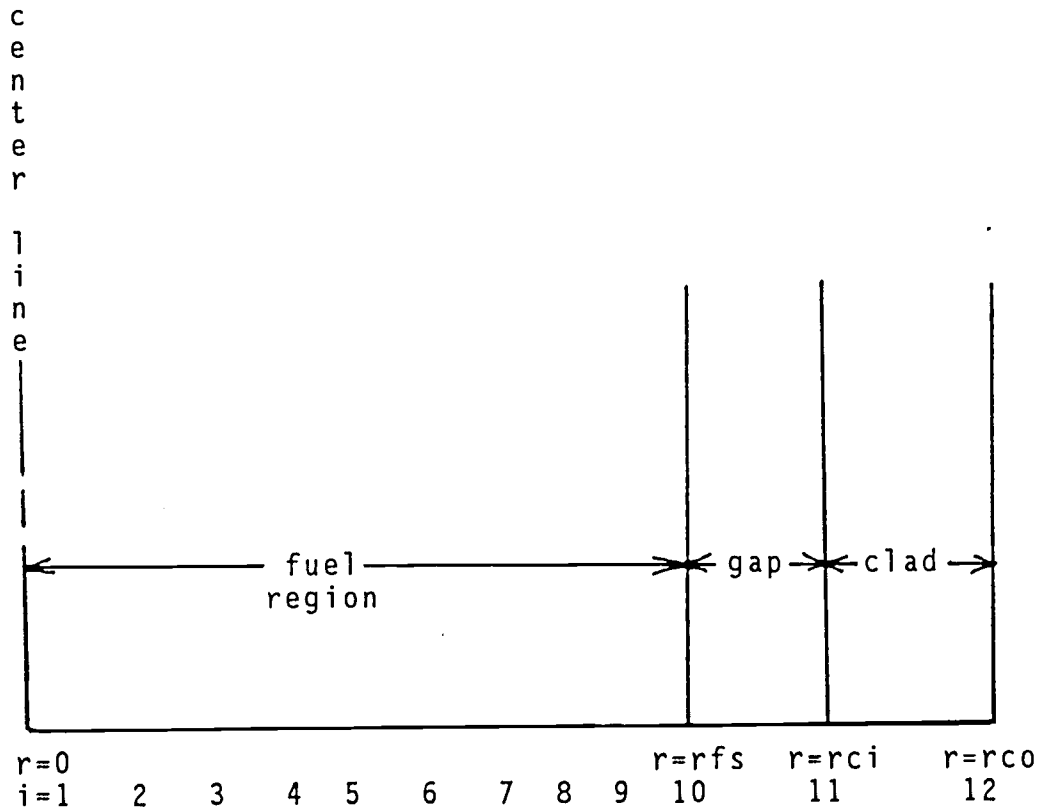

Figure 7.2
Fuel Pin Nodalization

The difference operator used at the cladding inner surface is:

$$L^i\left\{\frac{1}{r}\left[\frac{\partial}{\partial r}\left(rk\frac{\partial T}{\partial r}\right)\right]\right\}=\left(\frac{2H_g}{(r_{fs}-r_{fs-1})^2}\right)T^i_{fs}$$

$$-\left[\left(1+\frac{r_{ci+1}}{r_{ci}}\right)\left(\frac{k_{ci+\frac{1}{2}}}{(r_{ci+1}-r_{ci})^2}\right)+\left(\frac{2H_g}{(r_{ci+1}-r_{ci})^2}\right)\right]T^i_{ci}$$

$$+\left(1+\frac{r_{ci+1}}{r_{ci}}\right)\left(\frac{k_{ci+\frac{1}{2}}}{(r_{ci+1}-r_{ci})^2}\right)\Big]T^i_{ci+1} \qquad (7\text{-}23)$$

Finally the difference operator at the cladding surface nodes is:

$$L^i\left\{\frac{1}{r}\left[\frac{\partial}{\partial r}\left(rk\frac{\partial T}{\partial r}\right)\right]\right\}=\left(1+\frac{r_{ci}}{r_{co}}\right)\left(\frac{k_{co-\frac{1}{2}}}{(r_{co}-r_{ci})^2}\right)T^i_{ci}$$

$$-\left[\left(1+\frac{r_{ci}}{r_{co}}\right)\left(\frac{k_{co-\frac{1}{2}}}{(r_{co}-r_{ci})^2}\right)+\left(\frac{2H_\infty}{(r_{co}-r_{ci})^2}\right)\right]T^i_{co}$$

$$+\left(\frac{2H_\infty}{(r_{co}-r_{ci})^2}\right)\Big]T^i_{ci} \qquad (7\text{-}24)$$

where T_∞ is the bulk coolant temperature and H_∞ is the heat transfer coefficient.

Equation (7-19) and (7-21)-(7-24) can be arranged in a tridiagonal matrix equation. This can be solved using the Thomas Algorithm to find the radial fuel-clad temperature distribution. This is done for each axial node to find the axial temperature distribution.

7.3.Kinetics Equation

The region-wise point reactor kinetics model reduces the kinetics problem to solving the point reactor equations for each region in the core. OLAPS divides the core into 10 regions, one for each of the thermal-hydraulic nodes as shown in figure 7.1.

The point reactor kinetics equations are written:

$$\frac{dn}{dt} = \frac{\rho - \beta}{\Lambda} n(t) + \sum_{k=1}^{6} \lambda_k C_k(t)$$

$$\frac{dC_k}{dt} = \frac{\beta_k}{\Lambda} n(t) - \lambda_k C_k(t) \qquad k=1\text{-}6 \qquad (7\text{-}25)$$

These equations can be solved using the fully implicit matrix method. This method uses the following finite difference approximations:

$$n^{i+1} = n^i + \Delta t \frac{dn^{i+1}}{dt} \tag{7-26}$$

$$C_k^{i+1} = C_k^i + \Delta t \frac{dC_k^{i+1}}{dt} \qquad k=1-6$$

Using (7-26) with (7-25) and solving for n_i and C_k^i's:

$$[1-\Delta t(\frac{\rho-\beta}{\Lambda})]n^{i+1} - \Delta t \sum_{k=1}^{6} \lambda_k C_k^{i+1} = n^i \tag{7-27}$$

and

$$-\Delta t \frac{\beta_k}{\Lambda} n^{i+1} + [1+\Delta t\lambda_k]C_k^{i+1} = C_k^i \qquad k=1-6$$

In matrix form:

$$A\Phi^{i+1} = \Phi^i \tag{7-28}$$

This can be solved by elimination to find the values of n^{i+1} and C_k^{i+1}'s. A special elimination routine is used to take advantage of the sparseness of the A matrix and increase efficiency.

7.4. Solution Scheme

In keeping with the data flow design philosophy, the solution scheme used in OLAPS is highly modular. Separate subroutines are used for each major portion of the solution scheme. There are subroutines that handle the solution of the mass, energy and momentum equations and subroutines that are used to solve the conduction and kinetics equations. Additionally there are subroutines that handle the heat transfer package, pressurizer model, system pressure model, charging/letdown system model, the drift flux model, vapor generation rates and material properties. The major OLAPS routines are listed in Table 7.1.

Figure 7.3 shows a flow chart of the OLAPS solution scheme. After initial setup and start-up, the transient portion of the process proceeds by calls to USER and SCREEN for user input and screen output. Then the coolant properties, heat transfer coefficients, vapor generation rate, and phasic velocities are calculated by calls to PROPS, HXFER, GAMMA and DRIFT. After this, calls to MASS, ENERGY and MOMNTM setup and solve the mass, energy and momentum conservation equations. This section is followed by calls to various subroutines that model the charging/letdown systems (CNL), pressurizer

(PIZER), and system pressure (PRESSUR). The power distribution and fuel temperature distribution are updated by calls to REGKIN and PIN. Finally the time step is incremented and the process is repeated.

Table 7.1
OLAPS Major Subroutines

SETUP	Initial setup routines
USER	Reads Keyboard for user input
SCREEN	Write output to screen and output files
MOMNENTM	Solves mixture momnentum equations
MASS	Solves mass equations
ENERGY	Solves energy equations
DRIFT	Calculates phase velocities using a drift flux model
REGKIN	Solves regionwise kinetics equations
PIN	Solves conduction equation in fuel
PIZER	Calculates Pressurizer Pressure
PRESSUR	Calculates system pressure
PROPS	Calculates water properties
HXFER	Calculates heat transfer coefficients
CNL	Calculates charge and letdown flows
GAMMA	Calculates vapor generation rates

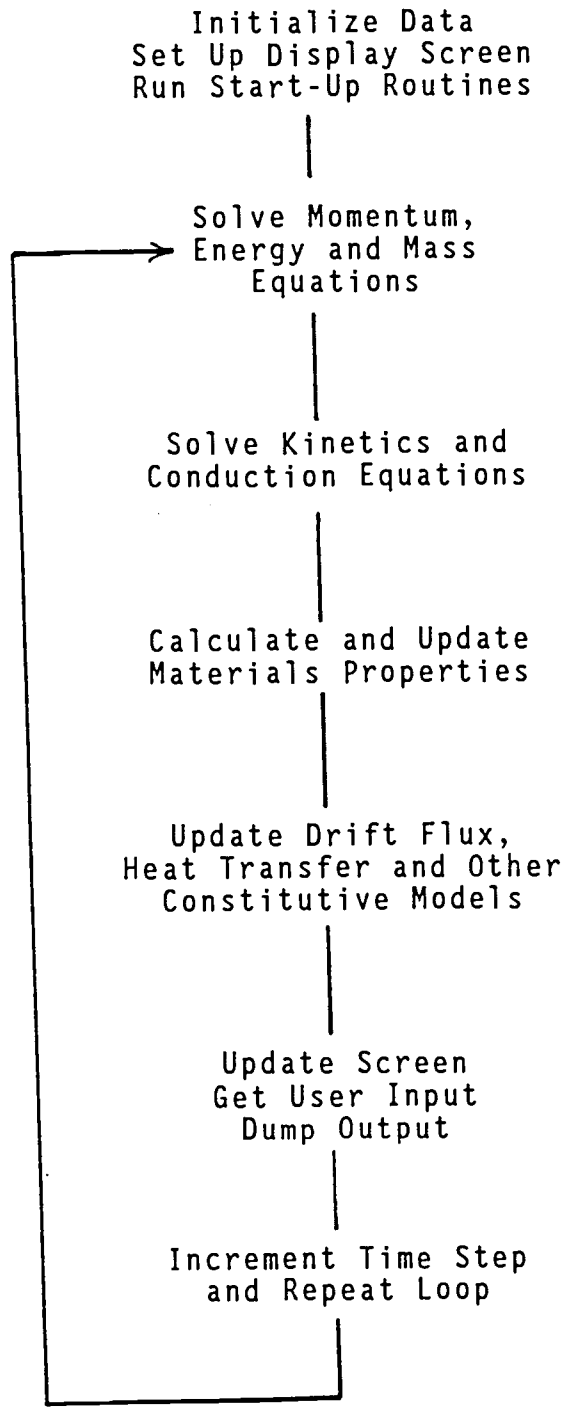

Figure 7.3
OLAPS Flow Chart

8. Results and Comparisons

As an initial test and validation three transients were simulated using OLAPS:

- Uncontrolled rod withdrawal at full power
- Reactor coolant pump locked rotor
- Large break loss of coolant accident (LOCA)

The results obtained from OLAPS were compared to those from the Trojan FSAR[46] and to results obtain from the COBRA-IV PC code. In addition to the transient results steady state results were compared.

8.1. Steady State

OLAPS does not in general have a built in steady state solution routine. Instead initial conditions are read in from various data files. In order to obtain a steady state solution from OLAPS an initial guess is input into these data files and a null transient is run (i.e. all forcing functions are held constant) and the system is allowed to settle. At the end of the run, OLAPS will save the current conditions to various output files. These files can be put into the input files for future

runs. This process can be repeated several times to produce accurate results.

Using this process, a steady state solution was obtained. The results are given in Table 8.1 where they are compared to the results from COBRA-IV PC and the Trojan FSAR data.

Table 8.1
Steady state results for the average channel from OLAPS, COBRA-IV PC and the Trojan FSAR.

	OLAPS	COBRA-IV PC	Trojan FSAR
Inlet Temp.	298 °C	300 °C	300 °C
Outlet	331 °C	332 °C	332 °C
Max Fuel Temp. (in average channel)	1104 °C	1138 °C	N/A
Max Clad Temp. (in average channel)	343 °C	345 °C	N/A
Delta P core	29.6 psi	5.88 psi	26.8 psi
mass flow core	18100 kg/s	17300 kg/s	16721 kg/s
delta P steam generator	35.1 psi	N/A	34.5 psi

N/A - Not Available

In the following discussion the percent differences are based on the OLAPS values. That is, the percent differences are calculated by taking the absolute value

of the difference between the compared value and the OLAPS value and dividing by the OLAPS value.

From Table 8.1, the inlet temperature calculated by OLAPS is 298 °C and is given as 300 °C by the Trojan FSAR and COBRA-IV (Note that the inlet temperature is an input value for COBRA-IV PC) this is a 0.671 percent difference. The outlet temperature calculated by OLAPS is 331 °C where as COBRA-IV PC calculates the outlet temperature as 332 °C. This is a 0.302 percent difference. The Trojan FSAR gives the outlet temperature as 333 °C which is a 0.604 percent difference.

The Trojan FSAR does not give values for the maximum fuel and cladding temperatures in the average channel. The values calculated by OLAPS and COBRA-IV PC for the maximum fuel temperature in the average channel are 1104 °C and 1138 °C respectively giving a 3.08 percent difference. The maximum cladding temperature in the average channel was calculated to be 343 °C by OLAPS and 345 °C by COBRA-IV PC, a 0.583 percent difference.

The pressure drop across the core, as given by the Trojan FSAR, is 26.8 psi. The value calculated by OLAPS is 29.6 psi. This is a 9.46 percent difference. The value for the pressure drop across the core calculated

by COBRA-IV PC is 5.88 psi. This gives an 80.1 percent difference from the OLAPS result. This large difference is most probably a result of the low quality of the available values for the drag coefficient for the spacer grids. The drag coefficients are needed by COBRA-IV PC to calculate the pressure loss. Because OLAPS uses a different method for calculating pressure losses it is not affected by the quality of the drag coefficients.

The pressure drop across the steam generators calculated by OLAPS is 35.1 psi. The value given in the Trojan FSAR is 34.5 psi. This is a 1.71 percent difference. COBRA-IV PC does not calculate the pressure drop across the steam generator.

The mass flow rate through the core calculated by OLAPS is 18,100 kg/s and the value given in the Trojan FSAR is 16,721 kg/s, a 7.62 percent difference. The value given by COBRA-IV PC is 17,300 kg/s which gives a 4.42 percent difference from the OLAPS values.

The above discussion indicates that for the steady state case OLAPS gives good results when compared to the Trojan FSAR data and COBRA-IV PC results. All the differences between OLAPS and the FSAR quoted data are less than 10 percent and in some cases less than one

percent. Except for the pressure drop across the core the same can be said for the COBRA-IV PC results. This is important in that these steady state conditions are used to provide the initial conditions for transient calculations described below.

8.2. Transient Calculations

Because OLAPS was written to simulate the transient behavior of the reactor system it is important to compare the transient results from OLAPS to those of other simulators. Below the results of three different transients are presented and compared to data from various sources. The transients were chosen to show results of transients from different initiating events. The uncontrolled rod withdrawal represents a reactivity induced transient. The locked rotor represents a flow induced transient. The large break LOCA is a pressure and flow induced transient.

8.2.1. Uncontrolled Rod Withdrawal

The uncontrolled rod withdrawal is simulated by a ramping in of reactivity at the rate of .005 Δk units (or \$0.78) per second. At 2.1 seconds into the event the

reactor is scrammed. This is simulated by the insertion of a total of .0576 Δk units (or $9.00) of negative reactivity over a 2 second period. The OLAPS calculation for this event was compared to data given in the Trojan FSAR.

The uncontrolled rod withdrawal power history, as calculated by OLAPS, is shown in figure 8.1. Figure 8.1 also shows the power history as given in the Trojan FSAR. There is good agreement between OLAPS and the FSAR data through most of the transient with the exception being the period when the scram reactivity is being inserted. This could be the result of using different models for the neutron kinetics and/or reactivity insertion. The FSAR does not describe any of the models used in this calculations.

Both sets of data show the power level peaking at approximately 2.1 seconds. The FSAR power level has a peak value of 117 percent full power while the OLAPS peak power level is 132 percent full power. This is a 15 percent difference based on full power or an 11.4 percent difference based on the OLAPS values. This difference is probably due to a difference in the reactivity coefficients used. The values of the reactivity coefficients used for this calculation are

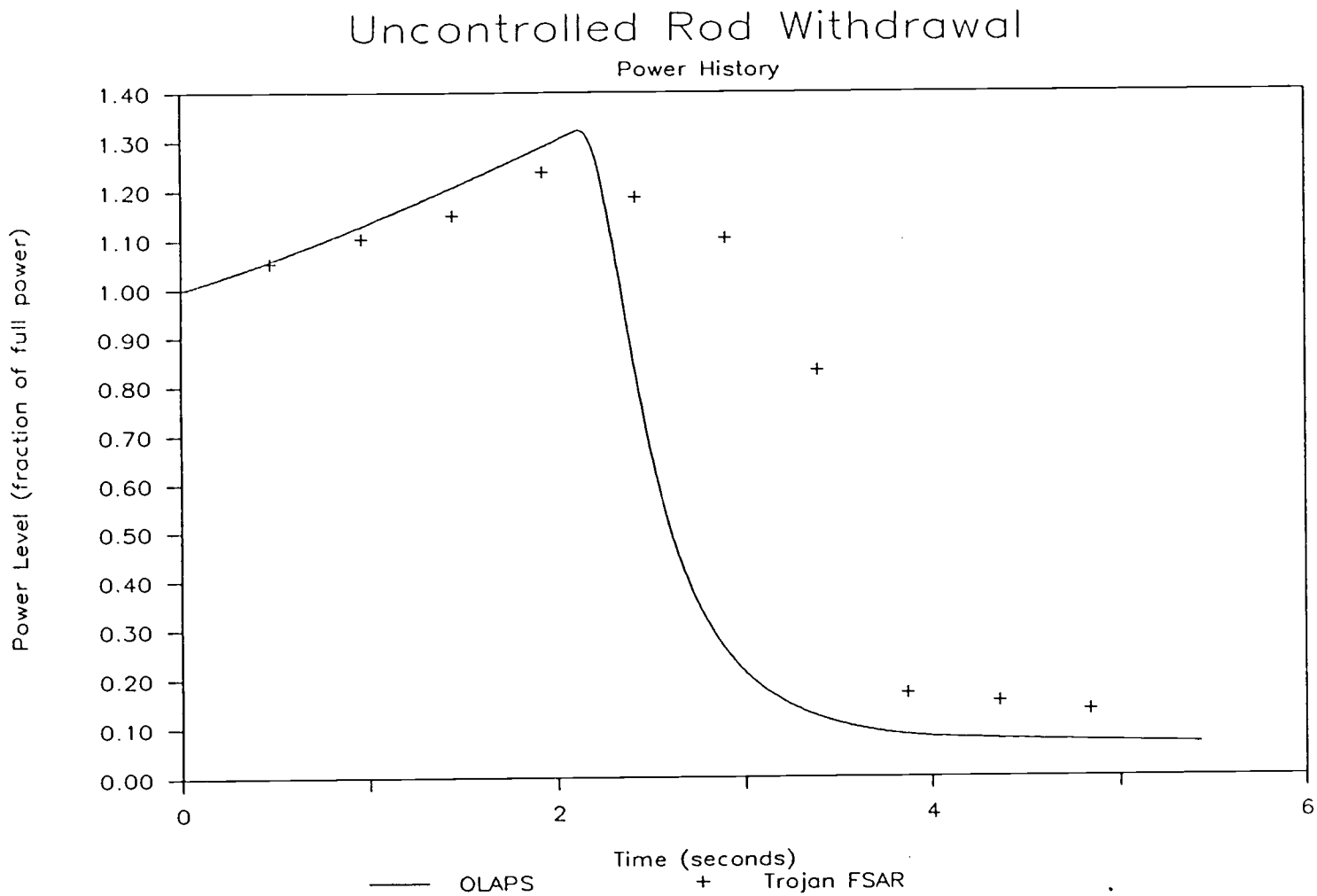

Figure 8.1
Uncontrolled Rod Withdrawal Power History.

not given in the FSAR.

The average core coolant temperature history for this transient as calculated by OLAPS is compared to the Trojan FSAR data in figure 8.2. For the OLAPS curve the average core coolant temperature is calculated by averaging the inlet and outlet temperatures. It is not possible to determine from the FSAR the algorithm used to calculate the quoted values of the average core coolant temperature. Therefore it is difficult to explain the differences between the initial values of average core coolant temperature. However the differences are small (4.1 °C or 1.3 percent) and do not represent a major concern.

Differences in initial temperatures aside, the two histories show a parallel trend. Both sets of data show an initial increase in temperature with a peak temperature occurring sometime after the scram. The FSAR data shows that the peak average core coolant temperature is 312.1 °C (1.5 °C above initial value) and occurs at 3.94 seconds, 1.84 seconds after the scram. The OLAPS data show a peak temperature of 315.7 °C (1.0 °C above initial value) occurring at 2.53 seconds. The difference in peak amplitudes and time to peak values

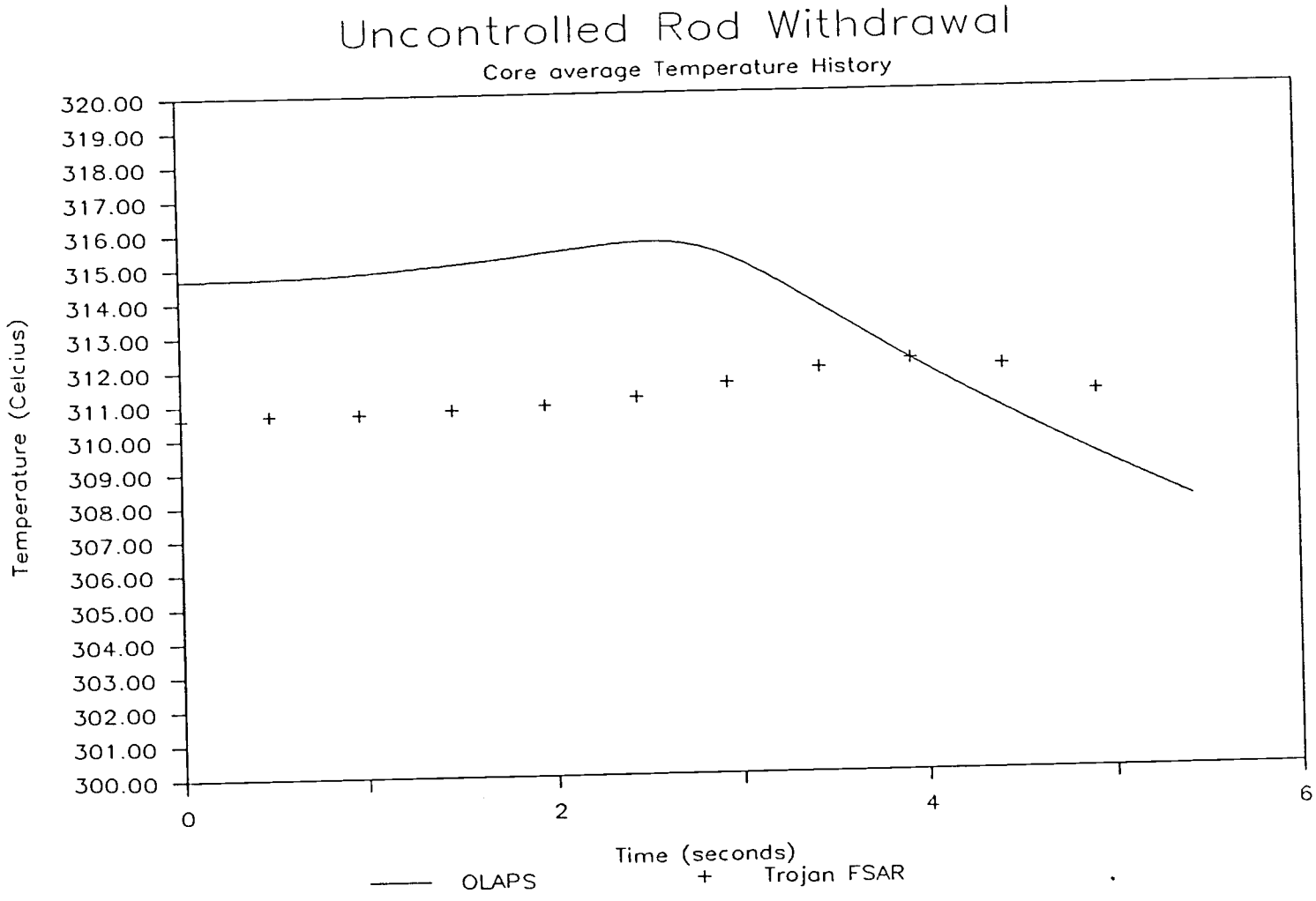

Figure 8.2
Uncontrolled Rod Withdrawal Coolant Temperature.

are consistent with differences in the power histories shown in figure 8.1.

Figure 8.3 shows the system pressure as a function of time as calculated by OLAPS and as given in the Trojan FSAR. Both sets of data show the same overall trend; an increase in pressure with a peak occurring sometime after the scram. OLAPS has the pressure increasing from an initial value of 15.40 MPa to 15.47 MPa with the peak at 2.74 seconds, while the FSAR shows the pressure from 15.30 MPa to 15.87 MPa peaking at 3.88 seconds. These differences in amplitude and time to peak values are consistent with the differences in power histories as shown in figure 8.1.

The time dependent behavior of the MDNBR calculated by OLAPS and as given by the Trojan FSAR are shown in figure 8.4. The data show an almost parallel behavior, again the differences are consistent with the differences in the power histories. The OLAPS data show the MDNBR value start from a value of 1.66 decrease to a minimum value of 1.52 at 2.25 seconds before starting to increase again. The FSAR data has the initial value of the MDNBR at 1.54 and reaching a minimum value of 1.39 at 2.9 seconds.

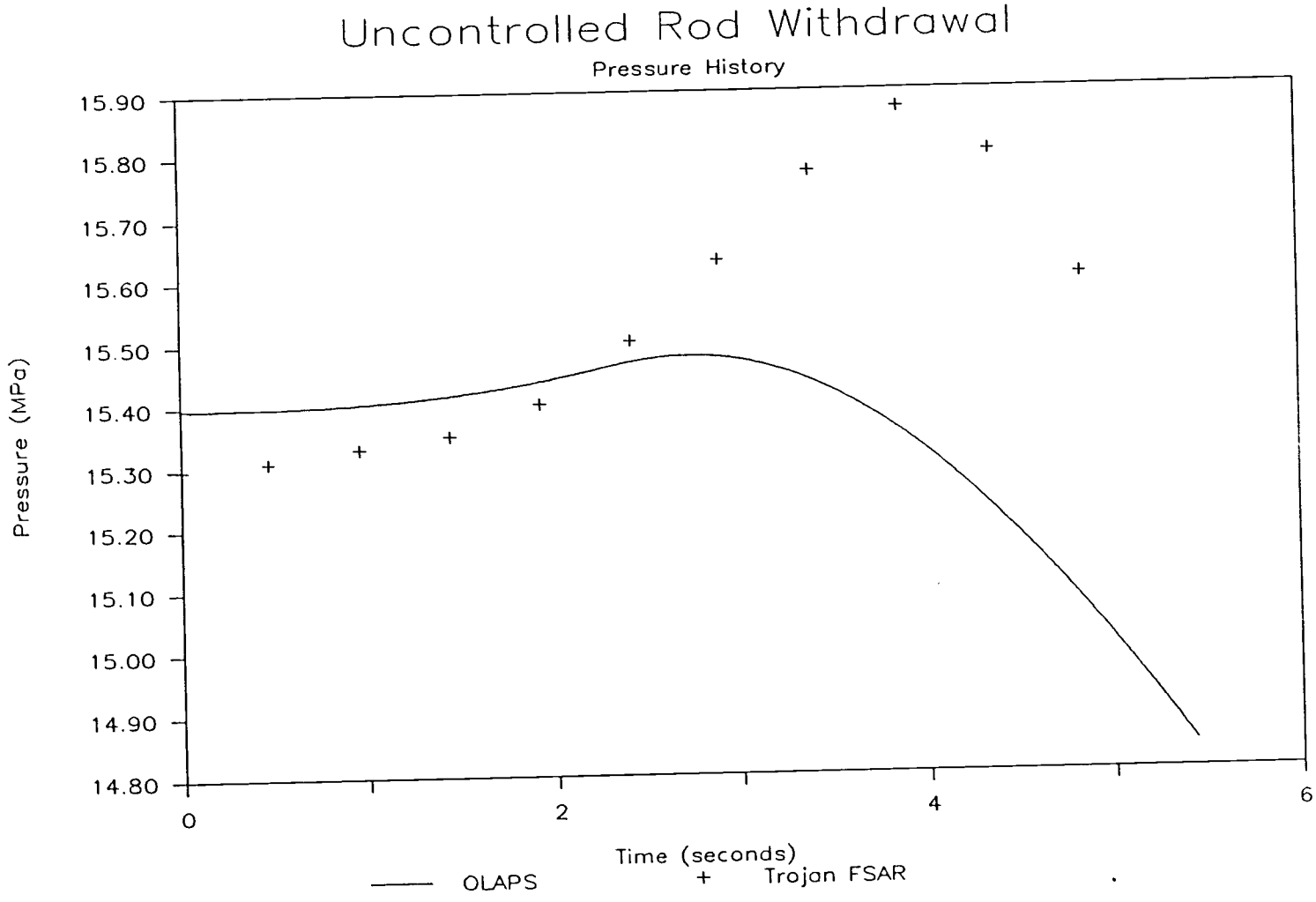

Figure 8.3
Uncontrolled Rod Withdrawal System Pressure.

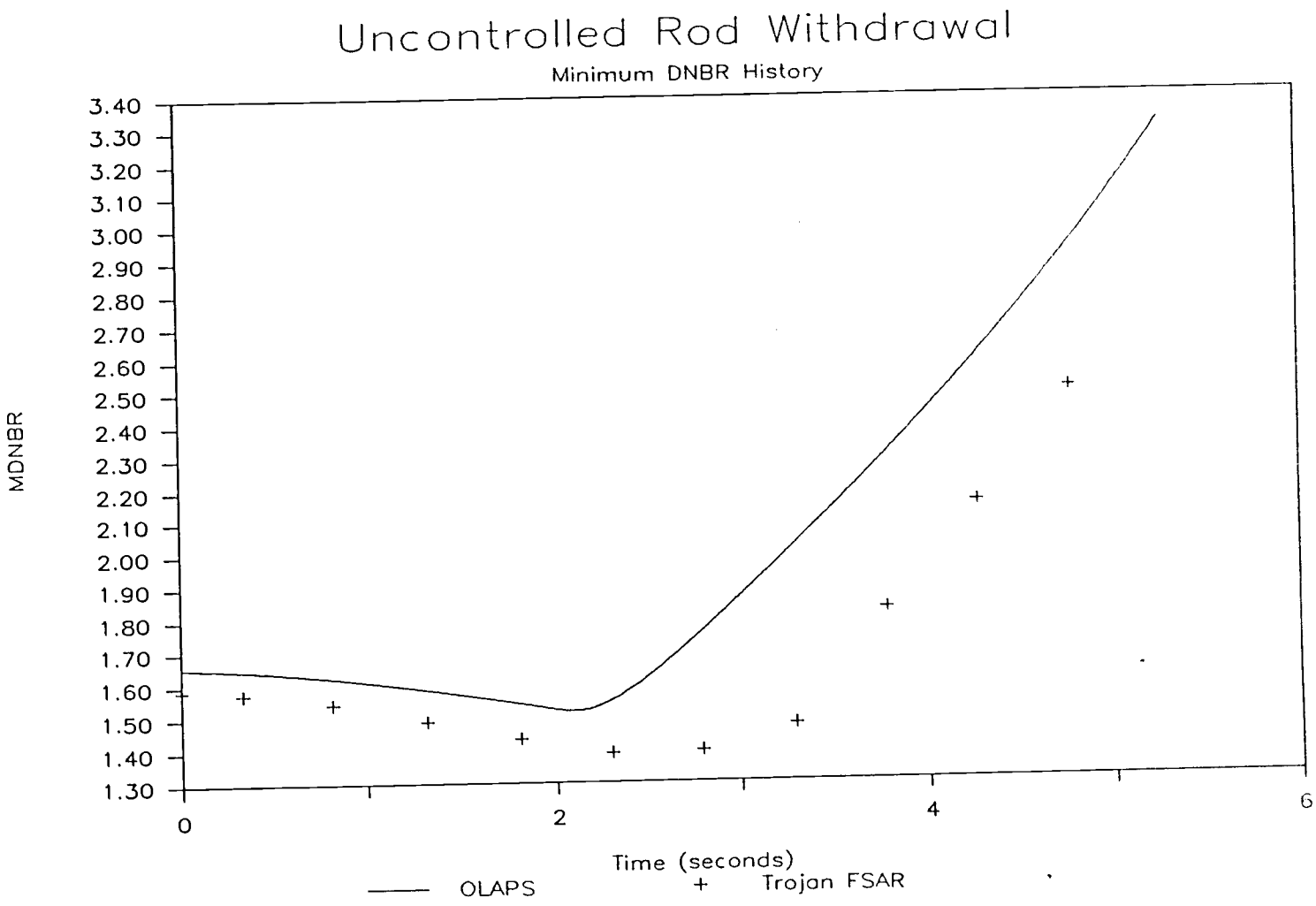

Figure 8.4
Uncontrolled Rod Withdrawal MDNBR History.

Figures 8.1 - 8.4 show good agreement between OLAPS and the Trojan FSAR. The magnitude of the differences invalues calculated between OLAPS and those quoted in the FSAR are small, less than 10 percent. The FSAR data was uniformly more conservative.

8.2.2. Locked Rotor

The next transient simulated using OLAPS and compared to Trojan FSAR data was a locked rotor transient. In this transient the pump shaft is assumed to seize and instantly stop. The reactor is scrammed 1.0 second after the flow rate through the core falls below 87 percent of nominal flow. For OLAPS this transient is initiated by turning off the single loop pump (pump No.2) and manually scramming the reactor.

Figure 8.5 shows the coolant mass flow through the core as a function of time as given by Trojan FSAR and as calculated by OLAPS. The Trojan data show the mass flow rate initially decreasing more rapidly and reaching a new higher steady flow than calculated by OLAPS. The agreement between the FSAR data and the OLAPS is good with the maximum difference being less then 11.0 percent. The new steady flow from the FSAR data is 74. percent of nominal and from OLAPS is 67. percent of

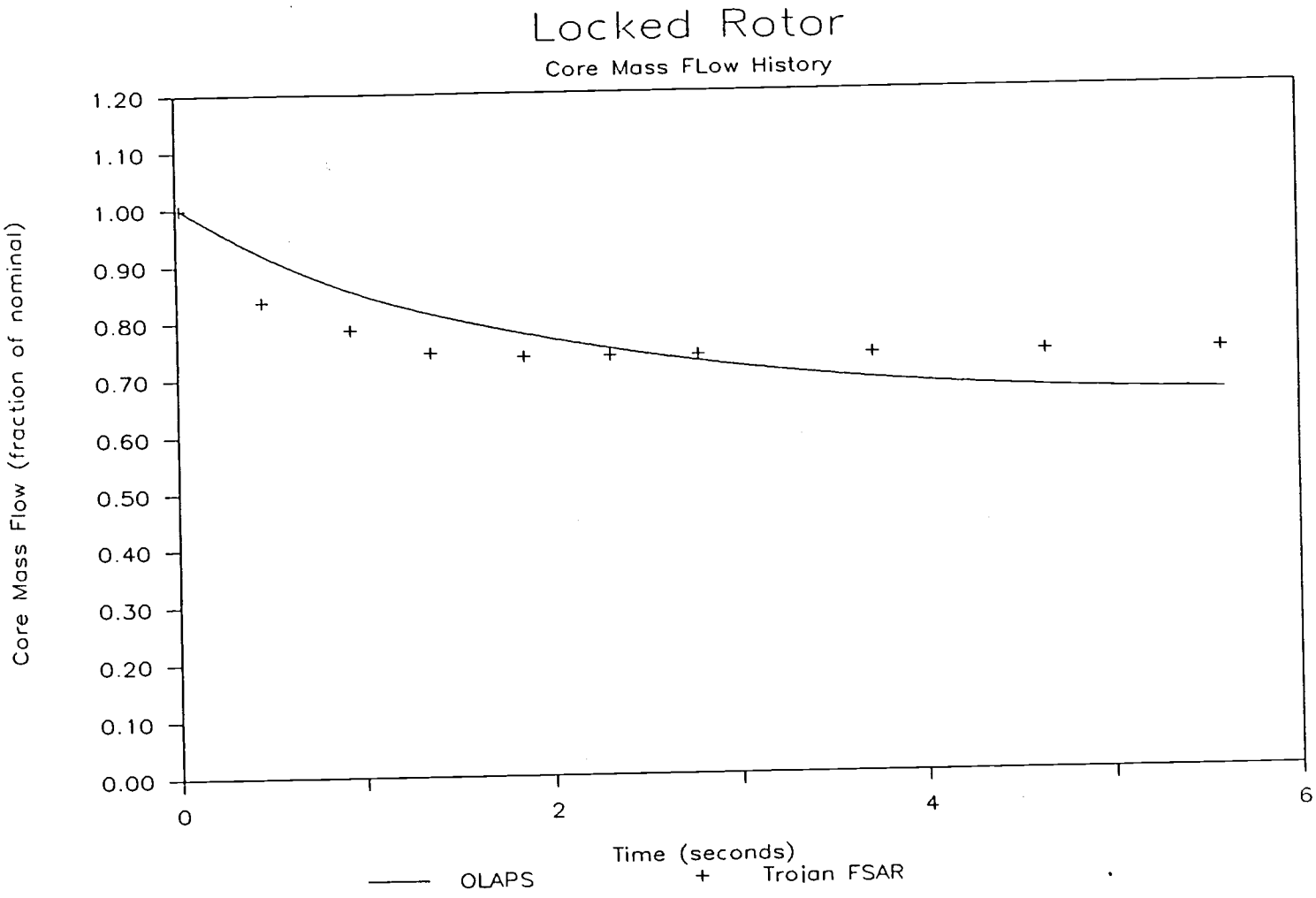

Figure 8.5
Locked Rotor Core Coolant Mass Flow Rate.

nominal. This is a difference of 7.0 percent based on nominal flow and a 10.4 percent based on the OLAPSvalue.

The power excursion induced by this transient is shown in figure 8.6. The significant difference between the Trojan FSAR and OLAPS power histories is that the FSAR data indicate an initial increase in power level after the shaft seizure while the OLAPS data show the power decreasing. This may be due to differences in the combined moderator density and temperature reactivity coefficients. The values for the moderator reactivity coefficients used in the FSAR calculation are not given but appear to be positive. The reactivity coefficients used in OLAPS is calculated using data from the cycle seven core reload and appear to negative for the given conditions.

This discrepancy may be due to the assumptions made for the FSAR calculation. The FSAR calculation assumes "adverse" steady state conditions for a worst case calculation. OLAPS conditions are based on normal operating conditions.

Even with these differences the overall agreement between the two calculations is good. With the difference being limited to a few percent throughout

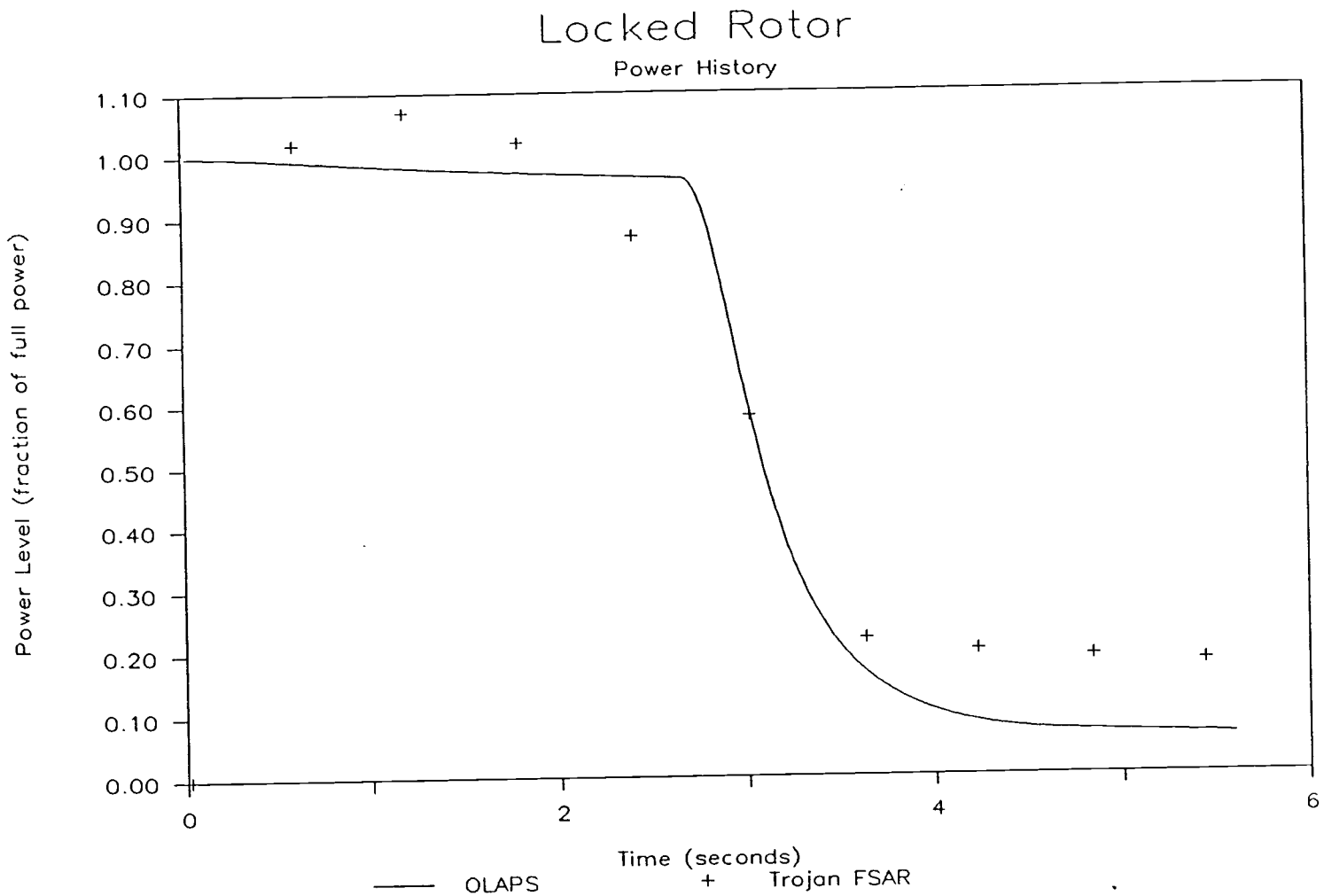

Figure 8.6
Locked Rotor Power Excursion

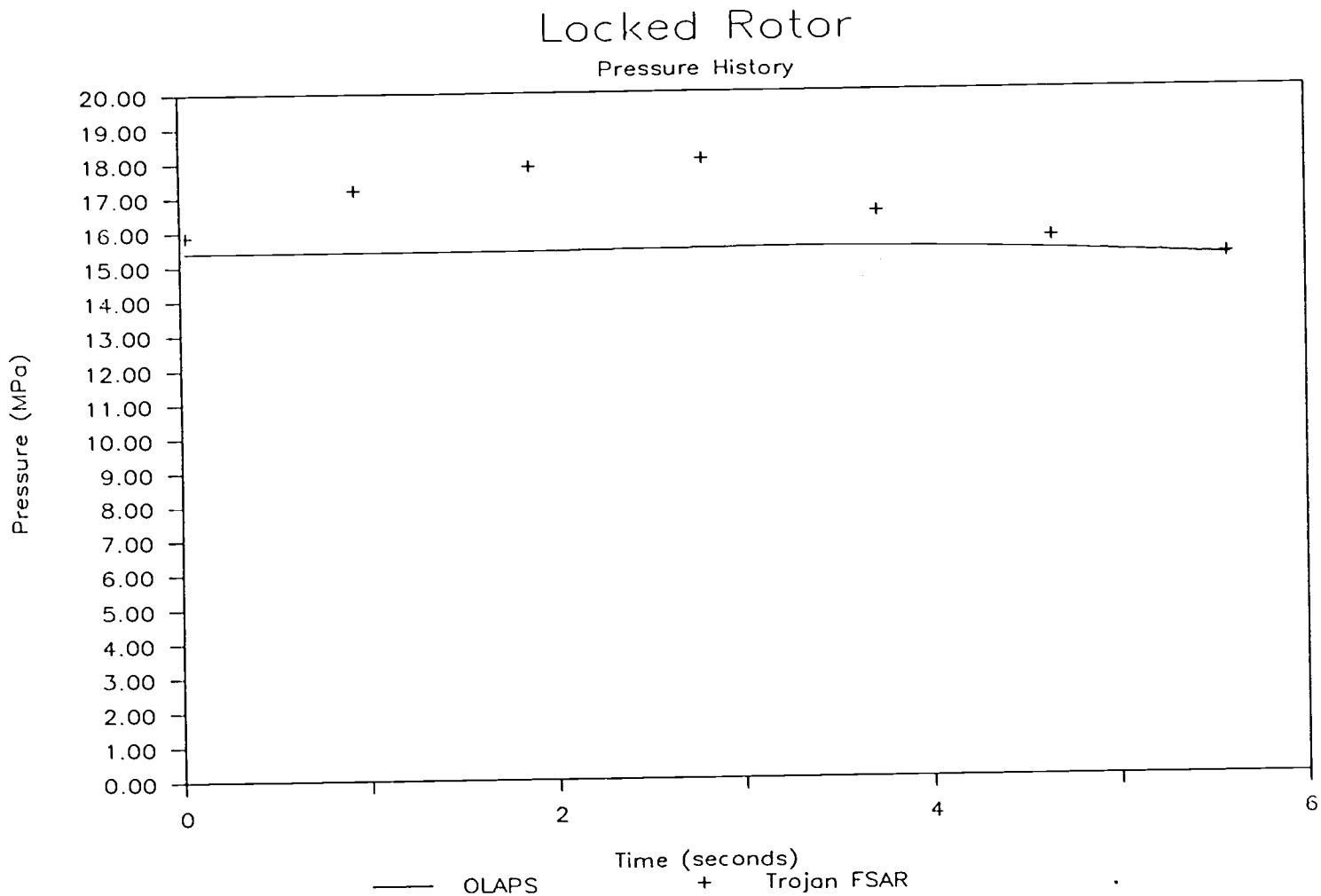

Figure 8.7
Locked Rotor System Pressure.

most of the transient.

The system pressure histories for the transient are given in figure 8.7. The differences between the OLAPS data and FSAR data are consistent with the differences in the power histories shown in figure 8.6. The maximum difference between the two calculations is 17 percent.

The overall agreement between OLAPS and the Trojan FSAR for the locked rotor transient is good. Differences are consistent with the assumptions made in each calculation with the FSAR results being more conservative.

8.2.3. Large Break LOCA

The large break loss of coolant accident is a double ended guillotine break in a cold leg pipe. Analysis of the accident plays a key roll in safety analysis of a power plant. In OLAPS this is simulated by forcing the mixture velocity in the single loop cold leg to be equal to the velocity of a mixture flowing out of a valve with hydraulic characteristics similar to the break. The

magnitude of the velocity is determined by the system pressure (see section 2.5).

The large break LOCA was run using three different values for the discharge coefficient 0.8, 0.6 and 0.4. The system pressure verses time for each case is compared to data from the Trojan FSAR in figures 8.8, 8.9, and 8.10.

In each case the OLAPS results track the system pressure well until the pressure falls below the saturation pressure of the hottest node. At this point the OLAPS program fails. This is caused by the limitations of the model used to describe the system pressure. This model requires the derivative of the density with pressure. When flashing occurs at saturation, these derivatives become too large and cause numerical over flow.

The mass flow out of the break is taken to be equal to the mass flow rate in the cold leg of the broken loop (Loop 2 for OLAPS). For each of the three cases above the break flow is given in figures 8.11, 8.12 and 8.13. The agreement between the OLAPS calculations and the Trojan FSAR is good during the early phases of the transient, but the agreement diminishes as the transient

progresses. This is probably due to limitations of the OLAPS choke flow model.

The limitations of the system pressure and break choke flow models limit the applicability of OLAPS to this class of transient. These limitations may be removed by improvements in the OLAPS models, and more testing would be required to determine the applicability of OLAPS to large break LOCA analysis.

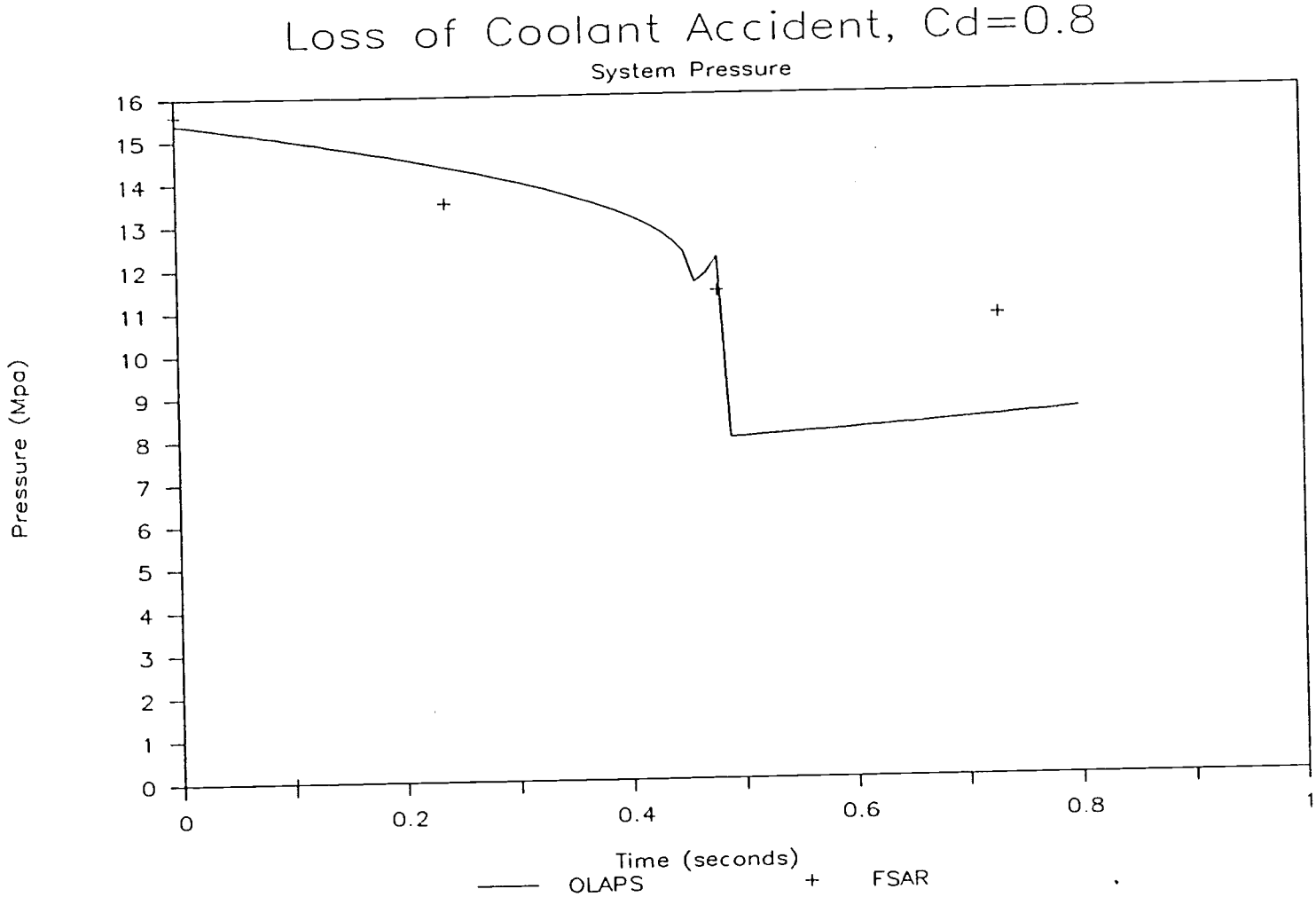

Figure 8.8
LOCA System Pressure, Cd=0.8

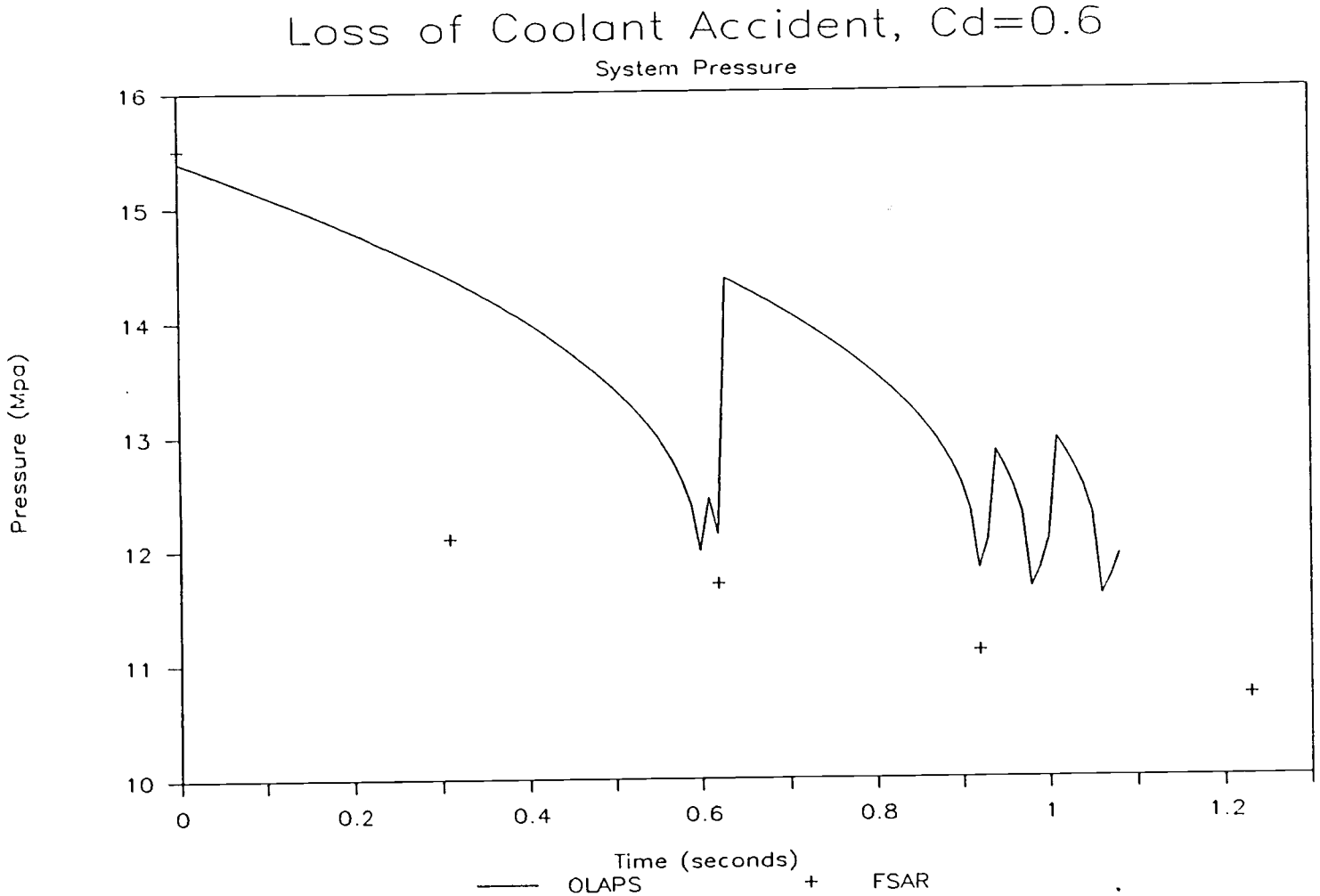

Figure 8.9
LOCA System Pressure, Cd=0.6

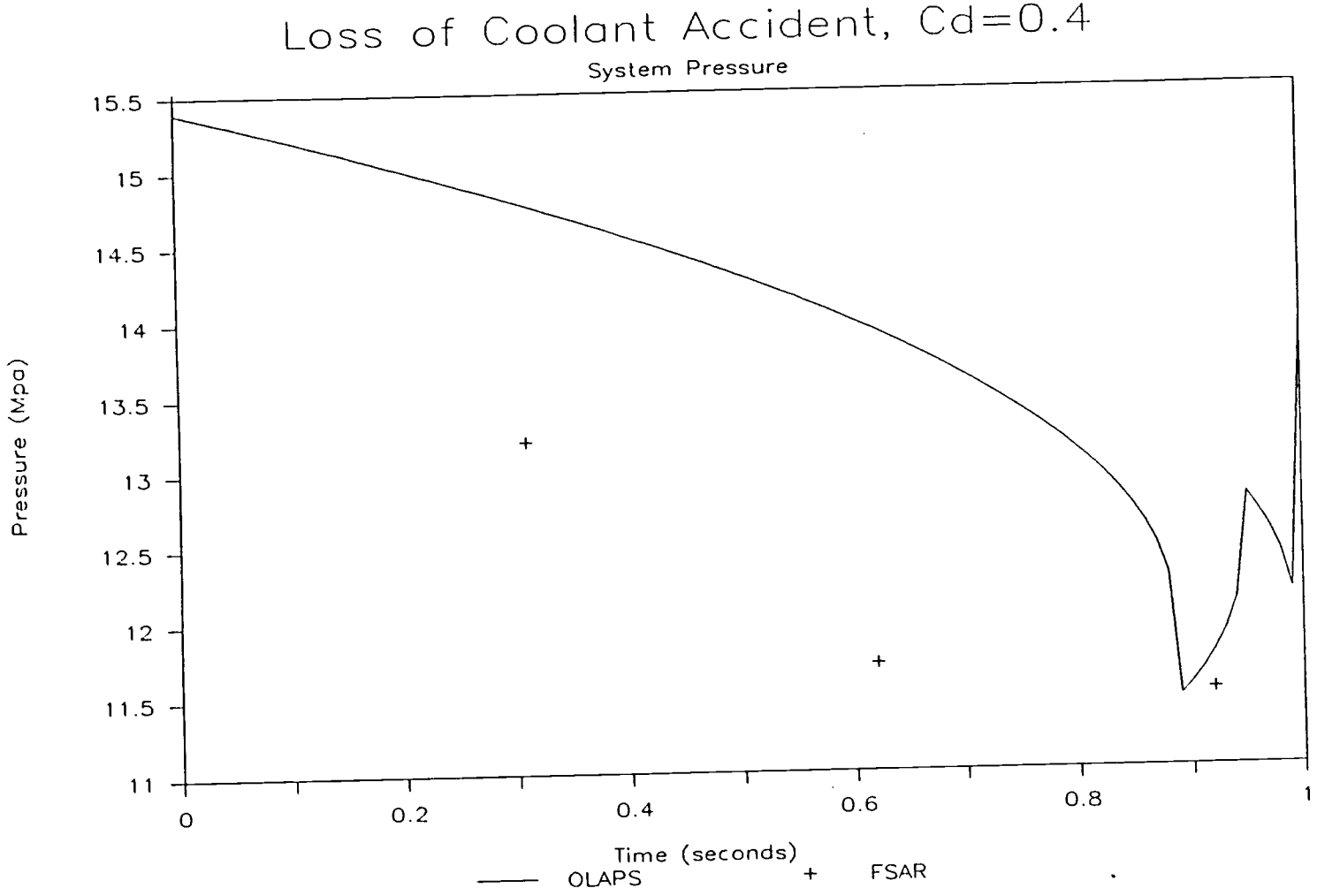

Figure 8.10
LOCA System Pressure, Cd=0.4

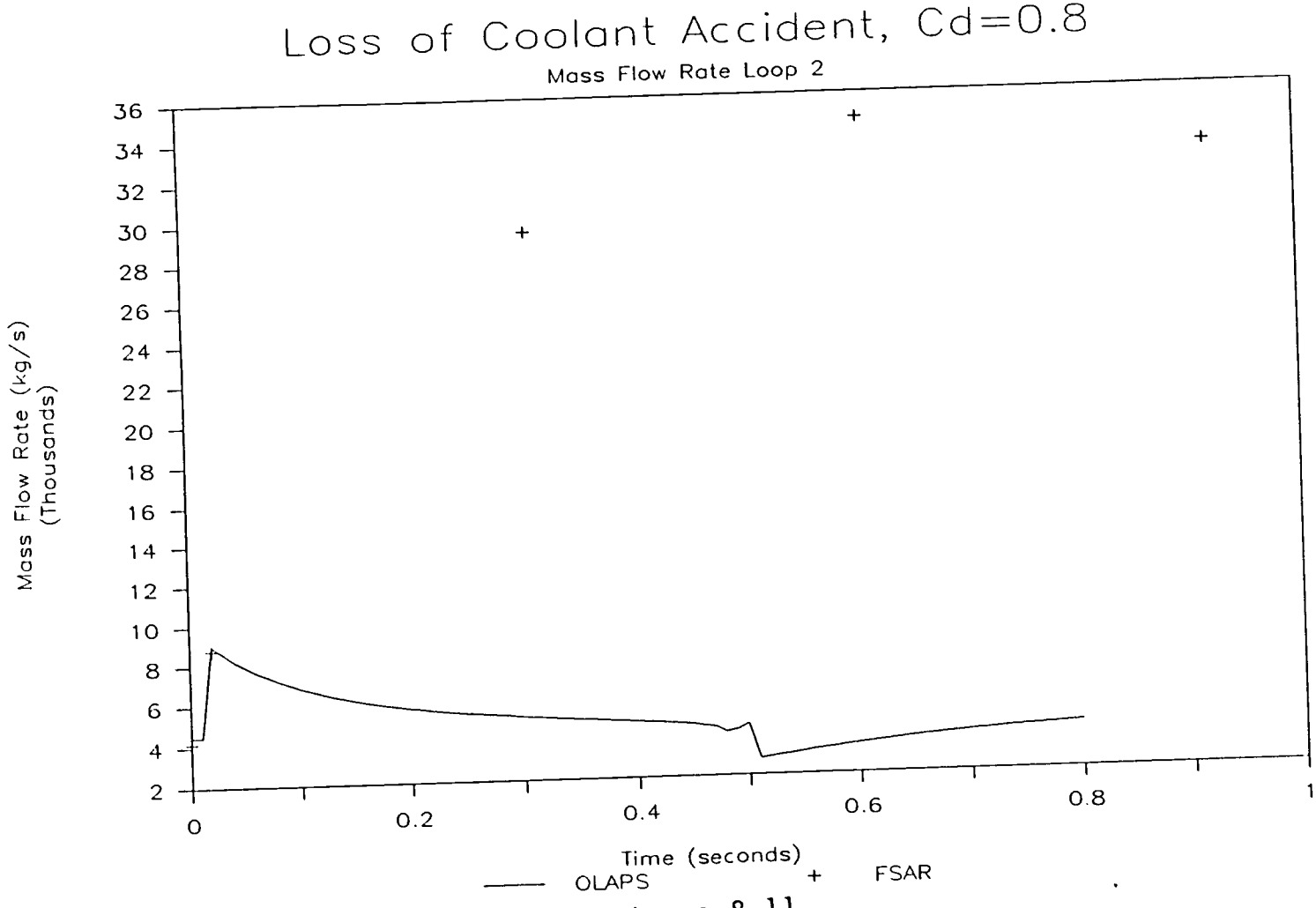

Figure 8.11
LOCA Break Mass Flow Rate, Cd=0.8

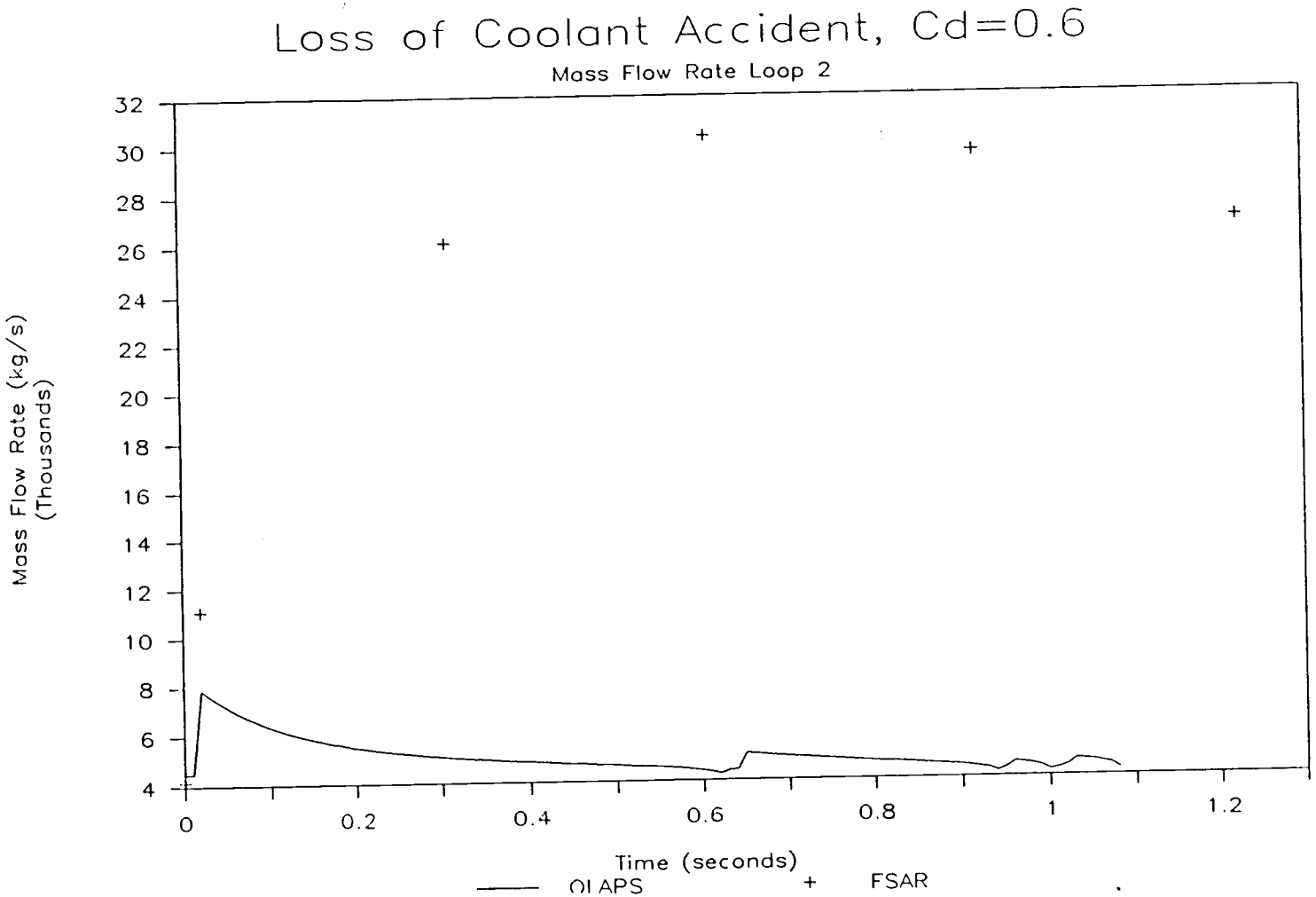

Figure 8.12
LOCA Break Mass Flow Rate, Cd=0.6

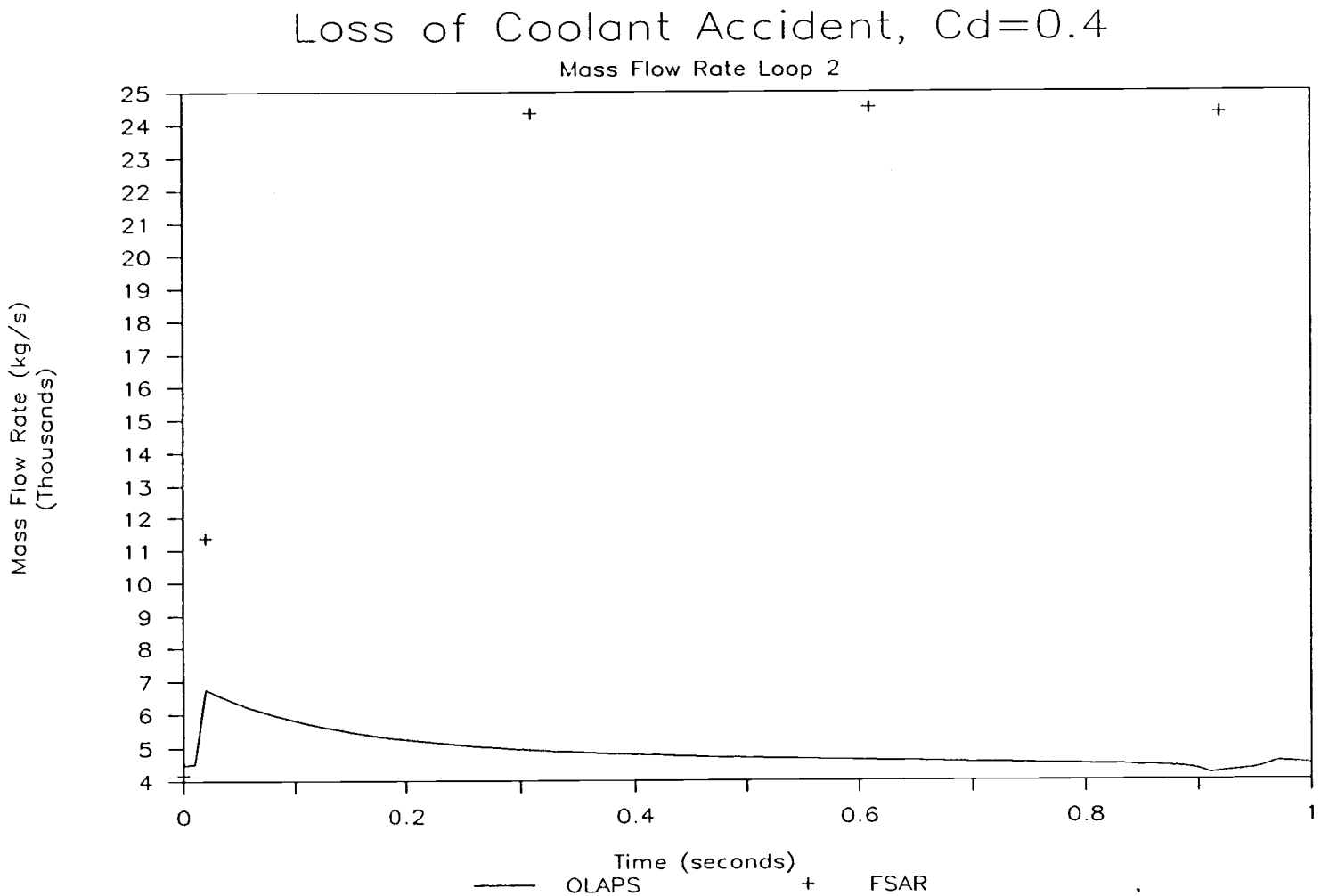

Figure 8.13
LOCA Break Mass Flow Rate, Cd=0.4

9. Comments and Conclusions

9.1. Comments

The stated objective of OLAPS was to provide a computer code with the following features:

- Accurate (approaching best estimate codes)
- User friendly (interactive,graphical output)
- On-line (interactive,ties to plant computer
- State of the Art Models
  (RWPRK, core thermalhydraulic detail).

Some of these features have been incorporated. By comparing OLAPS results to other codes and plant data it can be seen that the results are approaching those of the best estimate codes. The interactive keyboard and graphic representation of the system on the screen helps give a clearer understanding of the output. The models used in OLAPS are much more detailed than those of many of the available PC based simulators.

In addition to the above features data flow techniques were implemented in the programing. This resulted in a highly modular code that can be more easily ported to a data flow parallel processing machine.

Some of the features have yet to be incorporated. One of these is the on-line tie to the plant computer. This

feature is not currently feasible due to the relatively slow execution rate. The faster than realtime execution speed is another feature that has not been realized. When this limitation has been removed, then the ties to the plant computer can be contemplated and should not prove to be a large obstacle.

The slow execution speed is a direct result of the speed limitation of today's PC's. Even with the fastest of these machines such as the IBM Model-70 or the COMPAQ DeskPro 25, the execution speed would be very slow. If and when multiprocessor PC's with significant parallel processing capability become available then the ultimate goal of faster than real time execution may be realized.

Even though all of the desired features could not be implemented, OLAPS should and hopefully will prove to be a useful tool with several applications including:

- Teaching and Training Aid
- Preliminary Engineering Calculations
- Preliminary Safety Analysis.

9.2. Future Work

There is much room for future work in the development of OLAPS. Some areas of improvement are:

-Improvements of user Interface
-Improvements Steam Generator Model
-Improvements Pressurizer Controller
-Improvements Charge/Letdown Controller
-Addition of Controller for Power level
-Addition of more secondary systems.

Another and perhaps more important task is the further validation and verification of the models and programming of OLAPS. This task has two important phases. The first phase includes the continued comparison of OLAPS results to those of the best estimate codes; not only the thermal-hydraulics but kinetics as well, and plant data where possible.

The second phase would include a quality assurance study of the models and correlation used in OLAPS as has been done for RELAP5/MOD2 and as has been proposed for COBRA/TRAC. Here the models and correlations would be reviewed and retraced to original work to verify such things as range of validity. This study for OLAPS should be easier after the COBRA/TRAC study since they share many common elements.

Other work that should be carried out is the testing of OLAPS code on existing multiprocessing machines such as the Applied Dynamic AD-10 used by the BNL BWR Plant Analyzer (13). This should be very enlightening as to whether faster than realtime execution can be achieved.

9.3. Conclusions

OLAPS is a PC based thermalhydraulics and kinetic simulator for a four-loop Westinghouse PWR. The results show that the models used are of a high quality compared to most PC based simulators. At present one of the major limitations is the execution speed. The speed limitations should yield to advances in computer science and in computing machinery in the foreseeable future.

Even with the speed limitation, with current state of the art, personal computers OLAPS should enjoy a moderate utility , especially in the academic environment.

References

(1) Gonsalves, J. B., J.E. Proctor; "Nuclear Plant Simulators: The Past and the Present"; Nuclear News, June, 1987.

(2) D.S. Rowe "COBRA-IIIc A Digital Computer Program for Steady State and Transient Thermal Analysis of Rod Bundle Nuclear Fuel Elements",BNWL-1695,1973

(3) C.L. Wheeler, et. al.,"COBRA-IV: An Interim Version of COBRA for Thermal Hydraulic Analysis of Rod Bundle Nuclear Fuel Elements and Cores",BNWL-1962,Battelle Pacific Northwest Laboratory,1976

(4) "TORC-Code: A Computer Code for Determining the Thermal Margins of a Reactor Core",CENPD-161,Combustion Engineering,1975

(5) Stewart C.L., et al, "VIPRE-01 A Thermal-hydraulic Code Nuclear Reactor Cores",EPRI NP-2511, PNL, December 1982.

(6) Punches, W.C.,"MAYOU4: A method to evaluate Transient Thermal-hydraulic conditions in rod Bundles", GEAP-23517, General Electric Company, 1976.

(7) Hao, B.R., Alcorn, J.M., "LYNX1 - A Reactor Fuel Assembly Thermal-Hydraulic Analysis Code", BAW-10129, Babcock and Wilcox, 1976.

(8) Babcock and Wilcox Topical Report "LYNX2-Subchannel Thermal-Hydraulic Analysis Program", BAW-10130, Babcock and Wilcox, 1976

(9) K.V. Moore,et. al,"RETRAN - A Program for One Dimensional Transient Thermal Hydraulic Analysis of Complex Fluid Flow Systems",EPRI/NP-408,1977

(10) Ransom, V.H., et al. "RELAP5/MOD2 Code Manual", NUREG-4312, EGG-2396, Idaho National Engineering Laboratory, August 1985.

(11) D.R. Liles, et. al, "TRAC-PD2: An Advanced Best-Estimate Computer Program for Pressurized Water Reactor Loss-of-Coolant Accident Analysis",NUREG/CR-2054,1981.

(12) Thurgood, M.J., et al, "COBRA/TRAC - A Thermal-Hydraulic code for the analysis of Nuclear Reactor Vessels and Primary Coolant Systems", NUREG/CR-3046, PNL-4385, Pacific Northwest Laboratory, March 1984.

(13) Wulff, W., Cheng, H.S., Lekach, S.V., Mollen, A.N. "The BWR Plant Analyzer: Final Report", NUREG/CR-3943, BNL-NUREG-51812, Brookhaven National Laboratory, August 1984.

(14) Parveen, J.K. "A Dynamic Model for Pressurized Water Reactor Analysis on Microcomputers", Nuclear Technology, March 1986.

(15) Po, L.C., "PCTRAN- Personal Computer Transient Analyzer", 1985 Topical Meeting on Computer Applications for Nuclear Power Plants, September 1985

(16) Yackle, T.R., et al., "Generic Simulator for Personal Computers" National Heat Transfer Conference, Denver, August 1985.

(17) Webb, B.J., "COBRA-IV PC: A Personal Computer Version of COBRA-IV for Thermal Hydraulic Analysis of Rod Bundle nuclear Fuel Elements and Cores.", PNL-5476, Pacific Northwest Laboratories, January 1988.

(18) Fletcher, C.D., C.B. Davis, D.M. Ogden, "Thermal-Hydraulic Analysis of Overcooling Sequences for the H.B. Robinson unit 2 Pressurized Thermal Schock Studies", NUREG/CR-3935.

(19) Proceedings from the Boeing Computer Services SuperComputer Summer Institute, Session 1 Panel Discussion, Seattle Washington, June 1986.

(20) Pressman, R.S. "Software Engineering: A Practitioners Approach", McGraw-Hill, 1982.

(21) Samuels, J.W., S. Kaya, S.A. Anghie, "Kinetics Modeling for an On-line Advanced Plant Simulator," Proceedings International Conference on Simulation Methods in Nuclear Engineering Volume 2. Montreal ,1986

(22) Perry, J.R., Liang E., "Trojan Cycle Seven Design Report", Portland General Electric Company, Portland Oregon, June 1984.

(23) DeGreef, J.F.,"Simulating the Steam Generator and Pressurizer of a PWR Nuclear Power Plant", Proceedings International Conference on Nuclear Reactor Simulation Technology, 1984.

(24) Wallis, G.B., "One-Dimensional Two-Phase Flow", McGraw-Hill 1969.

(25) Samuels, J.W., Anghaie, S.A., "Prediction of Transient Axial Power Distribution for Calculation of DNBR Limit", AND Transactions, November 1986.

(26) Samuels, J.W., Anghaie, S.A. "Prediction of PWR Thermal-Hydraulic Margins During Transient Events", Topical Meeting on Anticipated and Abnormal Transients in Nuclear Power Plants, Atlanta Ga., April 1987.

(27) Stacey, W.M. "Space-time Nuclear Reactor Kinetics", Academic Press, 1969.

(28) Ash, M.H. "Nuclear Reactor Kinetics", McGraw-Hill, 1979.

(29) Duderstadt, J.J., Hamilton, L.R., "Nuclear Reactor Analysis", J. Wiley and Sons, 1976.

(30) Hottel, H.C., "Radiant Heat Transmission" in: McAdams, "Heat Transmission", McGraw-Hill 1954.

(31) Hagrman, D.L., Reymann, G.A., Manson, R.E., "MATPRO - Version 11 Rev(1): A Handbook of Materials Properties for Use in the Analysis of Light Water Reactor Fuel Rod Behavior", USNRC Report NUREG/CR-0497, TREE-1290, Idaho National Engineering Laboratory, February 1980.

(32) Edwards, D.K., "On The Use of Total Radiation Properties of Gases", ANL/RAS 75-12, Argonne National Laboratory, April 1975.

(33) Ishii, M., Grolmes, M.A., "Inception Criteria for Entrainment in Two-Phase Concurrent Film Flow", AIChE Journal, February 1975.

(34) Forslund, R.P., Rohsenow, W.M., "Dispersed Flow Film Boiling", Journal of Heat Transfer, June 1968.

(35) Bromely, L.A., "heat Transfer in Stable Film Boiling", Chemical Engineering Progress, May 1950.

(36) Chexial, B. Horowitz, J., Lellouche, G., "An Assessment of Eight Void Fraction Models for Vertical Flows", NSAC-107, EPRI, December 1986.

(37) Ohkawa, K., Lahey, R.T., "The Analysis of CCFL using Drift-flux Models", Nuclear Engineering and Design, Vol 61, 1980.

(38) Biasi, L., et al., "Studies in Burn Out Part 3", Energia Nucleare, September 1967.

(39) Shapiro A.H., "The Dynamics and Thermodynamics of Compressible Fluid Flow", Vol 1, Ronald Press Company, 1953.

(40) Hsu, Y.Y., Graham, R.W., "Transport Process in Boiling and Two-Phase Systems", Hemisphere Publishing Company, 1976.

(41) Delhaye, J.M., Giot, M., Reithmuller, M.L., "Thermohydraulics of Two-Phase Systems for Industrial Design and Nuclear Engineering", McGraw-Hill, 1981.

(42) Dimenna, R.A., et al. "RELAP5/MOD2 Models and Correlations", NUREG/CR-5194 EGG-2531, Idaho National Engineering Laboratory, August 1988.

(43) Cappiello, M.W., et al., "TRAC-PF1/MOD1 Models and Correlations", Los Alamos National Laboratory, December 1986.

(45) Reyes, J.N., NRC research grant proposal, Oregon State University, September 1988.

(46) Trojan Nuclear Facility Final Safety Analysis Report, Portland General Electric Company, July 21, 1984.